ECMWF COPERNICUS REPORT

Copernicus Atmosphere Monitoring Service

Validation of the CAMS regional services: concentrations above the surface

Status update for the period June – August 2019

Issued by: KNMI

Date: 9/12/2019 (final)

Ref: CAMS84_2018SC1_D4.1.1-JJA2019_v1.pdf

IMPLEMENTED BY ECMWF

Validation of the CAMS regional services: concentrations above the surface

Status update for June – August 2019

AUTHORS:
D. Akritidis (AUTH), T. Antonakaki (AA), Y. Bennouna (CNRS-LA),
A.-M. Blechschmidt (IUP-UB), T. Bösch (IUP-UB), H. Clark (CNRS-LA),
C. Gielen (BIRA-IASB), F. Hendrick (BIRA-IASB), J. Kapsomenakis (AA),
S. Kartsios (AUTH), E. Katragkou (AUTH), D. Melas (AUTH), A. Mortier (MetNo),
E. Peters (IUP-UB), K. Petersen (MPI), A. Piters (KNMI), A. Richter (IUP-UB),
M. van Roozendael (BIRA-IASB), M. Schulz (MetNo), N. Sudarchikova (MPI),
A. Wagner (MPI), P. Zanis (AUTH), C. Zerefos (AA)

EDITORS:
J. Douros (KNMI), H.J. Eskes (KNMI)

REPORT OF THE COPERNICUS ATMOSPHERE MONITORING SERVICE, VALIDATION SUBPROJECT (CAMS-84).

CITATION:
Douros, J., H.J. Eskes, D. Akritidis, T. Antonakaki, Y. Bennouna, A.-M. Blechschmidt, T. Bösch, H. Clark, C. Gielen, F. Hendrick, J. Kapsomenakis, S. Kartsios, E. Katragkou, D. Melas, A. Mortier, E. Peters, K. Petersen, A. Piters, A. Richter, M. van Roozendael, M. Schulz, N. Sudarchikova, A. Wagner, P. Zanis, C. Zerefos, Validation of CAMS regional services: concentrations above the surface, Status update for June - August 2019, Copernicus Atmosphere Monitoring Service (CAMS) report, CAMS84_2018SC1_D4.1.1-JJA2019_v1, December 2019, doi:10.24380/hwqd-mv32.

STATUS:
Version 1, final

DATE:
9/12/2019

REF:
CAMS84_2018SC1_D4.1.1-JJA2019_v1

Executive Summary

The Copernicus Atmosphere Monitoring Service (CAMS, http://atmosphere.copernicus.eu) is a component of the European Earth Observation programme Copernicus. The CAMS service consists of two major forecast and analysis systems. First, the CAMS global near-real time (NRT) service provides daily analyses and forecasts of reactive trace gases, greenhouse gases and aerosol concentrations, and is based on the ECMWF Integrated Forecast System (called CAMS-global in this document). Secondly, seven regional models in Europe perform air quality forecasts and analyses on a daily basis, nested within CAMS-global. Based on these individual forecasts and analyses, an ensemble forecast of air quality over Europe is produced and disseminated by Météo-France (called ENSEMBLE or CAMS-regional below). The seven regional members use the global forecasting results as boundary conditions at the sides and top of the domain.

This document reports on two validation activities, namely

- an evaluation of the consistency between the global and regional modelling components of CAMS, focussing on the boundaries of the regional domain, and
- an evaluation of the regional ensemble and the seven individual models contributing to the ensemble with independent observations, focusing on the concentrations above the surface.

The current analysis includes ozone (O_3), nitrogen dioxide (NO_2), aerosol (PM10/PM2.5/AOD) and carbon monoxide (CO) forecasts covering the period up to August 2019.

The forecasts from the regional models were compared with the following set of observations:

- aerosol lidar observations from the EARLINET network;
- aerosol AOD observations from the AERONET network;
- IAGOS routine aircraft measurements of ozone and CO;
- ozone sonde profiles;
- MaxDOAS NO_2 tropospheric columns;
- GOME-2/MetOp-A NO_2 satellite tropospheric column retrievals (IUP-UB v1.0 product);
- high-altitude ozone surface stations;
- CO and O_3 from GAW mountain stations; and
- CO observations from the MOPITT satellite instrument.

These observations are available to CAMS within one month after the observations were made.

This report is based on regional model data available for the months February 2016 to August 2019, with a focus on June – August 2019 (JJA2019). The report is updated every 3 months. The main results are summarised below. This summary is focusing on the performance of the regional Ensemble. Detailed results, also for the seven individual models, are presented in sections 3 to 11, and each of these sections starts with a summary of the main results.

During the reporting period there were upgrades implemented for CAMS-global (on 9 July 2019, moving from 60 to 137 vertical levels) and for CAMS regional (on June 12, e.g. implementing new anthropogenic emissions including emissions outside of Europe).

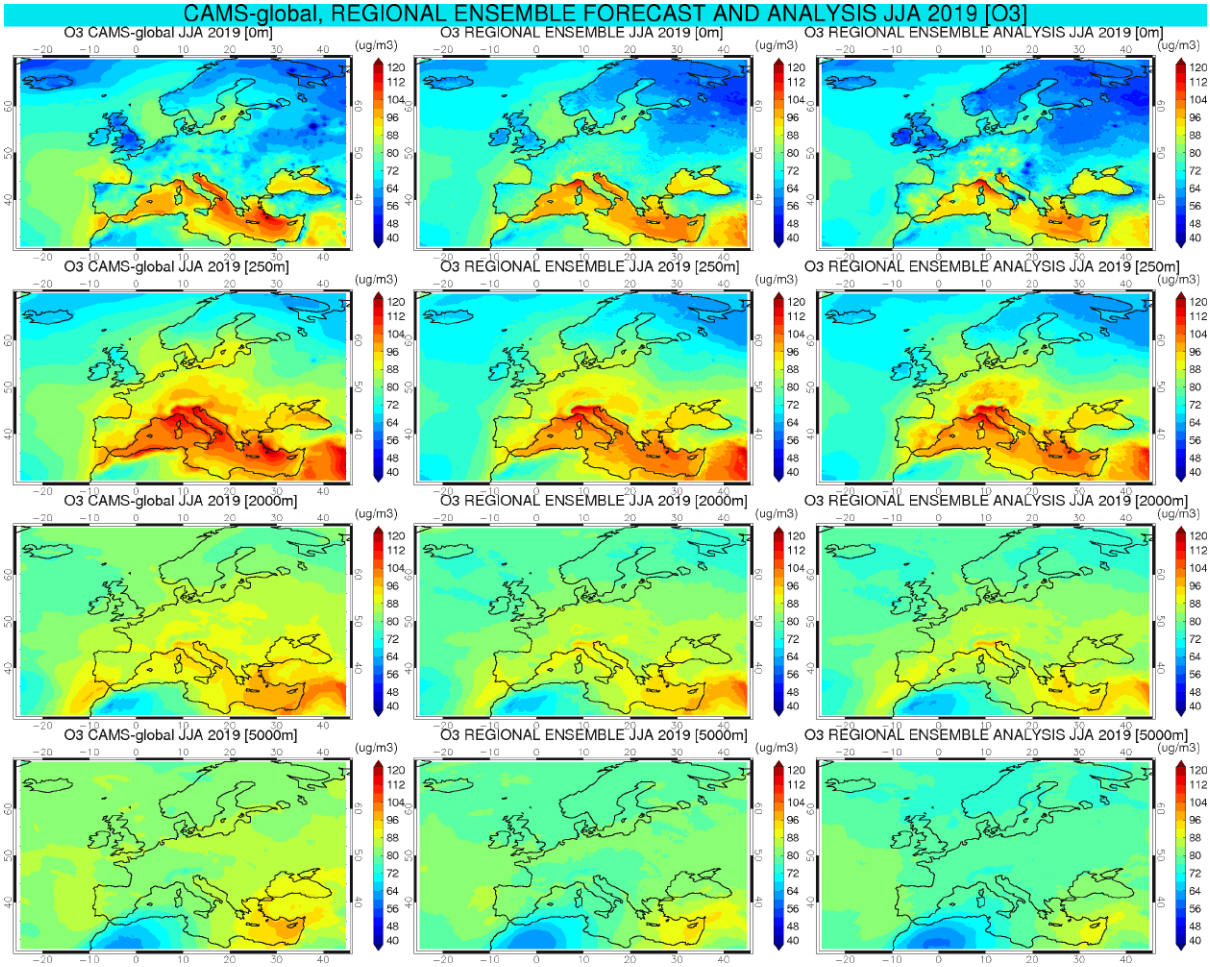

Figure S.1. CAMS global ozone forecast for day 1 (left), CAMS regional ensemble ozone forecast for day 1 (middle), CAMS regional ensemble ozone analysis (right). From top to bottom: 0, 250, 2000, 5000m altitude level. The results are averaged over the June - August 2019 period.

General conclusions for the regional ensemble forecasts

The comparison of the European regional CAMS ensemble air quality forecasts and analyses against above-surface observations of O_3, NO_2, CO for the period up to 1st of September 2019 demonstrates that overall, the biases observed are small, often within the uncertainty of the validation approach while the temporal correlations for ozone and CO show that the CAMS-regional system describes the main episodes observed. Performance of the ensemble analysis product is found to be generally superior to that of the ensemble forecasts. Regional models - and thus the ensemble - benefit from the use of the global CAMS boundary conditions, which are implemented efficiently. The ensemble model performs generally better than any of the individual models for ozone, NO_2 and CO, showing the strength of the ensemble approach adopted in CAMS.

The upgrade of CAMS-global from 60 to 137 vertical levels on 9 July and the impact on the boundary conditions for the regional models was studied. No significant change in the performance or discontinuities at the domain boundaries were observed, showing that the transition was smooth.

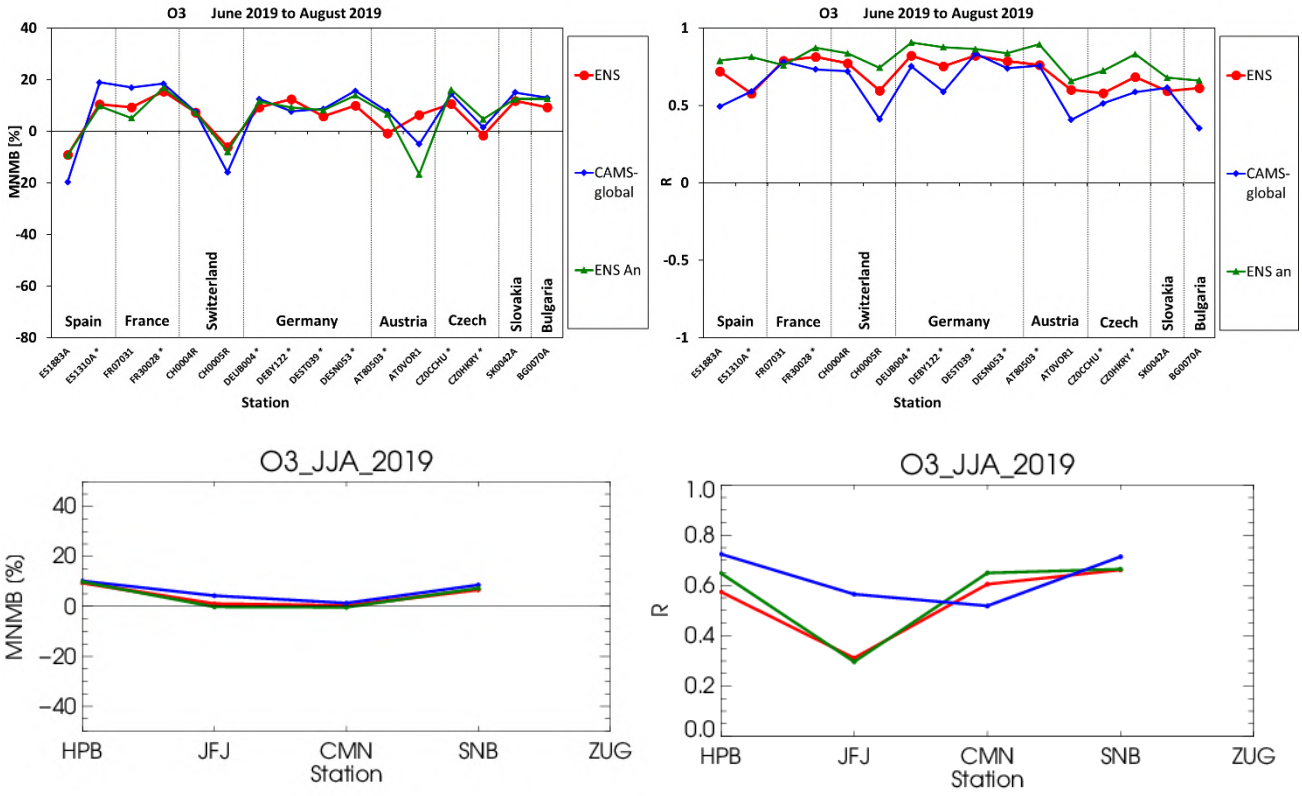

Figure S.2. Normalised bias (left) and correlation coefficient (right) for ozone for the high-altitude (above 1 km) EEA Air Quality e-reporting stations (top) and the 5 high-altitude European GAW stations (bottom). Lines represent ENSEMBLE forecast (solid red), ENSEMBLE analysis (solid green) and CAMS-global system (blue) for June-August 2019. The horizontal axis is the station identifier referring to Hohenpeissenberg (HPB), Jungfraujoch (JFJ), Monte Cimone (CMN), Sonnblick (SNB) and Zugspitze (ZUG, no observations this quarter).

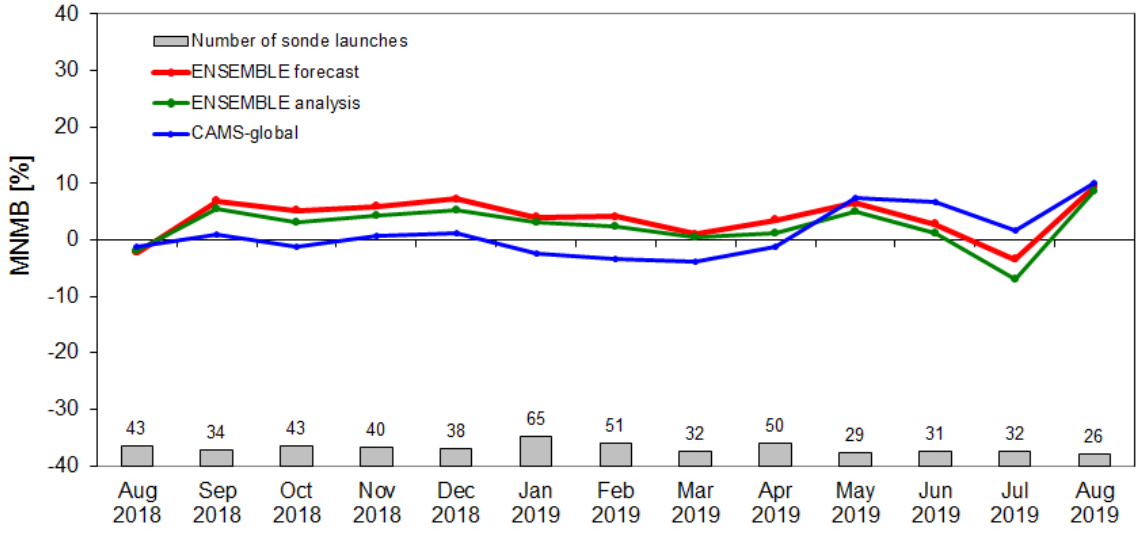

Figure S.3. Modified normalised mean bias (MNMB) against ozone sondes for the regional ENSEMBLE forecasts (red) and analyses (green) from August 2018 to August 2019 (horizontal axis). Ozone was averaged over the lower-middle free troposphere region, 500 hPa < p < 850 hPa.

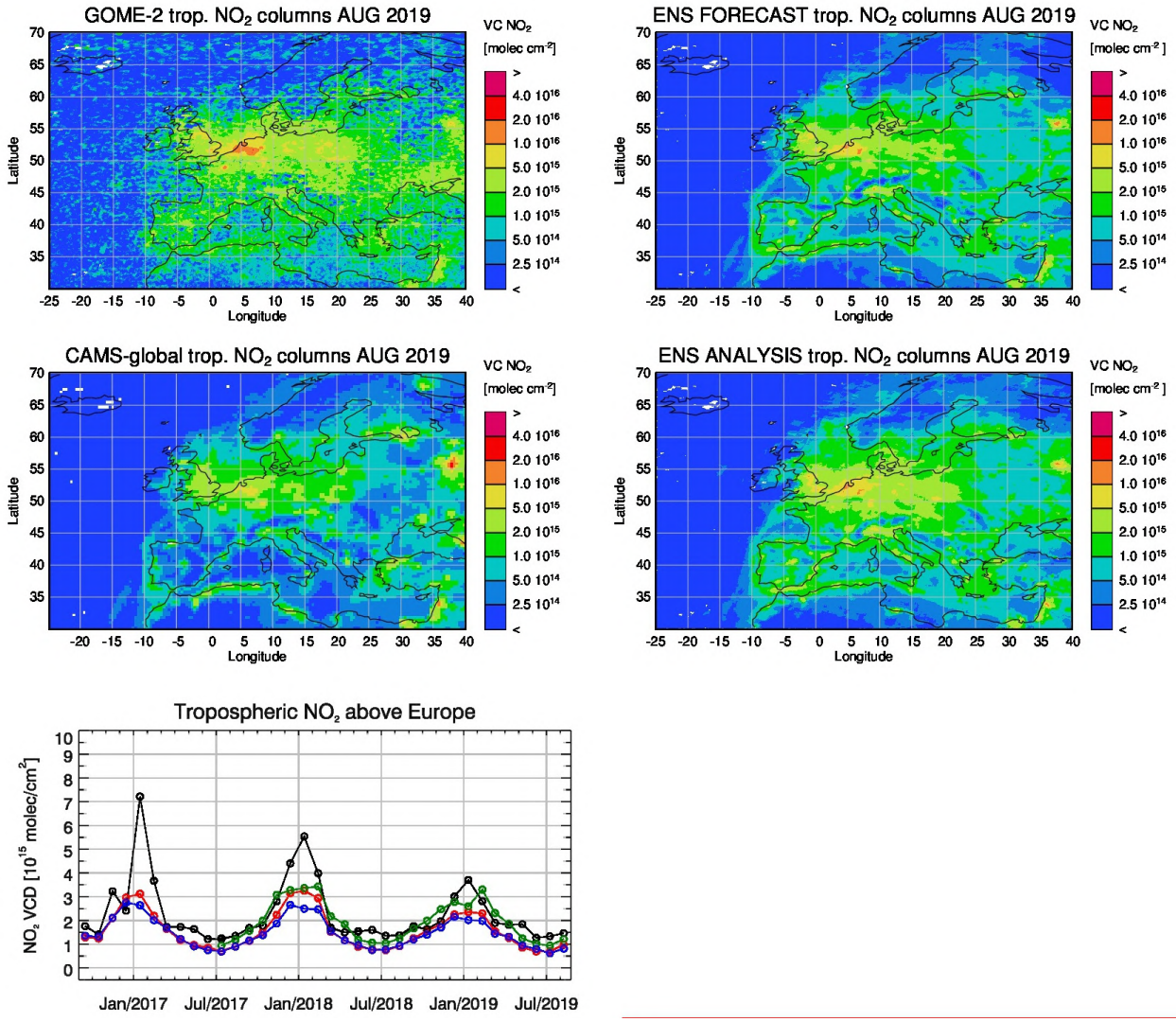

Figure S.4. Maps of satellite retrieved and model simulated tropospheric NO_2 columns [molec cm^{-2}] for May 2019 for GOME-2 (top left), regional ENSEMBLE forecasts (top right) CAMS-global forecasts (middle left) and regional ENSEMBLE analyses (middle right) The panel at the bottom shows corresponding time series of average tropospheric NO_2 columns [10^{15} molec cm^{-2}] from GOME-2 (black), regional ENSEMBLE forecasts (red), CAMS-global forecasts (blue) and regional ENSEMBLE analyses (green). GOME-2 data were gridded to regional model resolution (i.e. 0.1° x 0.1°). Model data were treated with the same reference sector (25°W - 20°E) subtraction approach as the satellite data and linearly interpolated to the satellite overpass time (9:30 LT).

Ozone

A comparison of the regional analysis product with the regional day 1 forecast (Fig. S.1) reveals some small differences between the regional ENSEMBLE forecast and analysis, with the analysis generally showing lower concentrations near the surface. As in the previous quarter, there is a very good match between the global and regional CAMS analyses and forecasts between 1 and 5 km altitude. The differences between the global and regional systems reveal themselves in the

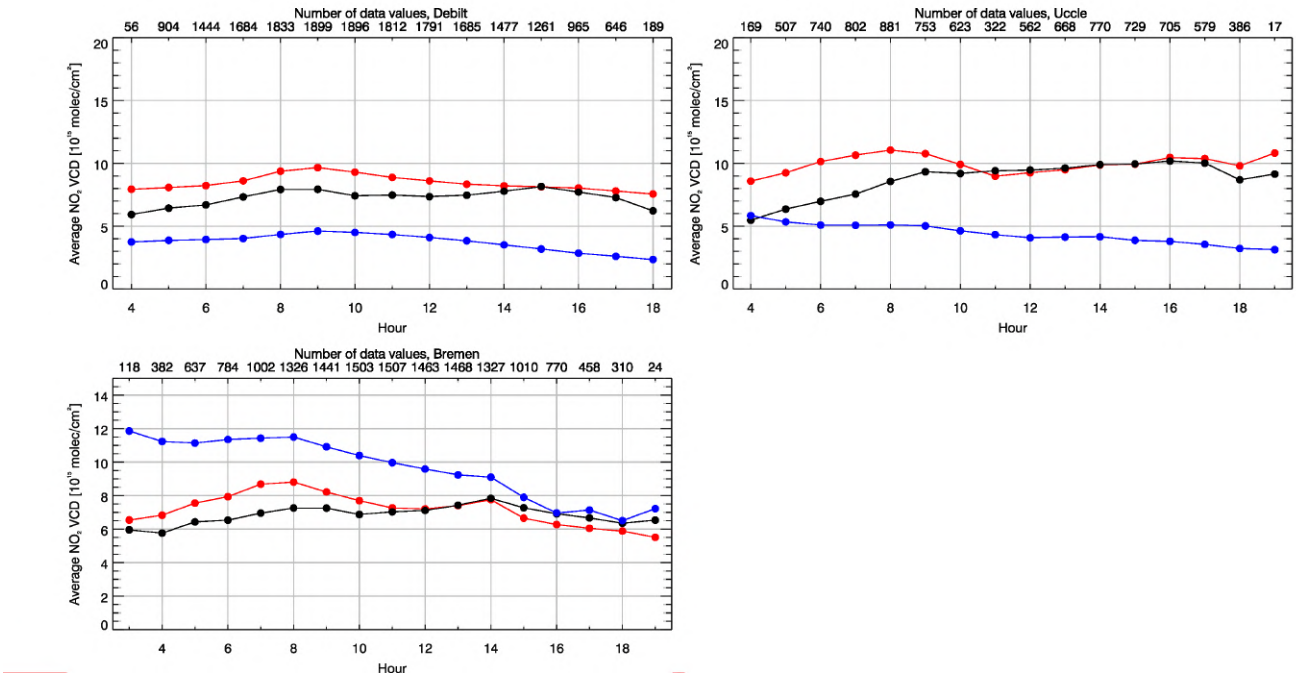

Figure S.5: Diurnal cycles (averages over hourly bins) of tropospheric NO_2 VCDs [10^{15} molec. cm^{-2}] from MAX-DOAS and models for De Bilt (Netherlands) (top left), Uccle (Belgium) (top right) and Bremen (Germany) (bottom). The coloured lines show (black) MAX-DOAS retrievals, (red) regional ENSEMBLE forecasts and (blue) CAMS-global.

boundary layer and at the surface over land, as expected. At the boundaries of the regional domain, the ENSEMBLE agrees well with CAMS-global, indicating that the implementation of the boundary conditions was done properly.

For high altitude stations, Fig. S.2, as well as for comparisons against ozone sondes, Fig. S.3, mostly an overestimation is also apparent, but only up to 20% at some stations for the former and up to 10% for the latter. Time correlations at high-altitude and GAW stations range between 0.3 and 0.85 during this period, with noticeably improved figures for the ENSEMBLE analyses as compared to the ENSEMBLE forecast in the case of the high-altitude stations. Such improvement is not so evident for the GAW stations.

IAGOS aircraft observations indicate that ozone is well represented by both the regional ensemble the CAMS-Global during the heat wave periods with slightly better results from the regional ensemble. Quantitative comparisons at Frankfurt (not shown) are complicated due to IAGOS instrumental issues over the summer. The comparisons show the ability of the models to capture the correct diurnal cycle in the boundary layer and the concentration up to 5000m.

Nitrogen dioxide (NO_2)

The overall spatial distribution of tropospheric NO_2 as observed from space by GOME-2 is reproduced by the ensemble during JJA 2019 (see Fig. S.4). As described in previous reports, winter values over European emission hotspots simulated by the regional ensemble analysis, forecasts and

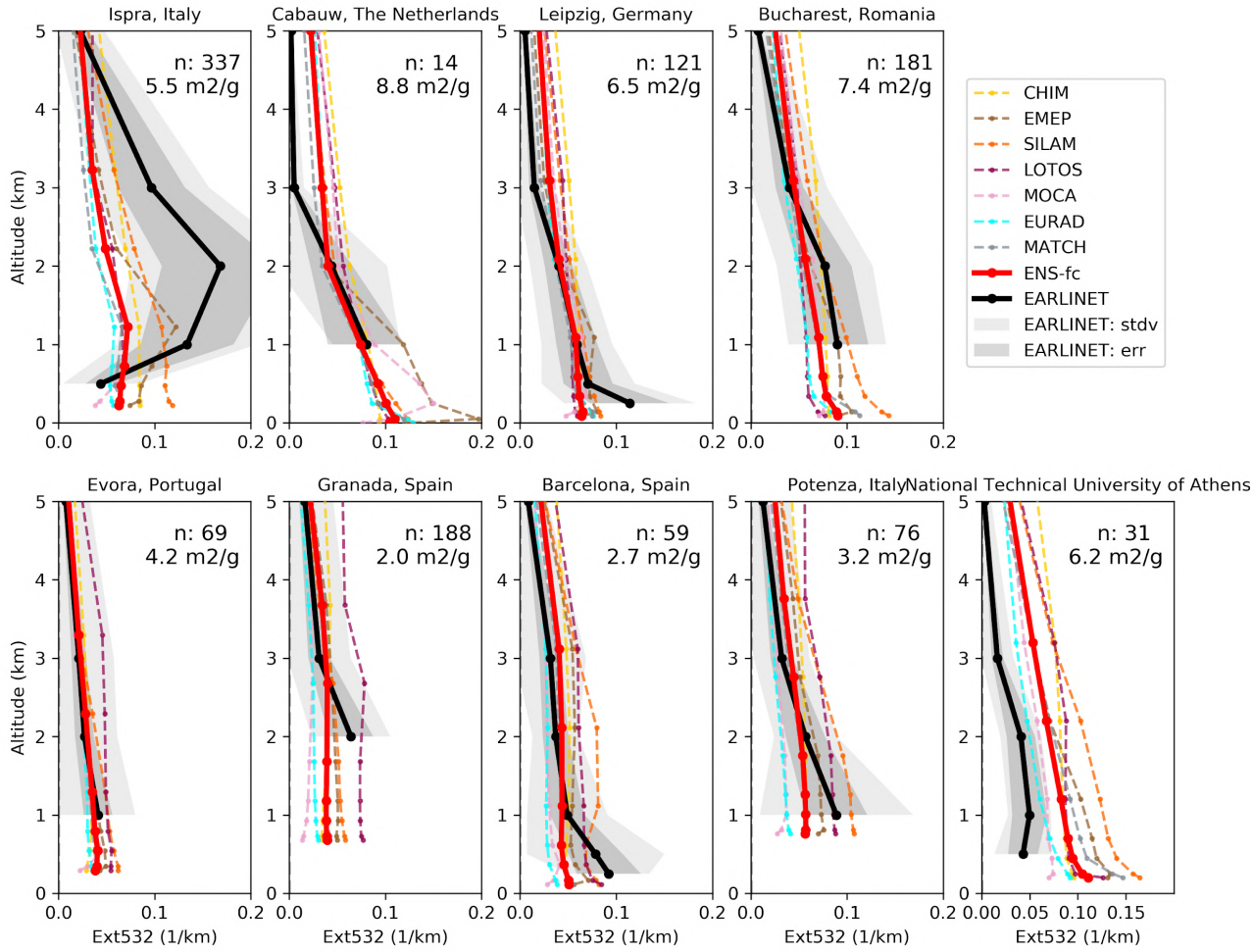

Figure S.6. Extinction profiles June - August 2019 derived from the ENSEMBLE forecast mass concentration profiles (red envelope) and from EARLINET (climatology) backscatter profiles (grey envelope: lidar ratio uncertainty, light grey: including sampling error). "n: XX means number of individual EARLINET profiles assembled (June - August 2006-2018). The EMC used for the calculation of the extinction from the concentration profiles is indicated for each station below the number of EARLINET profiles "n" used for the calculation of the climatology.

CAMS-global show significantly smaller values than GOME-2 but the difference appears to be decreasing over the last three years mainly driven by a reduction in GOME-2 observations while the modelled columns remain on the same order of magnitude. Values over European emission hotspots during other seasons are better represented by the regional ensemble analysis and forecasts than by CAMS-global. As a result of a major regional model upgrade in June (2019), which includes the use of an updated European emissions inventory with improved estimates for North African and Middle Eastern anthropogenic emissions, enhanced tropospheric columns of NO_2 are now reproduced by all model runs.

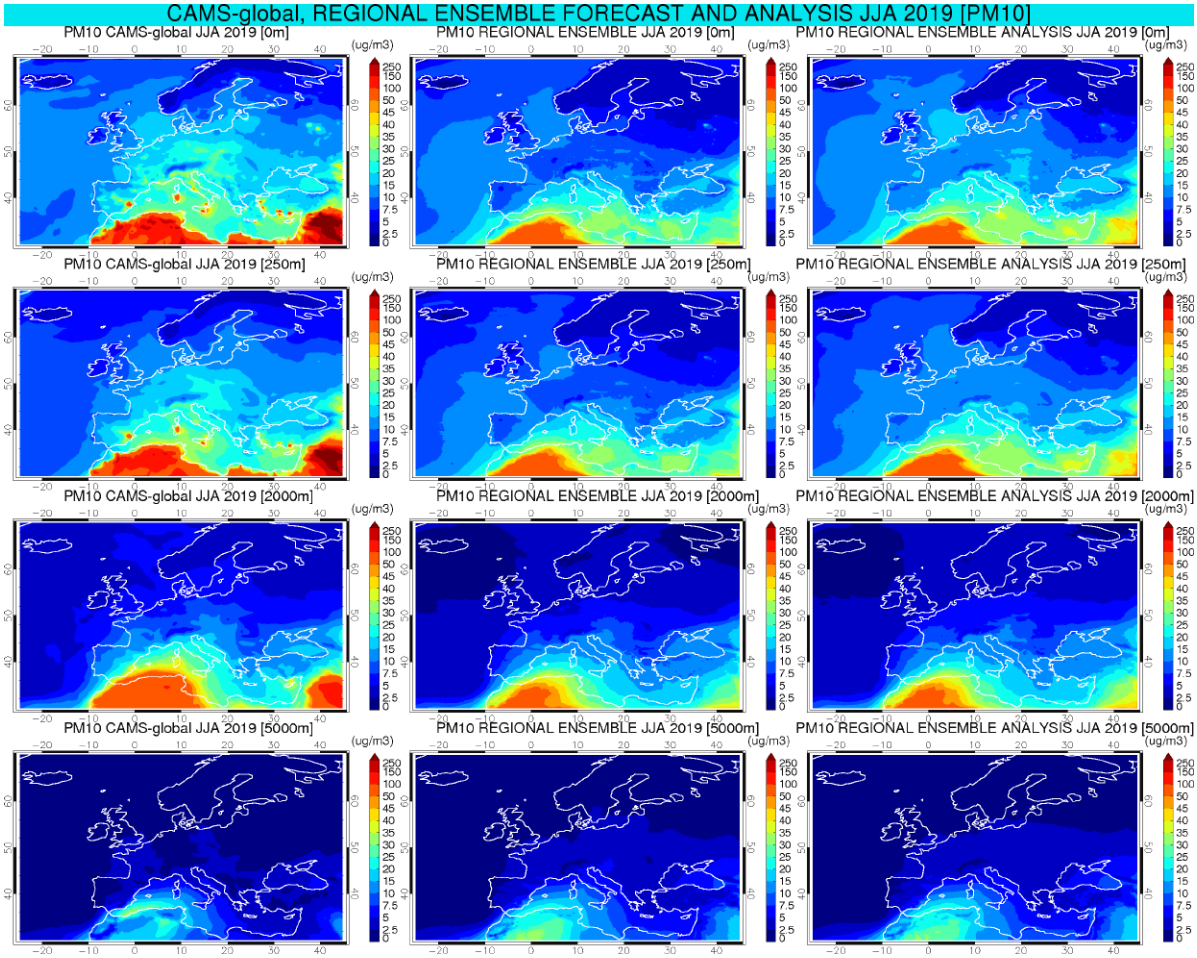

Figure S.7. CAMS global PM10 forecast for day 1 (left), CAMS regional ensemble PM10 forecast for day 1 (middle), CAMS regional PM10 analysis (right). From top to bottom: 0, 250, 2000, 5000m altitude level. Period: June to August 2019.

Systematic uncertainties in the retrievals (on average on the order of 20% – 30% over polluted regions) depend on the season, with winter values in mid and high latitudes normally associated with larger error margins. Conclusions may differ for comparisons to other satellite NO_2 products (e.g. TEMIS GOME-2, http://www.temis.nl). We note that since the CAMS-global upgrade of 26 June 2018, GOME-2 observations are assimilated by the global system. This is, however, a different retrieval product than what is used in the validation reported here (University of Bremen retrieval).

Comparisons to ground based remote sensing MAX-DOAS retrievals at three different European stations (see Figure S.5) show that regional ENSEMBLE forecasts are closer to the urban station observations than CAMS-global, mainly attributed to the difference in spatial resolution. The performance of simulations for diurnal cycles of tropospheric NO_2 columns depends on the location, but generally shows a good performance for the ENSEMBLE products.

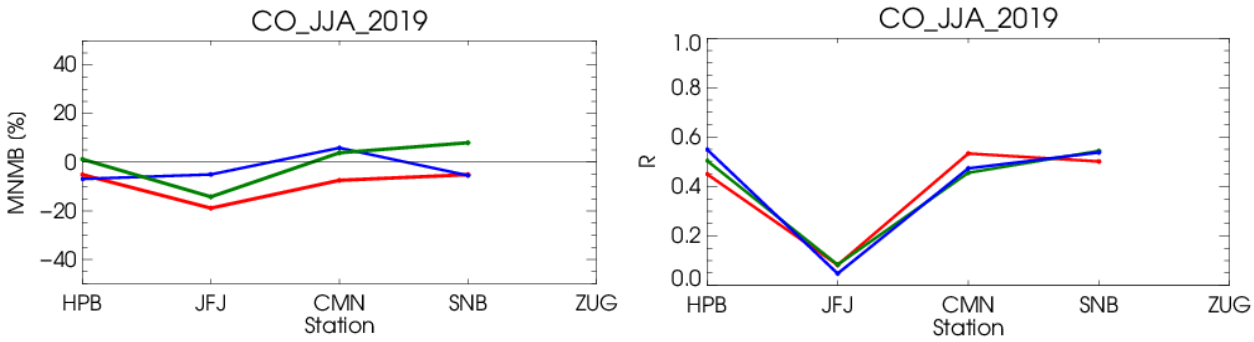

Figure S.8. MNMBs [%] (top) and correlation coefficients (bottom) for CO regional ensemble forecasts (red), analyses (green) and CAMS-global (blue) compared to observations at GAW stations. Period: June - August 2019.

Aerosol / PM

The regional models are compared with EARLINET climatological lidar profiles for the same season (data from 2006-2019), Fig. S.6. Missing information on composition, size and humidity growth of the aerosol in the models introduces considerable uncertainty to the PM derived extinction, which conservatively spans a factor 10 for absolute extinction values. Relative differences among nearby stations and the form of extinction profiles are more certain. The order of magnitude in extinction is similar between the models and the lidar profiles, with Ispra, Italy, close to the Alps, and Athens, Greece, being the most notable exceptions. The decrease in extinction with height seems to be generally steeper in the observations, such that upper level extinction in the models is higher in some locations. Considerable spread exists among the models, especially for Ispra and Athens.

The PM10 concentrations in the regional ENSEMBLE forecasts and analyses are quite similar, but larger PM values are observed for the analysis over Eastern Europe and the North Sea, see Figure S.7. For PM2.5 the difference between the CAMS-global and CAMS-regional is more pronounced than for PM10 within the PBL especially for dust near the southern boundary and over the Middle East (exceeding 50 µg/m^3). Note that on 9 July 2019 there was an upgrade of CAMS-global, which showed higher dust over the Mediterranean compared to the previous version, and a positive bias in PM10 when compared to European surface observations in the western Mediterranean. CAMS-global and CAMS-regional overall compare quite well over mainland Europe this quarter although CAMS-global shows much more structure over land at the surface. The agreement between CAMS-global and the ENSEMBLE products is better for PM10 and PM2.5 in the upper layers compared to the lower layers.

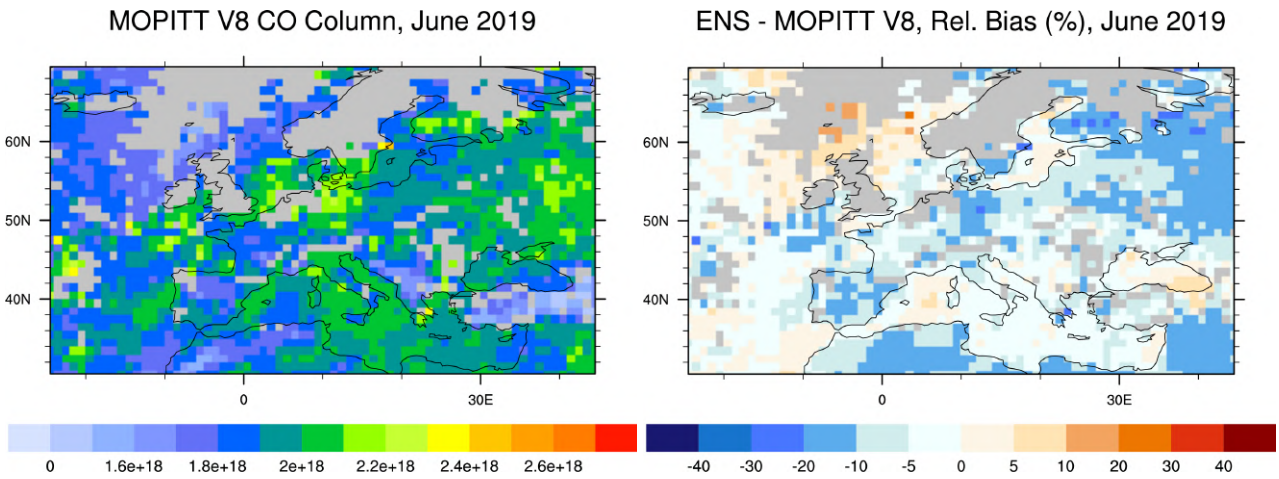

Figure S.9. CO total column for MOPITT v8 satellite retrievals (left, in molecules/cm^2) and relative difference between the regional ensemble forecasts and MOPITT (right) for the first weeks of June 2019. Grey colour indicates missing values.

Carbon monoxide (CO)

Comparison at the GAW stations reveal biases between -18% and 8%, and temporal correlations are between 0.1 and 0.54 (Fig. S.8). The comparison against IAGOS aircraft observations shows that, in the lower layers, CO is mostly underestimated by all models with, in some cases, a better performance from the regional ensemble. In the free troposphere CAMS-global performs well while the regional ensemble underestimates CO.

Comparisons with MOPITT CO satellite observations (version 8, Fig. S.9) shows on average a negative model bias between 0 and -20% for this period. MOPITT averaging kernels peak in the middle troposphere. Taking this into account the findings are consistent with GAW comparisons. Note that the MOPITT observations are assimilated in the CAMS-global system.

Table of Contents

1 Introduction

The Copernicus Atmosphere Monitoring Service (CAMS, https://atmosphere.copernicus.eu) is a component of the European Earth Observation programme Copernicus. The CAMS near-real time services consist of daily analysis and forecasts with the IFS system with data assimilation of trace gas concentrations and aerosol properties. The global modelling system is also used to provide the boundary conditions for an ensemble of more detailed regional air quality models that are used to zoom in on the European domain and produce 4-day forecasts of air quality. The regional forecasting service provides daily 4-days forecasts of the main air quality species and analyses of the day before, based on the results from 7 state-of-the-art atmospheric chemistry models. The ensemble represents the median of the 7 model forecasts.

Routine validation of the regional models against surface observations from the European member states (EEA Air Quality e-reporting) is provided for each model individually as well as the ensemble in separate quarterly validation reports. Validation reports of the CAMS regional products are available in the following portal:
https://atmosphere.copernicus.eu/regional-air-quality-production-systems.
This web page provides access to the quarterly reports on the daily analyses and forecast activities and verification of the regional ensemble. An overview of the regional air quality forecasting system is provided by Marécal et al (2015).

Validation reports (e.g. Wagner et al., 2019) for the CAMS global products are available at
https://atmosphere.copernicus.eu/node/325,
including the evaluation on Earth's troposphere, stratosphere, aerosols and greenhouse gases, with state-of-the art observational datasets (GAW, IAGOS, MOPPIT, EMEP, GOME-2, OMPS-LP, BASCOE, AERONET etc.). A published overview on the validation of reactive gases and aerosols in the global analysis and forecast system can be found in Eskes et al (2015). A validation study of the global surface ozone reanalysis for Europe is provided by Katragkou et al (2015).

Details of the various observational datasets can be found in Eskes et al. (2018), "Observations characterisation and validation methods document", also available at:
https://atmosphere.copernicus.eu/sites/default/files/2018-12/CAMS84_2015SC3_D84.8.1.1-2018_observations_v3.pdf.

This document presents an evaluation of the concentrations above the surface as modelled by the set of 7 regional models and the ensemble forecasts derived from these individual forecasts and analyses, and the consistency between the global and regional modelling systems of CAMS.

2 Regional and global CAMS forecasting systems

2.1 Regional models

The European Air Quality products are provided from the Copernicus Atmosphere Monitoring Service (http://atmosphere.copernicus.eu/). These data are available in NetCDF or Grib-Edition2 format. The files are available each day through ftp protocol from the Météo-France server (ftp.cnrm-game-meteo.fr). The products are available in Near Real Time (NRT) for four forecast days, following the protocol below:

- Each day 96h model forecasts and 24h analyses for the previous day are provided with hourly resolution. Consistent provision of the analysis product started on the 5th of July 2017.
- Products are available at eight vertical height levels: surface, 50, 250, 500, 1000, 2000, 3000, 5000 meters.
- The pollutants are O_3, CO, NO_2, SO_2, PM2.5, PM10, NO, NH_3, birch, grass, olive, ragweed and pollen. Since the upgrade of June 12th 2019, dust aerosols (fraction below 10µm) and secondary inorganic aerosols (SIA, fraction below 2.5 µm) are also available.
- The regional datasets cover the longitudes 335.05°E to 44.95°E every 0.1°, and latitudes 69.95°N – 30.05°N also at 0.1° resolution (~10km). Since June 12th, 2019, the northern boundary of the domain extends to 71.95°N.
- The forecasts until the 48th hour are available before 7:30 UTC
- The forecasts 49-96th hour are available before 9:30 UTC
- The analyses are provided before 12:00 UTC
- Since the June 2019 upgrade, the regional models make use of the updated CAMS-REG-AP_v2_2_1 emissions.

The NRT forecast and analysis regional air quality data are available for the seven air quality models and their ensemble mean (CAMS-regional):

- MOCAGE model (MFM)
- LOTOS-EUROS model (KNM)
- EMEP MSC-W model (EMP)
- MATCH model (SMH)
- EURAD-IM model (RIU)
- CHIMERE model (CHI)
- SILAM model (FMI)

Every evening, a full download of the 96h forecasts and 24h analyses fields to KNMI at full resolution is performed. These fields are co-located to the set of surface stations used, and this largely reduced datasets is shared with all validation partners.

Documentation about the 7 regional models may be found at the address https://atmosphere.copernicus.eu/regional-air-quality-production-systems. For the purposes of this report however, it's useful to indicate what kinds of observations are actively assimilated in each model (Table 2.1).

Table 2.1: Surface and other observations that are actively assimilated in regional models.

Model	Method	Surface	Other
CHIMERE	Kriging	O_3, NO_2, PM10, PM2.5	
EMEP	Intermittent 3D-var	O_3, SO_2, NO_2, PM10, PM2.5	OMI NO_2
EURAD	Intermittent 3D-var	O_3, SO_2, NO_2, PM10, PM2.5	OMI and MetOp/GOME-2 NO_2 and SO_2, MOPITT and IASI CO
LOTOS-EUROS	Ensemble Kalman filter	O_3, NO_2, PM10, PM2.5	OMI NO_2
MATCH	Intermittent 3D-var	O_3, NO_2, CO, PM10, PM2.5	
MOCAGE	3D-var	O_3, NO_2, PM10	
SILAM	Intermittent 3D-var	O_3, NO_2, CO, PM10, PM2.5	

Validation reports of the CAMS regional products are available in the following portal: https://atmosphere.copernicus.eu/regional-services.

Whenever possible, in this report, models follow the naming and colour scheme of Table 2.2.

Table 2.2: Naming and colour scheme followed throughout this report. In the near future the ensemble of 7 models will be extended with two new models, DEHM and GEM-AQ, which have already been included in the table below.

Model	*Short model name*	*Colour name*	*Colour*
CAMS-global	CAMSg	Blue	
ENSEMBLE forecast	ENS-fc	Red	
ENSEMBLE analysis	ENS-an	Green	
CHIMERE	CHIM	Yellow	
EMEP	EMEP	Brown	
EURAD	EURAD	Cyan	
LOTOS-EUROS	LOTOS	Purple	
MATCH	MATCH	Grey	
MOCAGE	MOCA	Pink	
SILAM	SILAM	Orange	
DEHM	DEHM	Fuchsia	
GEM-AQ	GEMAQ	Light Green	

2.2 Global CAMS system based on the ECMWF IFS model

The CAMS-global operational assimilation/forecast system consists of the IFS-CB05 chemistry combined with the MACC aerosol model. The chemistry is described in Flemming et al. (2015); aerosol is described by the bulk aerosol scheme (Morcrette et al., 2009). Dissemination of CAMS-global forecasts is twice a day, at about 10:00 and 22:00UTC. The forecast length is 120 h. Users can get access at https://atmosphere.copernicus.eu/catalogue#. Table 2.3 provides information on the satellite data used in CAMS-global.

Table 2.3: Satellite retrievals of reactive gases and aerosol optical depth that are actively assimilated in CAMS-global.

Instrument	Satellite	Provider	Version	Type	Status
MLS	AURA	NASA	V4	O_3 Profiles	20130107 -
OMI	AURA	NASA	V883	O_3 Total column	20090901 -
GOME-2A	Metop-A	Eumetsat	GDP 4.8	O_3 Total column	20131007 - 20181231
GOME-2B	Metop-B	Eumetsat	GDP 4.8	O_3 Total column	20140512 -
SBUV-2	NOAA-19	NOAA	V8	O_3 21 layer profiles	20121007 -
OMPS	Suomi-NPP	NOAA / EUMETSAT		O_3 Profiles	20170124 - 20190409
IASI	MetOp-A	LATMOS/ULB EUMETSAT	-	CO Total column	20090901 - 20180621 20180622 -
IASI	MetOp-B	LATMOS/ULB EUMETSAT	-	CO Total column	20140918 - 20180621 20180622 -
MOPITT	TERRA	NCAR	V5-TIR V7-TIR V7-TIR Lance V8-TIR Lance	CO Total column	20130129 - 20160124 - 20180626 20180626 20190702
OMI	AURA	KNMI	DOMINO V2.0	NO_2 Tropospheric column	20120705 -
OMI	AURA	NASA	v003	SO_2 Tropospheric column	20120705 - 20150901
GOME-2A/2B	METOP A/B	Eumetsat	GDP 4.8	SO_2 Tropospheric column	20150902-
MODIS	AQUA / TERRA	NASA	Col. 6 Deep Blue	Aerosol total optical depth, fire radiative power	20090901 - 20150902 -
PMAp	METOP-A METOP-B	EUMETSAT		AOD	20170124 - 20170926 -
GOME-2A/2B	METOP A/B	Eumetsat	GDP 4.8	NO_2 Tropospheric column	20180624-

The most recent upgrade relevant to this report took place on 9 July 2019 and involves a change from 60 to 137 vertical levels. A detailed changelog and the corresponding validation reports for this last upgrade can be found on the following page: https://atmosphere.copernicus.eu/node/472.

Upgrade and version information is available here: https://atmosphere.copernicus.eu/changes-cams-global-production-system.

Documentation on the global system can be found here: https://atmosphere.copernicus.eu/global-production-system.

2.3 Methodology for the comparisons of CAMS-global and CAMS-regional

Operational download

The daily regional CAMS forecasts are retrieved on a daily basis. This includes the 3-hourly (0,3,6,9 etc.) regional forecast data (ensemble members and regional ensemble) for all provided species at all vertical layers for the 5 forecast days extracted from the Météo-France ftp server, and the 3-hourly (0, 3, 6, 9 etc.) global forecast data for 5 forecast days extracted from the ECMWF CAMS ftp server.

Methodology of global-regional comparison

The following methodology is used to a) convert CAMS-global species from mass mixing ratio (kg/kg) to concentration (µg/m^3) and, b) extract CAMS-global species concentrations from the vertical levels that lie closest to the regional height levels.

The following parameters are used from the CAMS-global model: hybrid layer coefficients; temperature, surface pressure; "GEMS" ozone; carbon monoxide; "aermr01" to "aermr11" (aerosol species, kg/kg). Data from the first 28 vertical layers (from the surface) are used.

The thickness of each vertical layer Δz (m) is calculated:

$$\Delta z_k = \frac{R * T_k}{M_{air} * g} * \ln\left(\frac{p_{i_{k+1}}}{p_{i_k}}\right) \qquad (E.1)$$

where R=8.314 J/mol·K the gas constant, T the temperature at vertical layer midpoint, M_{air}=28.97·10^{-3} kg/mol the molecular weight of air and g=9.8 m/s^2 the gravity acceleration.

The mass-mixing ratio (kg/kg) for ozone (go3) and carbon monoxide (CO) is initially provided. Conversion from mass mixing ratio (kg/kg) to concentration (µg/m^3) is performed using the following approach:

$$\rho_{O3} = mmr_{O3} * \left(\frac{p_m * M_{air}}{R * T}\right) \qquad (E.2)$$

where ρ_{O3} is the ozone concentration (kg/m^3) and mmr_{O3} the ozone mass mixing ratio (kg/kg). The expression inside the parentheses in E.2 corresponds to the air concentration (kg/m^3). The same approach is also used for the CO unit conversion from kg/kg to µg/m^3.

The mass mixing ratio for all aermr01 to aermr11 species (see Table 2.4) is initially provided. The PM10 and PM2P5 species are both produced and converted to μg/m^3 as follows:

$$\rho_{PM10} = \left[\frac{aermr01 + aermr02}{4.3} + aermr04 + aermr05 + 0.4 * aermr06 + aermr07 + aemr08 + aerm09 + aermr10 + aermr11\right] * \left(\frac{p_m}{R_{spec} * T}\right) \quad (E.3)$$

$$\rho_{PM2P5} = \left[\frac{aermr01 + 0.5 * aermr02}{4.3} + aermr04 + aermr05 + 0.7 * (aermr07 + aemr08 + aerm11) + aermr09 + aermr10\right] * \left(\frac{p_m}{R_{spec} * T}\right) \quad (E.4)$$

where R_{spec}=287.058 J/(kg·K) is the specific gas constant for dry air. The expression inside the parentheses in E.3 and E.4 corresponds to the dry air concentration (kg/m^3).

Since the IFS-cycle46r1 implementation and on the above methodology is applied using data from the first 58 vertical layers (from the surface). Moreover, with the addition of three new aerosol species (aermr16 - Nitrate fine mode aerosol; aermr17 – Nitrate coarse mode aerosol; aermr18 – Ammonium aerosol) the calculation of PM10 and PM2P5 is performed according to the following formulas:

$$\rho_{PM10} = \left[\frac{aermr01}{4.3} + \frac{aermr02}{4.3} + aermr04 + aermr05 + 0.4 * aermr06 + aermr07 + aemr08 + aermr11 + aerm09 + aermr10 + aermr16 + aemr17 + aermr18\right] * \left(\frac{p_m}{R_{spec} * T}\right) \quad (E.5)$$

$$\rho_{PM2P5} = \left[\frac{aermr01}{4.3} + \frac{aermr02 * 0.5}{4.3} + aermr04 + aermr05 + 0.7 * aermr07 + 0.7 * aemr08 + 0.7 * aermr11 + aermr09 + aermr10 + 0.7 * aermr16 + 0.25 * aermr17 + 0.7 * aermr18\right] * \left(\frac{p_m}{R_{spec} * T}\right) \quad (E.6)$$

Regional model products are provided at the height levels of 0, 50, 250, 500, 1000, 2000, 3000 and 5000m. For every grid point and time step of the CAMS-global model, the differences between the height of each vertical layer midpoint z_m and the regional model height (e.g. 5000m) is calculated. The layer midpoint that exhibits the minimum height difference is the one that lies closest to the regional height level and is therefore selected for extraction of both chemical and aerosol species concentrations. The above procedure is performed for every regional height level. The final global product contains the O_3, CO, PM10 and PM2.5 concentrations in eight height levels that correspond to the CAMS-global vertical levels that lie closest to the regional height levels.

Table 2.4: Aerosol species description.

Label		Name	Size (µm)
aermr01	SS1	Sea Salt Aerosol	0.03-0.5
aermr02	SS2	Sea Salt Aerosol	0.5-5
aermr03	SS3	Sea Salt Aerosol	5-20
aermr04	DD1	Dust Aerosol	0.03-0.55
aermr05	DD2	Dust Aerosol	0.55-0.9
aermr06	DD3	Dust Aerosol	0.9-20
aermr07	OM1	Hydrophobic Organic Matter Aerosol	
aermr08	OM2	Hydrophilic Organic Matter Aerosol	
aermr09	BC1	Hydrophobic Black Carbon Aerosol	
aermr10	BC2	Hydrophilic Black Carbon Aerosol	
aermr11	SU1	Sulphate Aerosol	

3 Consistency between the global and regional modelling components of CAMS

3.1 Summary

This chapter reports on the consistency between the global and regional modelling components of CAMS, and the impact of global CAMS boundary conditions on regional forecasts. The current evaluation includes ozone (O_3) carbon monoxide (CO) and aerosol (PM10/PM2.5) forecasts covering the period from June to August 2019.

Global and regional ensemble forecasts: The two forecast products compare well, with some differences in the surface CO (higher in the global forecast) and surface PM10 (higher over the south-eastern boundary in the global forecast).

Regional forecast variability: The regional ensemble members exhibit the expected regional variability for O_3, CO and particulate matter. Minor deviations (compared to CAMS-global and the majority of regional models) are generally noted, with CHIMERE exhibiting some spurious features in the boundary implementations.

Regional forecast and analysis: The comparison of regional analyses and forecasts shows strong model and species dependence. The MOCAGE analysis plots are not included in this report due to data unavailability.

- Ozone: Consistent discrepancies between forecast and analysis in CHIMERE (surface only), and MATCH, LOTOS-EUROS (the whole vertical extent)/
- Carbon monoxide: SILAM (up to 2 Km altitude) and MATCH over the whole vertical extent.
- Particulate matter: Minor discrepancies for LOTOS-EUROS over the southern boundary and MATCH over the south-eastern boundary.

Case study During the last week of July 2019 several Central European have experienced record high temperatures, due to the prevailing heatwave. The CAMS-forecasted implications for near-surface ozone. Noteworthy is the agreement of ozone fields between the CAMS global and regional forecast systems during the heatwave event.

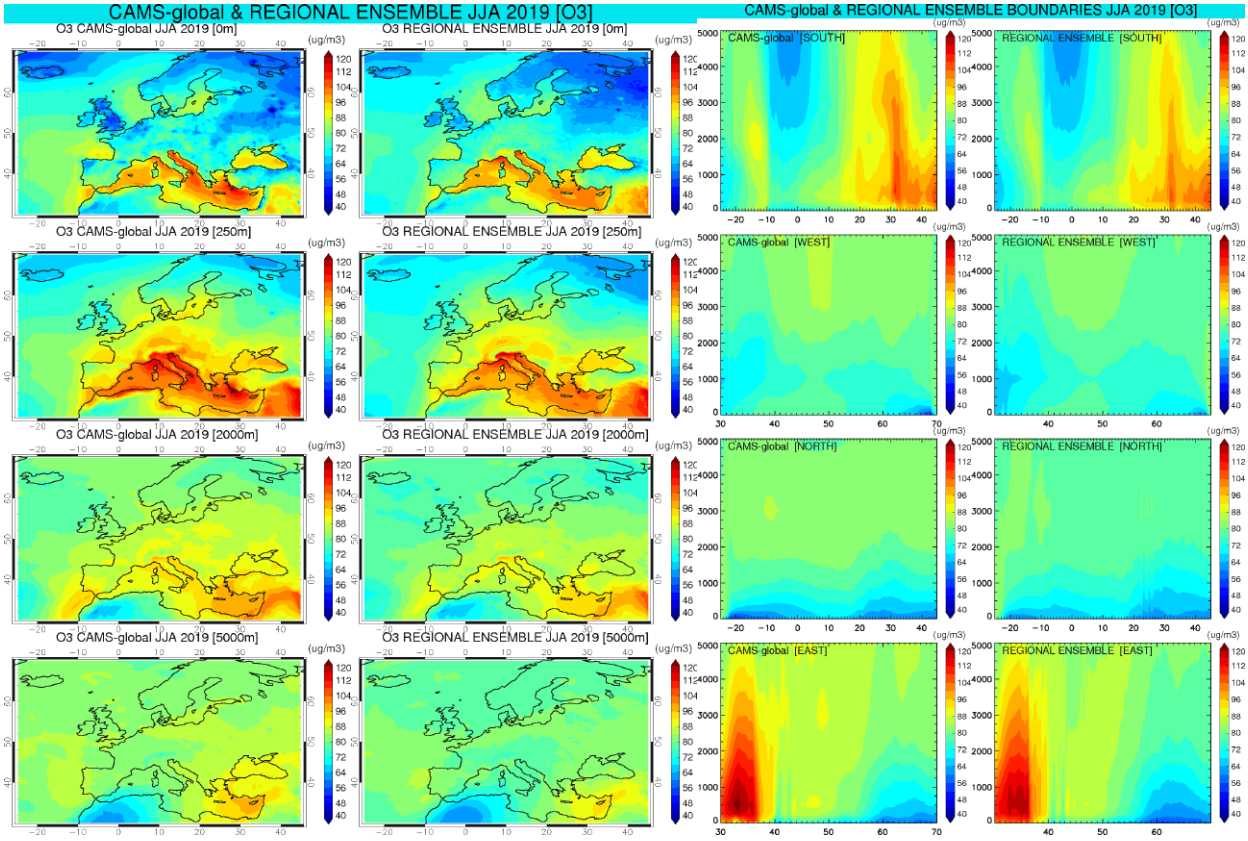

Figure 3.1. Left: Mean global and regional ensemble forecast ozone fields for four different vertical layers (0, 250, 2000, 5000 m) for JJA2019. Right: Cross sections for the same period of the global and regional ensemble ozone boundaries (south, west, north, east).

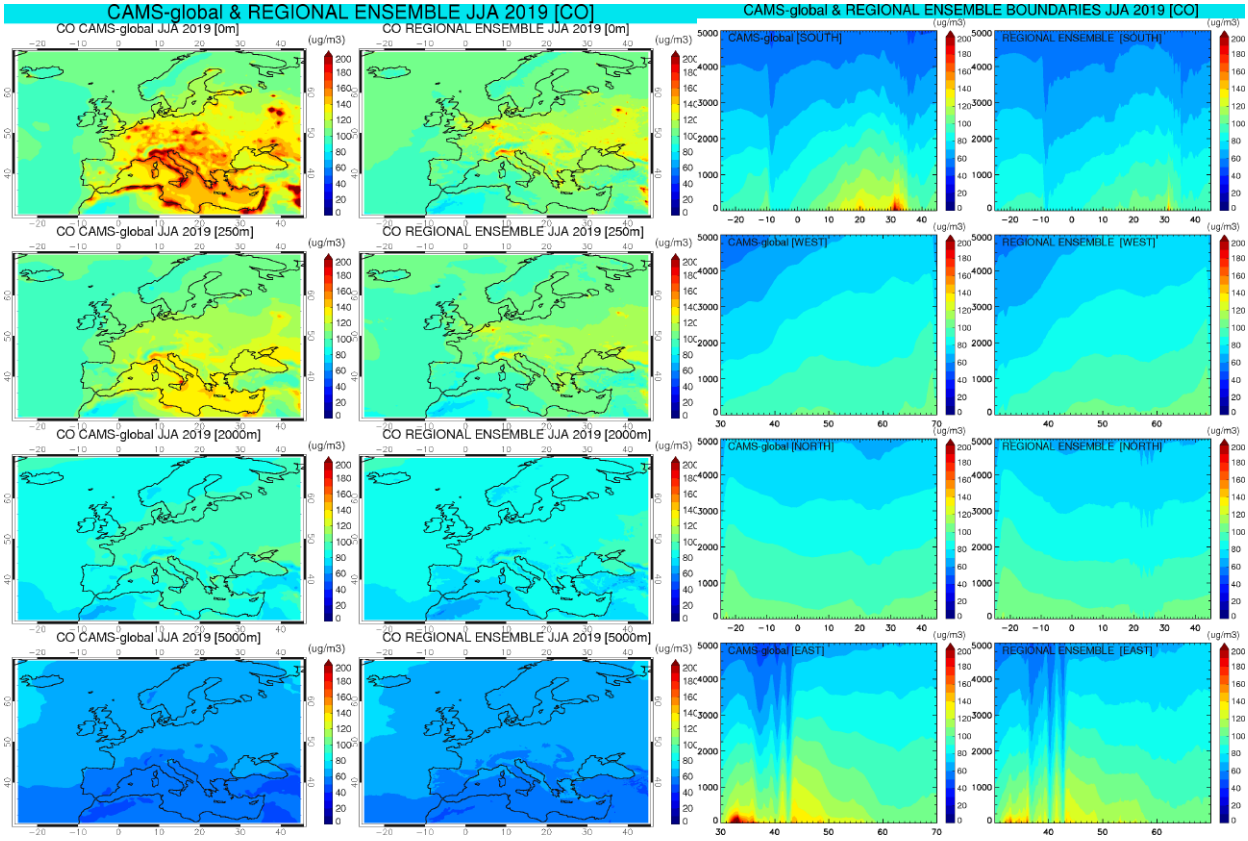

Figure 3.2. Left: Mean global and regional ensemble forecast CO fields for four different vertical layers (0, 250, 2000, 5000 m) for JJA2019. Right: Cross sections for the same period of the global and regional ensemble ozone boundaries (south, west, north, east).

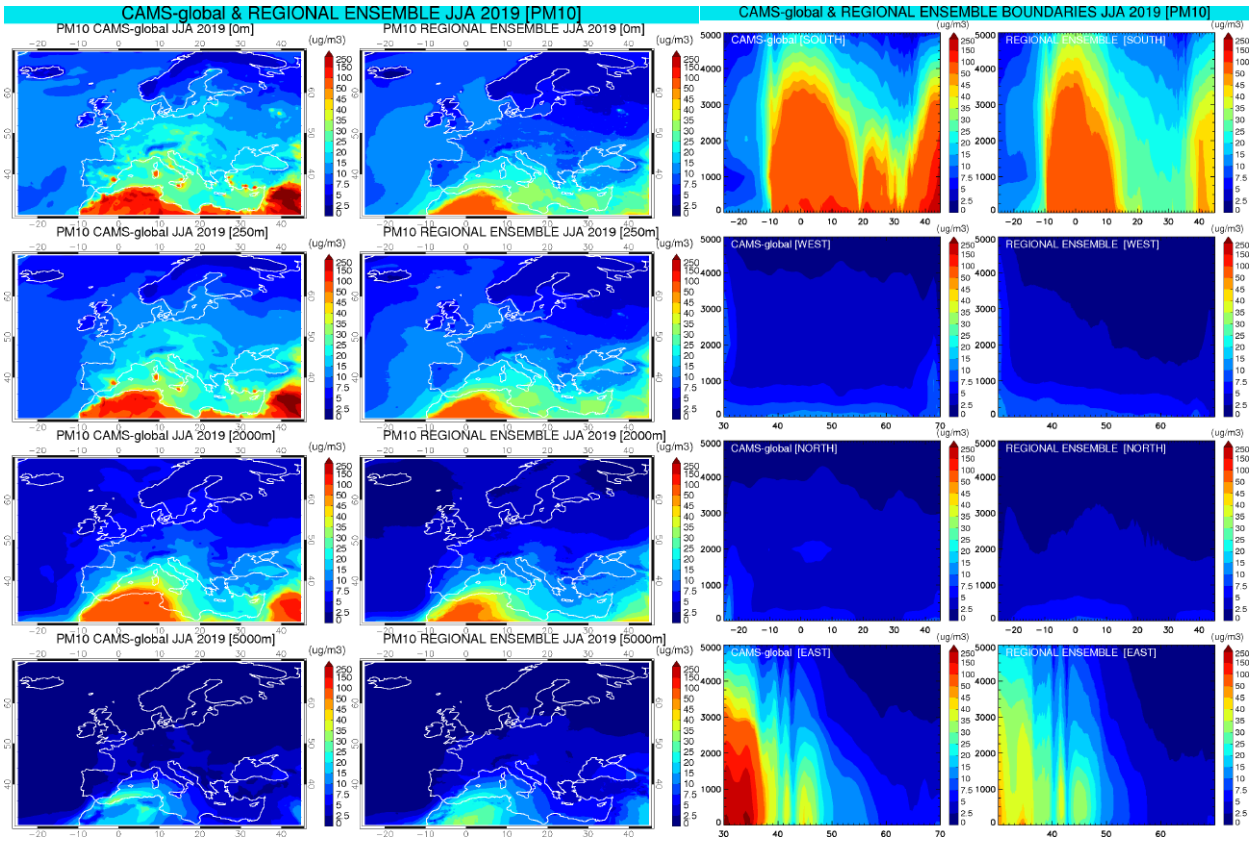

Figure 3.3. Left: Mean global and regional ensemble forecast PM10 fields for four different vertical layers (0, 250, 2000, 5000 m) for JJA2019. Right: Cross sections for the same period of the global and regional ensemble ozone boundaries (south, west, north, east).

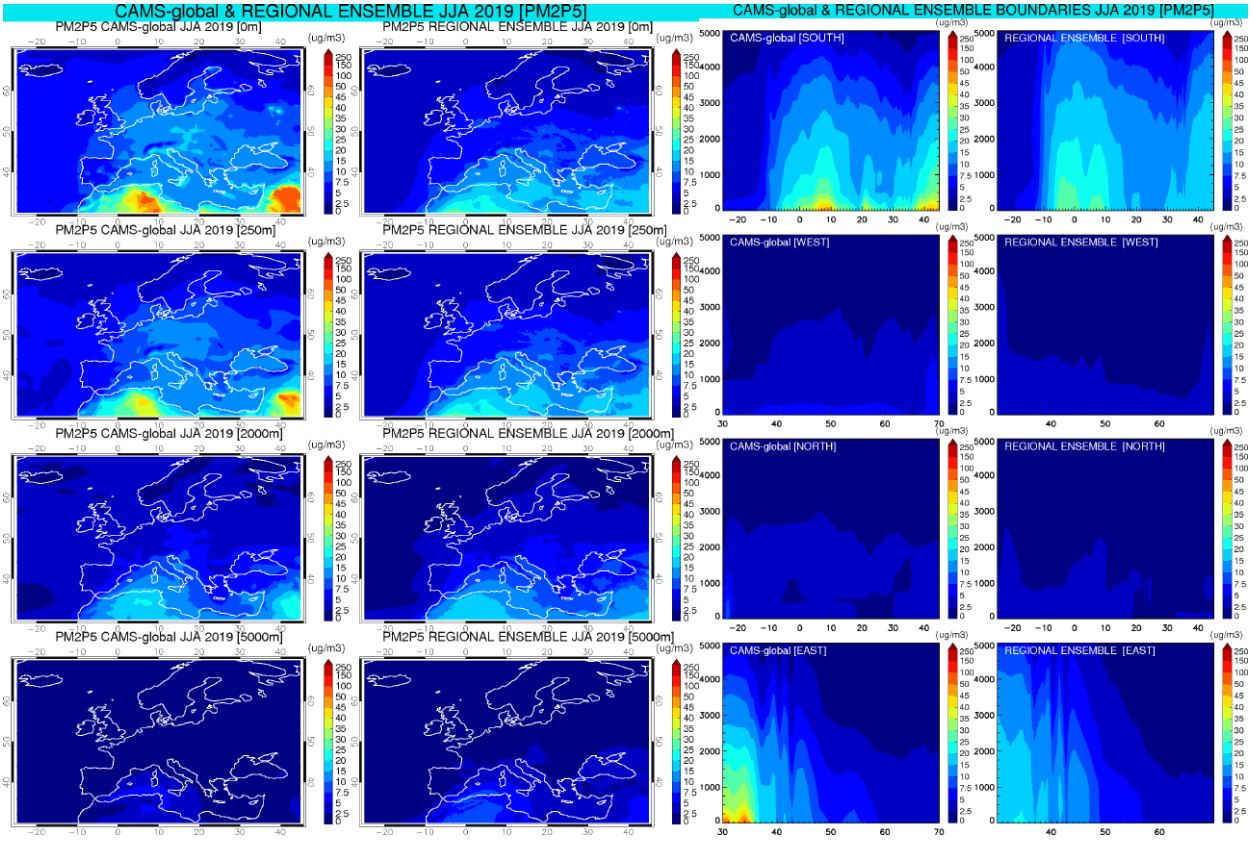

Figure 3.4 Left: Mean global and regional ensemble forecast PM2.5 fields for four different vertical layers (0, 250, 2000, 5000 m) for JJA2019. Right: Cross sections for the same period of the global and regional ensemble ozone boundaries (south, west, north, east).

3.2 Consistency between the global and regional forecasts

This section reports on the consistency of the global and regional ensemble forecast. The analysis is performed for O_3, CO, PM10 and PM2.5 at four levels (0, 250, 2000 and 5000 m) for the time period from June to August 2019.

Ozone (O_3)

Figure 3.1 shows the average JJA2019 spatial distribution of O_3 for different vertical layers (left) and the cross sections of the lateral boundaries (right) for the global forecast CAMS-global and the regional ENSEMBLE. The two products are very similar.

Carbon monoxide (CO)

Figure 3.2 illustrates the seasonal mean fields of CO and the cross sections of lateral boundaries (right) for ENSEMBLE and CAMS-global. Global surface CO is higher than the regional ensemble CO. The agreement becomes better at higher levels.

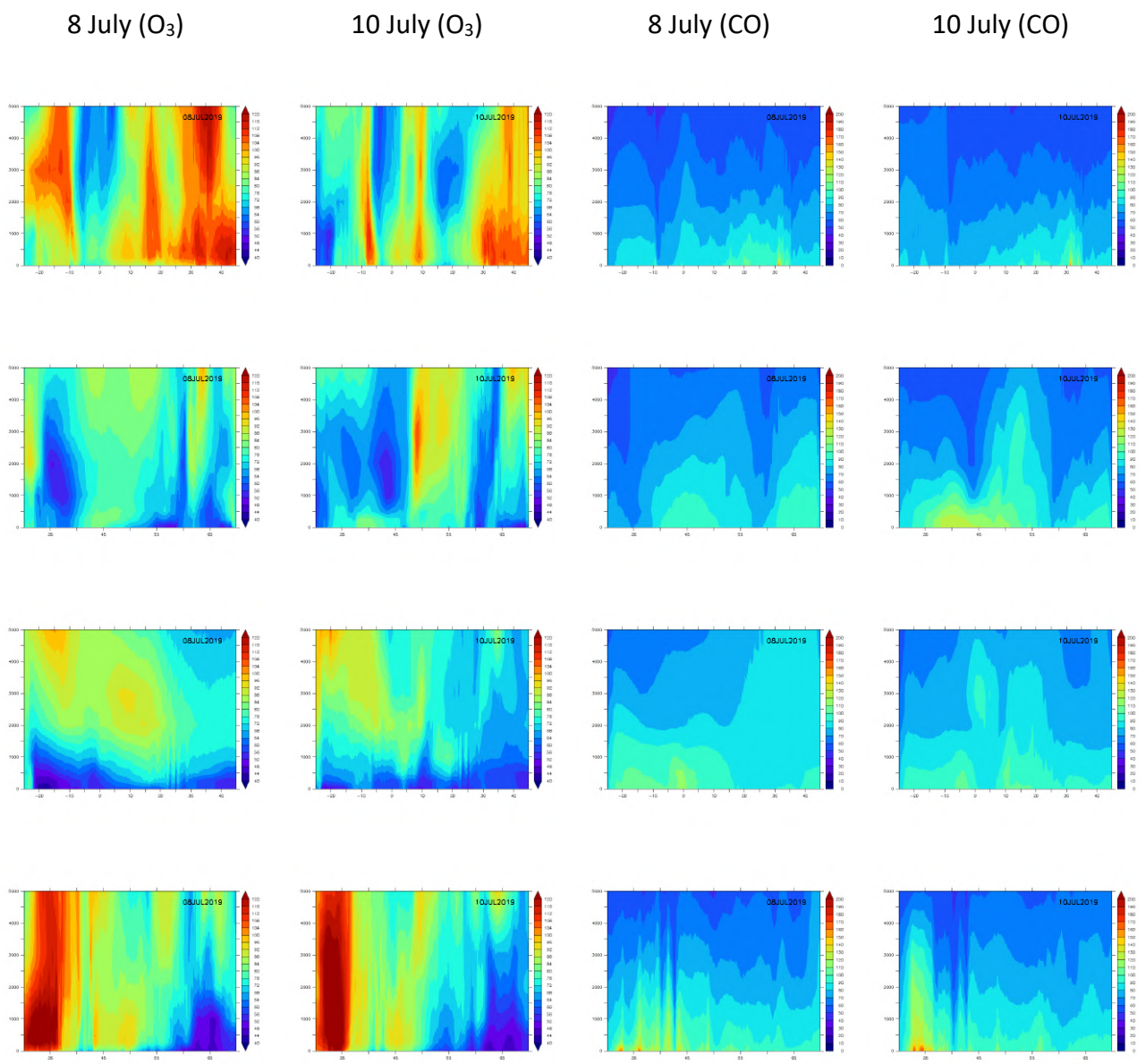

Figure 3.5. Cross sections for the regional ensemble ozone (two left columns) and CO (two right columns) boundaries for the 8th and 10th of July 2019. Rows are southern, western, northern and eastern boundary respectively.

Aerosols (PM10 and PM2.5)

Figures 3.3 and 3.4 illustrate the CAMS-global and ENSEMBLE spatial distributions (left) and lateral boundary cross sections (right) of PM10 and PM2.5 mean fields, respectively. Differences between surface and PBL PM10 and PM2.5 are seen over the south-eastern boundary. The global forecast system has higher and spatially more extended dust concentrations than the regional ensemble below < 2 Km.

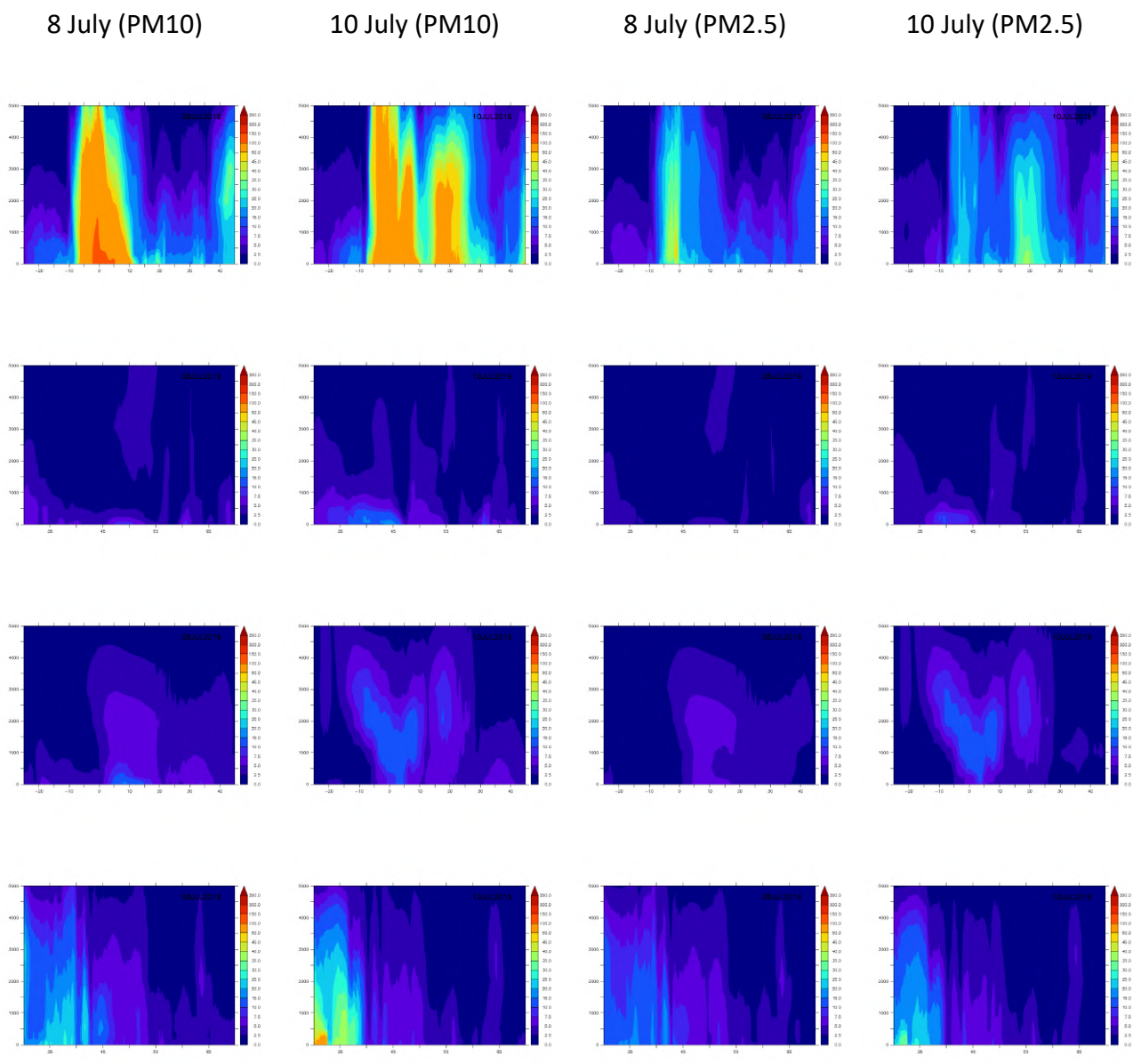

Figure 3.6. Cross sections for the regional ensemble PM10 (two left columns) and PM2.5 (two right columns) boundaries for the 8th and 10th of July 2019. Rows are southern, western, northern and eastern boundary respectively.

Figures 3.5 and 3.6 illustrate the lateral boundary cross sections for O_3, CO, PM10 and PM2.5 for two days before and after the CAMS-global upgrade that happened on the 9th of July. Despite some differences that can be attributed to the meteorological impact on the fields, as far as regional models are concerned, there seems to be an undisturbed transition to the use of the 137 levels of cycle 46R1 of the global system. A notable exception has been the EMEP model, which for the first hours of 9 July exhibited a peculiar western CO boundary (not shown), a feature which slowly disappeared in the days after the upgrade.

3.3 Regional variability

Ozone (O_3)

Figure 3.7 illustrates ozone mean fields for JJA2019 of the individual regional ensemble members and CAMS-global (bottom panel) for selected altitudes (0, 250, 2000, 5000 m). There is good agreement between the forecast products, within reasonable ranges of variability.

Carbon monoxide (CO)

The JJA2019 mean fields of carbon monoxide for the regional ensemble members as well as for CAMS-global are illustrated in Figure 3.8 for different vertical layers. There are generally no discrepancies.

Aerosols (PM10 and PM2.5)

The mean PM10 and PM2.5 fields for JJA2019 are illustrated in Figures 3.9 and 3.10, respectively. The model with the most distinct behavior is MOCAGE with different western and southern PM boundaries compared to other regional ensemble members and the CAMS-global.

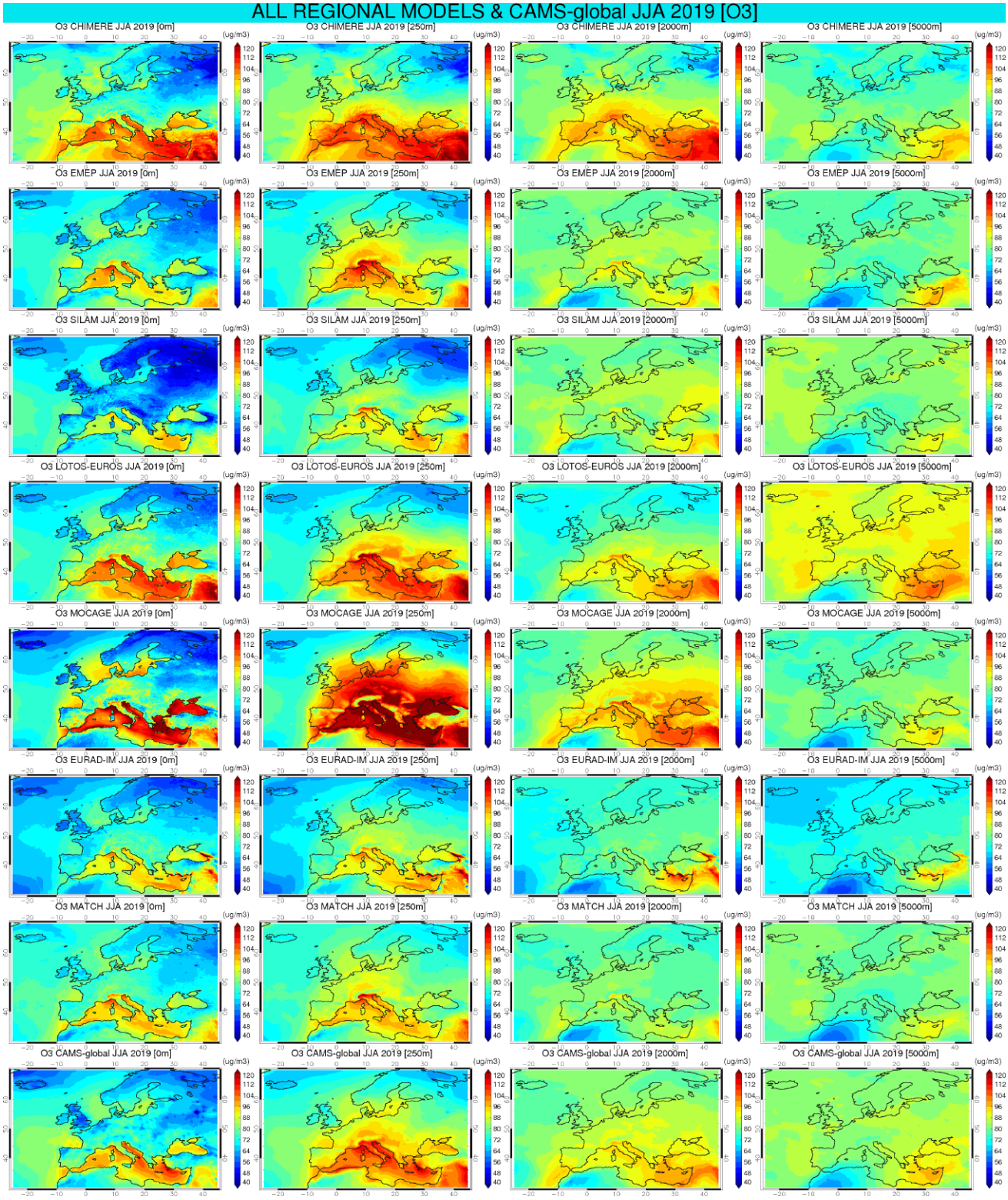

Figure 3.7. Mean regional ozone forecasts for JJA2019 for four different vertical layers (0, 250, 2000, 5000 m) from the seven ensemble members and CAMS-global (top to bottom: CHIMERE, EMEP, SILAM, LOTOS-EUROS, MOCAGE, EURAD-IM, MATCH and CAMS-global).

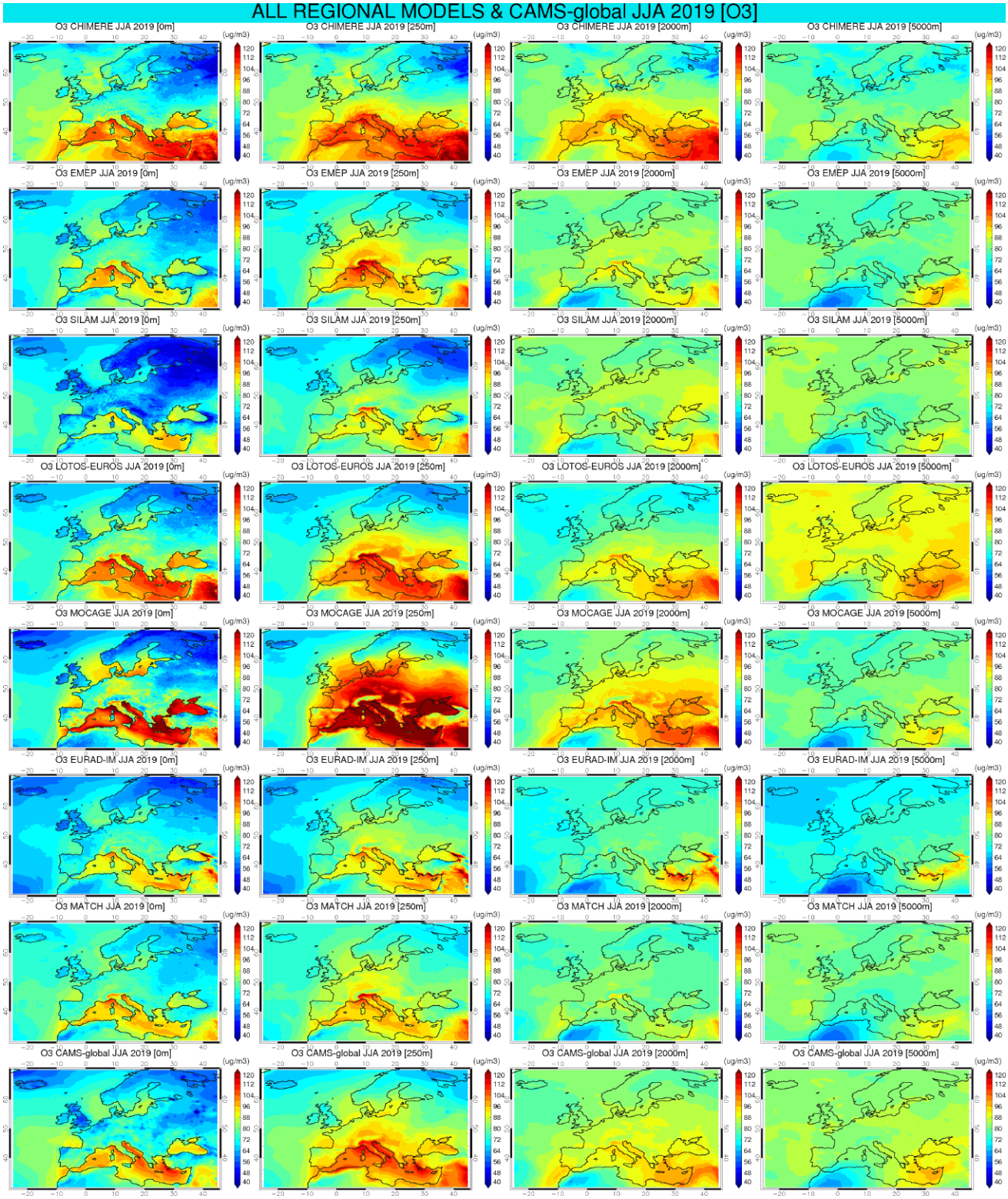

Figure 3.8. Mean regional CO forecasts for JJA2019 for four different vertical layers (0, 250, 2000, 5000 m) from the seven ensemble members and CAMS-global (top to bottom: CHIMERE, EMEP, SILAM, LOTOS-EUROS, MOCAGE, EURAD-IM, MATCH and CAMS-global).

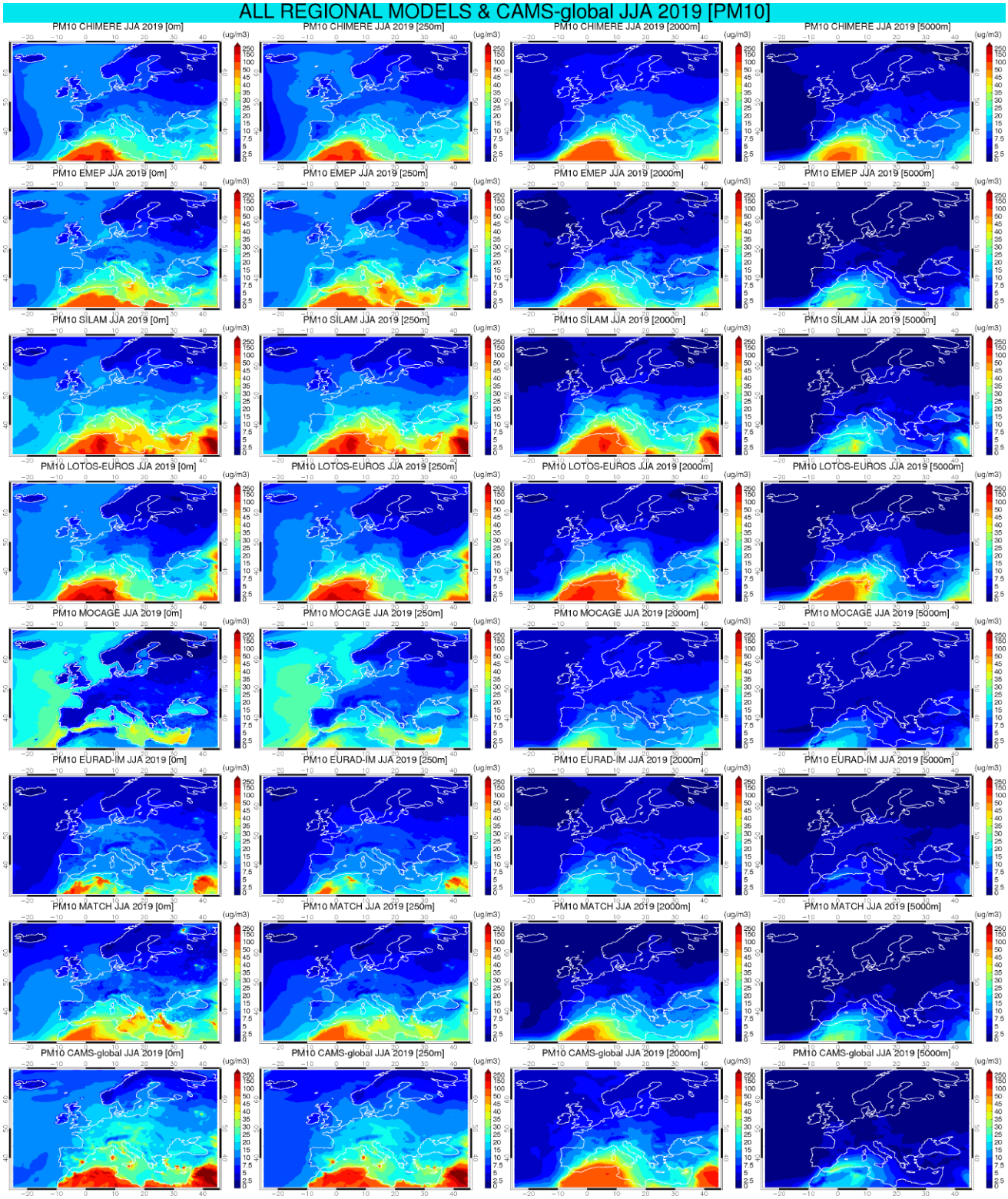

Figure 3.9. Mean regional PM10 forecasts for JJA2019 for four different vertical layers (0, 250, 2000, 5000 m) from the seven ensemble members and CAMS-global (top to bottom: CHIMERE, EMEP, SILAM, LOTOS-EUROS, MOCAGE, EURAD-IM, MATCH and CAMS-global).

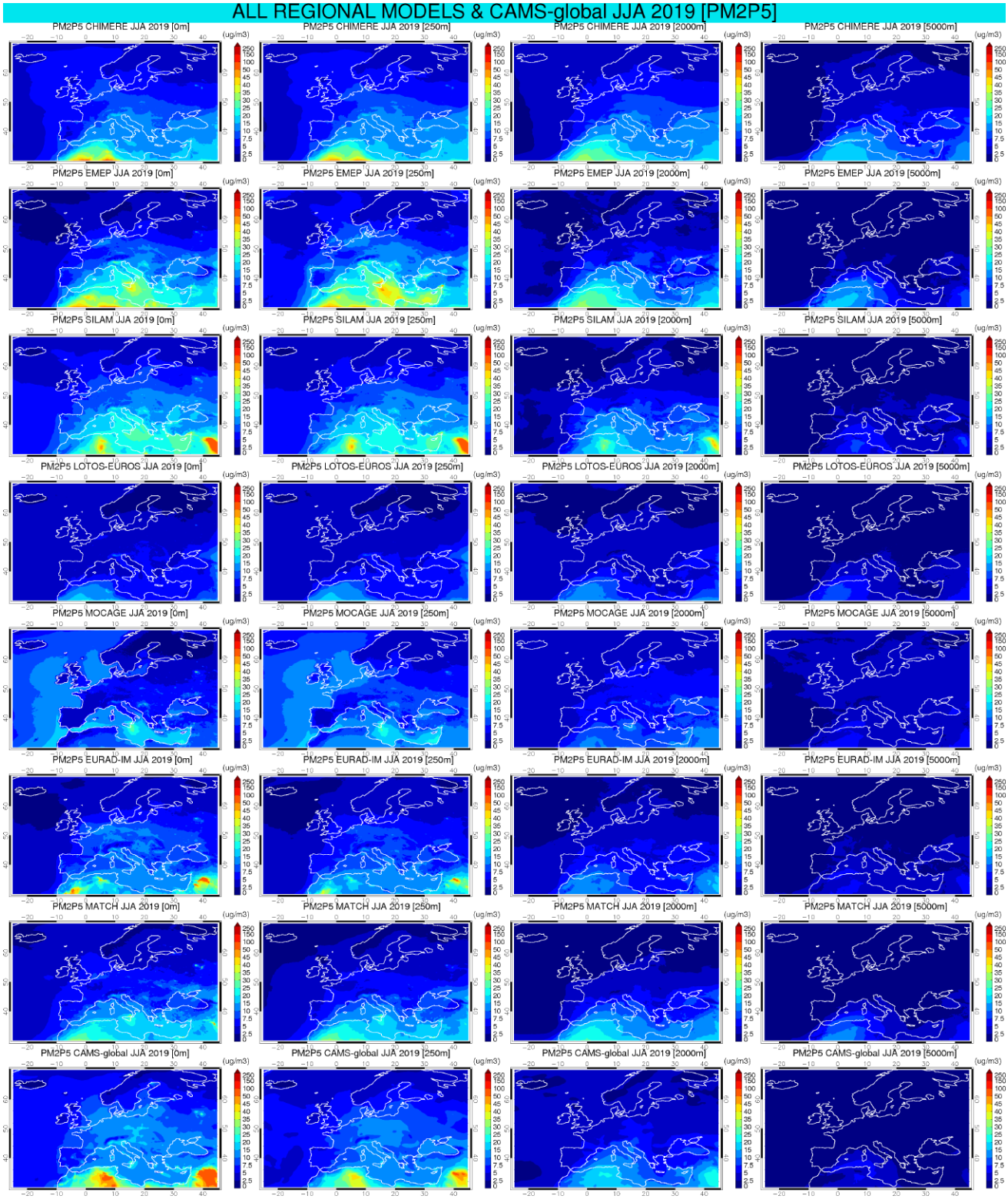

Figure 3.10. Mean regional PM2.5 forecasts for JJA2019 for four different vertical layers (0, 250, 2000, 5000 m) from the seven ensemble members and CAMS-global (top to bottom: CHIMERE, EMEP, SILAM, LOTOS-EUROS, MOCAGE, EURAD-IM, MATCH and CAMS-global).

3.4 Time series

Figure 3.11 shows the mean daily time series from June to August 2019 for the four species, namely O_3, CO, PM10, PM2.5 (from left to right) for different European sub-regions (from top to bottom): Alps (AL), British Isles (BI), East Europe (EA), France (FR), Iberian Peninsula (IP), Mediterranean (MD), Mid-Europe (ME), Scandinavia (SC).

Each subregion is defined with the following latitude/longitude boundaries:

Name = (BI, IP, FR, ME, SC, AL, MD, EA)

West = (-10, -10, -5, 2, 5, 5, 3, 16)

East = (2, 3, 5, 16, 30, 15, 25, 30)

South = (50, 36, 44, 48, 55, 44, 36, 44)

North = (59, 44, 50, 55, 70, 48, 44, 55)

The red colour is used for the regional ensemble forecast and the blue for CAMS-global. The letter R denotes the temporal correlation between the two products. Only concentrations over land are used.

For O_3 the temporal correlation ranges from 0.31 (AL) to 0.94 (SC). The agreement between the regional ensemble and the global forecast is very good.

The global forecast has higher surface CO in comparison to all regional ensemble members, with the exception of the EURAD model, which has higher concentrations during June in most of the European subregions. The temporal correlations range from 0.35 over the Iberian Peninsula and the best over Mid Europe and the British Isles (0.93).

Some regional models capture higher PM10 variability in June and July over central and southern Europe (AL, FR, IP, MD). The global forecast and the regional ensemble are more similar with R ranging from 0.45 (ME) to 0.69 (IP). In better agreement are the PM2.5 products.

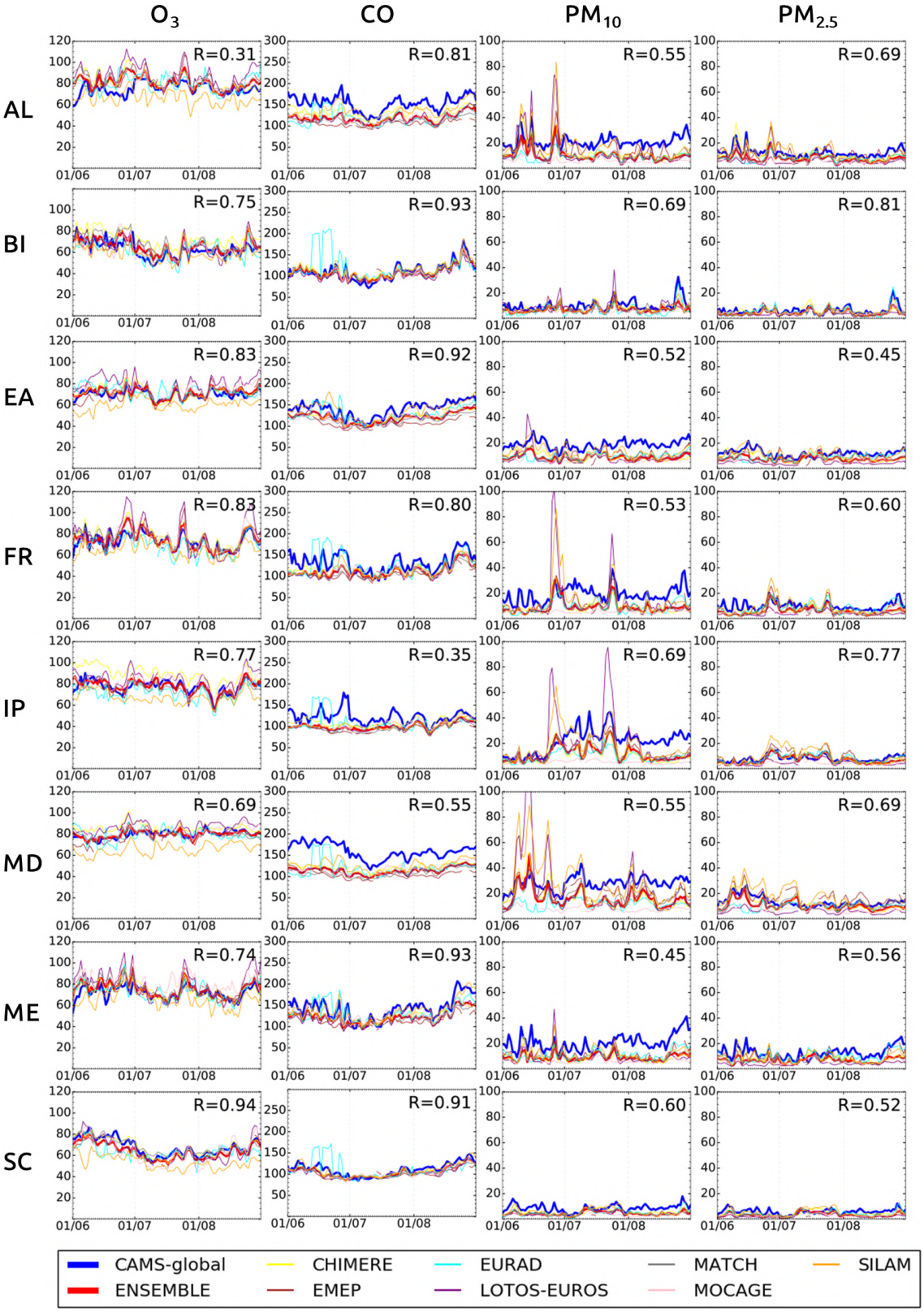

Figure 3.11. Mean daily time series for surface O_3, CO, PM10 and PM2.5 for JJA2019 (unit µg/m^3). The blue line is CAMS-global and the red line the ENSEMBLE forecasts. Each line in the composite plot denotes a different European subregion.

3.5 Diurnal cycles

Figure 3.12 shows the diurnal cycles for surface O_3, CO, PM10 and PM2.5 averaged over the period JJA2019 for different European sub-regions (from top to bottom): Alps (AL), British Isles (BI), East Europe (EA), France (FR), Iberian Peninsula (IP), Mediterranean (MD), Mid-Europe (ME), Scandinavia (SC). The red colour is used for the regional ensemble and the blue for CAMS-global.

There is a good agreement between the O_3 CAMS-global and ENSEMBLE diurnal cycles and the regional ensemble members.

The CO values in CAMS-global are higher during the night-time, minimizing at 15:00 to 16:00 UTC. The majority of the regional models either exhibits a very small diurnal variability or almost none.

The PM10 mass densities are higher in the global forecast with more pronounced diurnal cycles. The agreement is better with PM2.5.

We are noting here, that PM10 is a mix product of aerosol properties with different chemical speciation (dust, sea salt, sulfate, carbon etc.) which may have different diurnal cycles, however, this information is lost in the sum product of PM10.

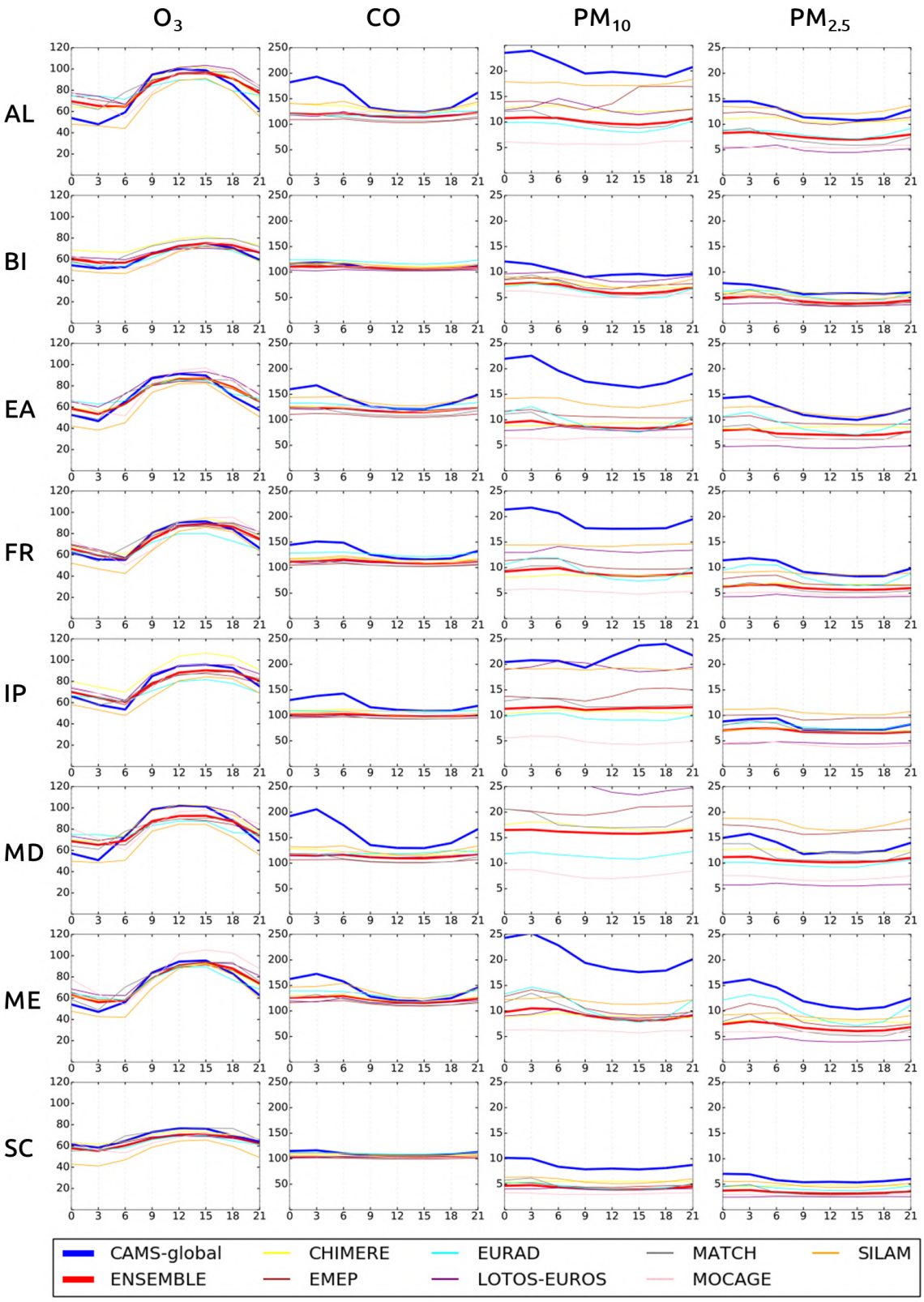

Figure 3.12. Diurnal cycles for surface O_3, CO, PM10 and PM2.5 for the period JJA2019 (unit µg/m^3). The blue line is CAMS-global and the red line the ENSEMBLE forecast. Each line in the composite plot denotes a different European sub-region.

3.6 Regional domain boundary cross sections

Ozone (O_3)

Figure 3.13 shows the regional variability in the lateral domain boundary cross sections of O_3 (from left to right): south, west, north, east and the different ensemble members and CAMS-global (from top to bottom) averaged over the period JJA2019. No major inconsistencies identified, except for CHIMERE, which has higher O3 southern (and east) boundaries, compared to the other regional models (also seen in Fig. 3.7).

Carbon monoxide (CO)

Figure 3.14 shows the regional variability in the lateral cross sections of CO (from left to right): south, west, north, east and the different ensemble members and CAMS-global (from top to bottom) averaged over the period JJA2019. We identify only in CHIMERE an inconsistency in the east/south boundary, which seems to have wrong south-north/east-west direction.

Aerosols (PM10 and PM2.5)

Figure 3.15/3.16 shows the regional variability in the lateral cross sections of PM10/PM2.5 respectively (left to right): south, west, north, east and the different ensemble members and CAMS-global (top to bottom) averaged over the period JJA2019. There is higher variability over the southern boundary in the regional ensemble members.

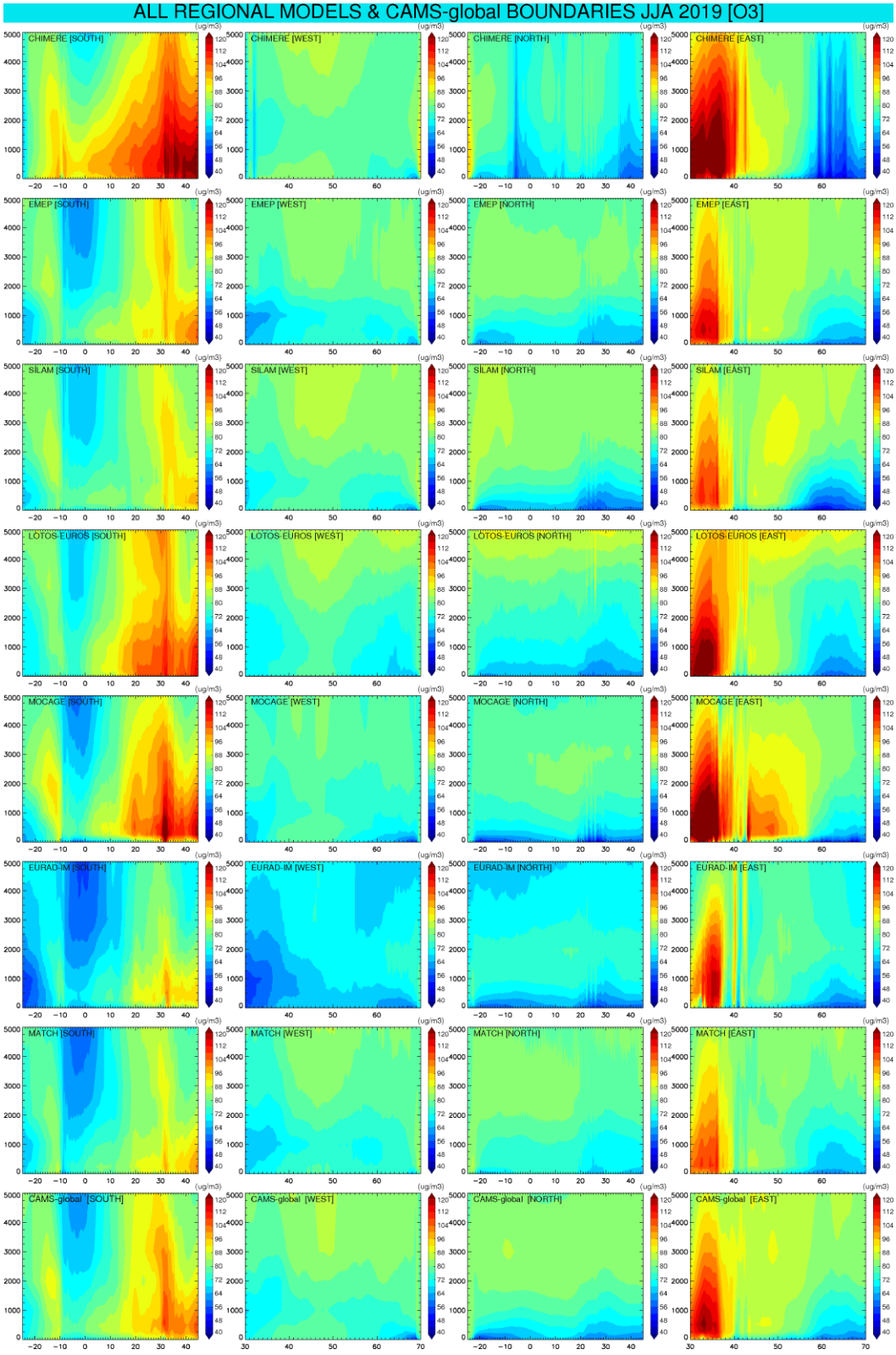

Figure 3.13. Ozone cross sections for JJA2019 for the seven ensemble members and CAMS-global (top to bottom: CHIMERE, EMEP, SILAM, LOTOS-EUROS, MOCAGE, EURAD-IM, MATCH and CAMS-global) and the lateral boundaries (left to right: south, west, north, east).

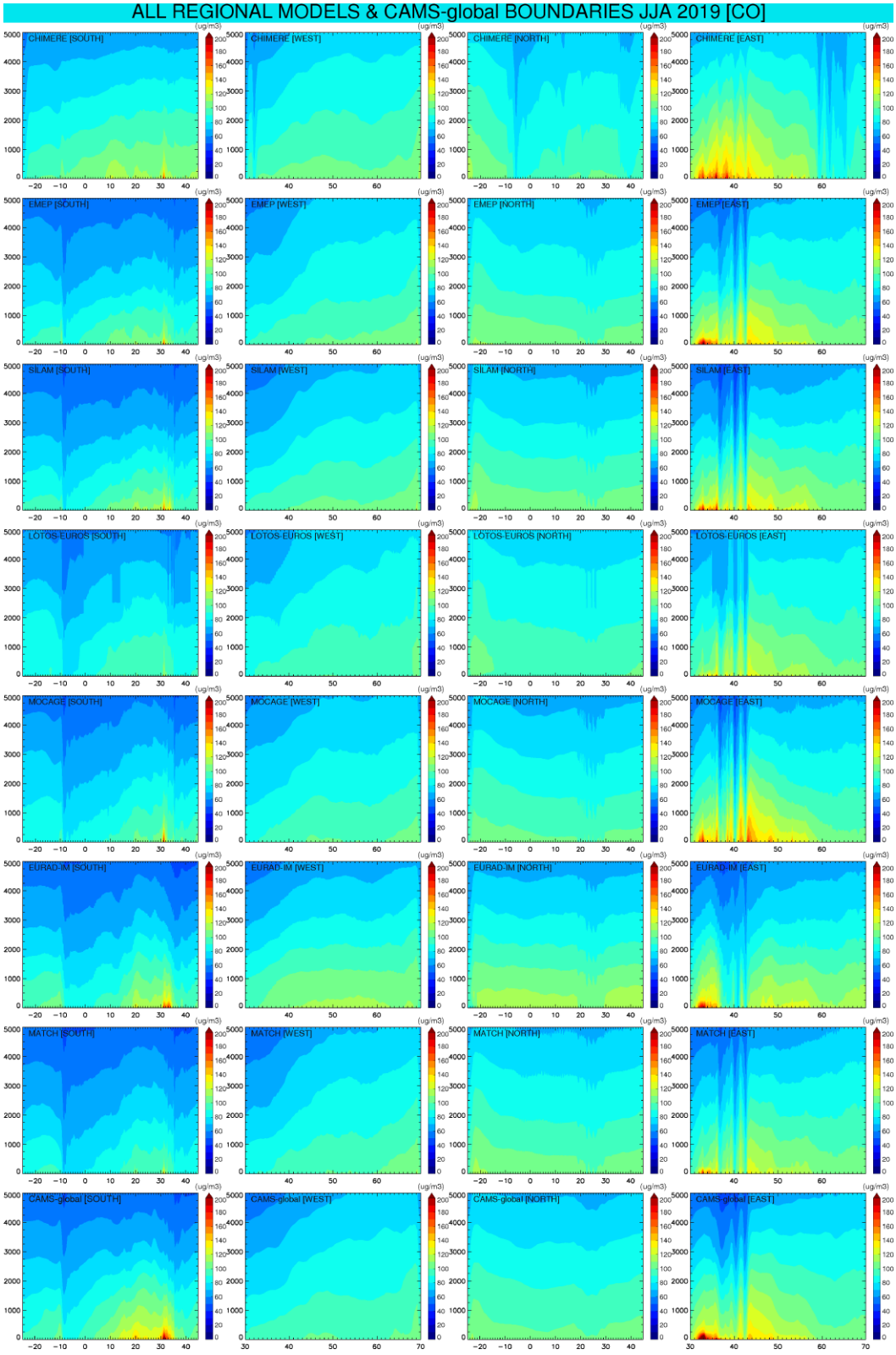

Figure 3.14. Carbon Monoxide cross sections for JJA2019 for the seven ensemble members and CAMS-global (top to bottom: CHIMERE, EMEP, SILAM, LOTOS-EUROS, MOCAGE, EURAD-IM, MATCH and CAMS-global) and the lateral boundaries (left to right: south, west, north, east).

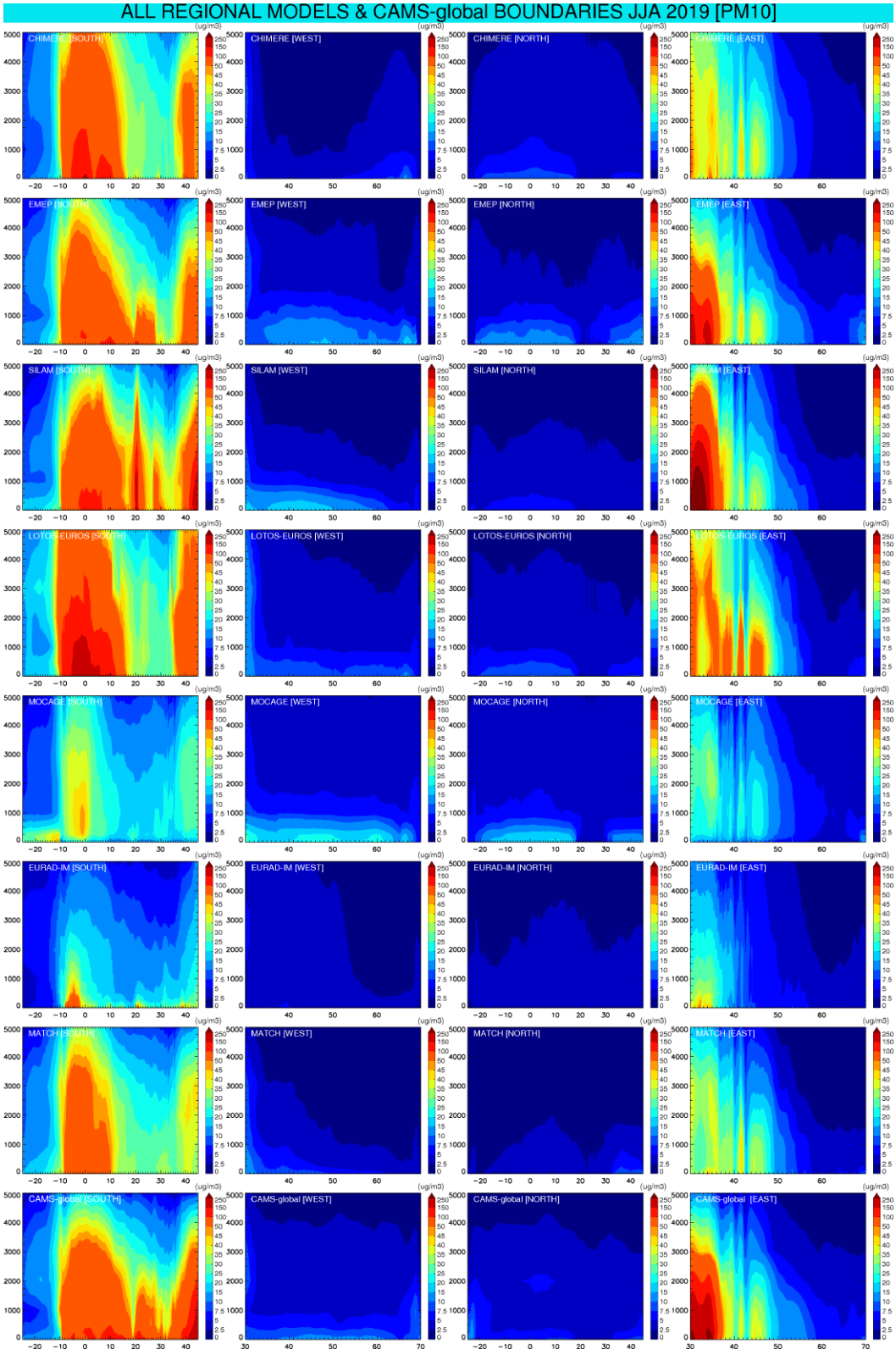

Figure 3.15. Aerosol PM10 cross sections for JJA2019 for the seven ensemble members and CAMS-global (top to bottom: CHIMERE, EMEP, SILAM, LOTOS-EUROS, MOCAGE, EURAD-IM, MATCH and CAMS-global) and the lateral boundaries (left to right: south, west, north, east).

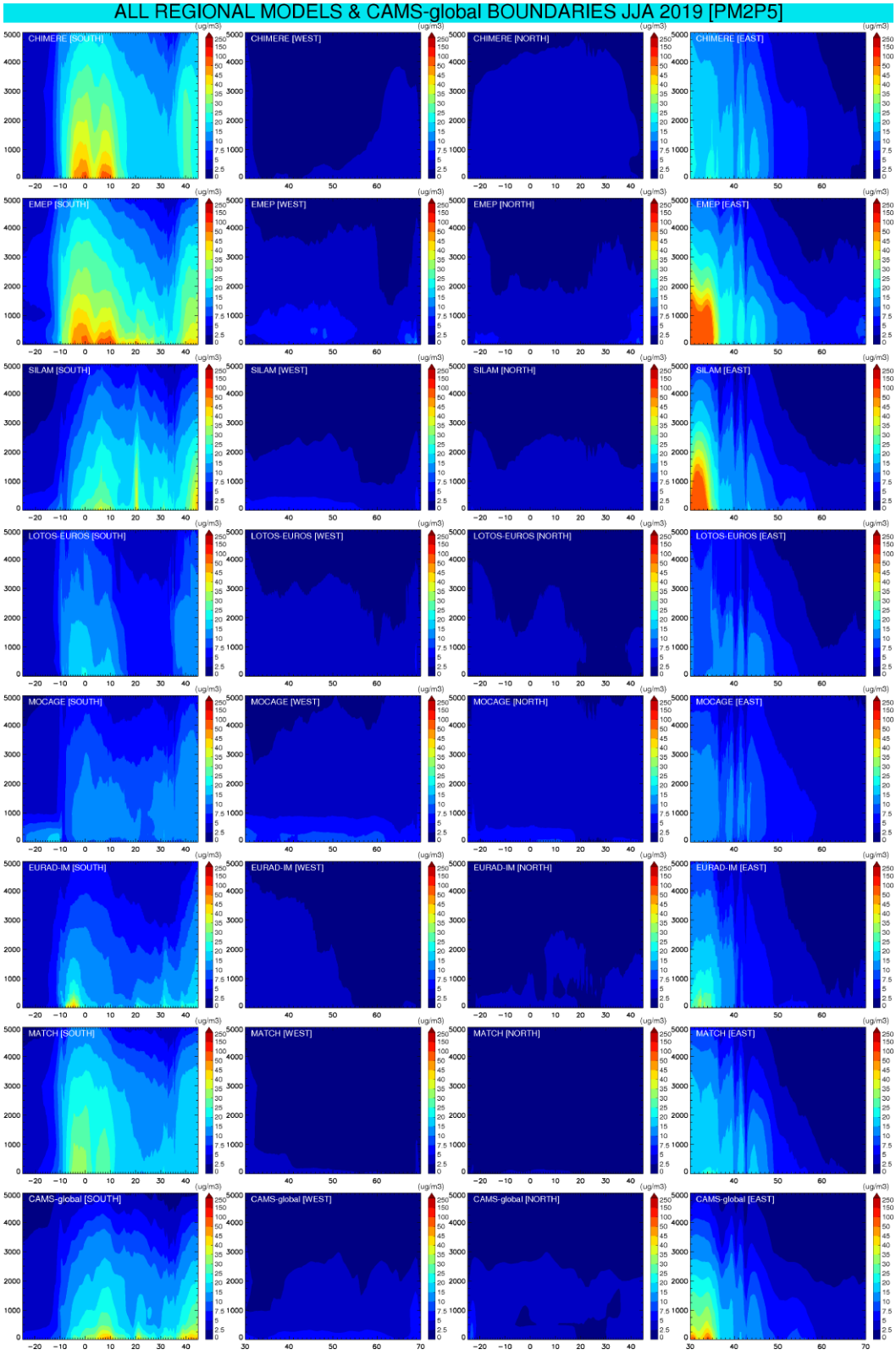

Figure 3.16. Aerosol PM2.5 cross sections for JJA2019 for the seven ensemble members and CAMS-global (top to bottom: CHIMERE, EMEP, SILAM, LOTOS-EUROS, MOCAGE, EURAD-IM, MATCH and CAMS-global) and the lateral boundaries (left to right: south, west, north, east).

3.7 Regional analysis vs. regional forecasts

In the following sections we compare the regional analysis products with the regional forecasts (Day1). The four following figures (3.17-3.20) show the mean regional differences between analysis and forecasts for the time period JJA2019 at four different vertical layers (0, 250, 2000, 5000 m, left to right) including O_3, CO, PM10 and PM2.5, respectively.

Regional models with the largest differences between the analyses and the 1st day forecasts are for:

Ozone

- CHIMERE in the surface layer.
- EMEP and SILAM mostly within the PBL (patchy patterns)
- MATCH over the total vertical extent, mostly pronounced at the top level.

Carbon monoxide

- SILAM up to 2km altitude and MATCH over the total vertical extent. Please note that SILAM and MATCH are the only two models actively assimilating ground CO observations. Some differences are also present in other models but this is probably due to chemistry effects as most models assimilate ozone which may affect CO.

PM10 and PM2.5

- Minor differences in some models, LOTOS-EUROS over the southern boundary and MOCAGE extending to the top layers.

It is important to note that the differences observed between the analysis and forecast do not only reflect the impact of the assimilation but may also result from differences in the model setup between the analysis systems and the forecast systems.

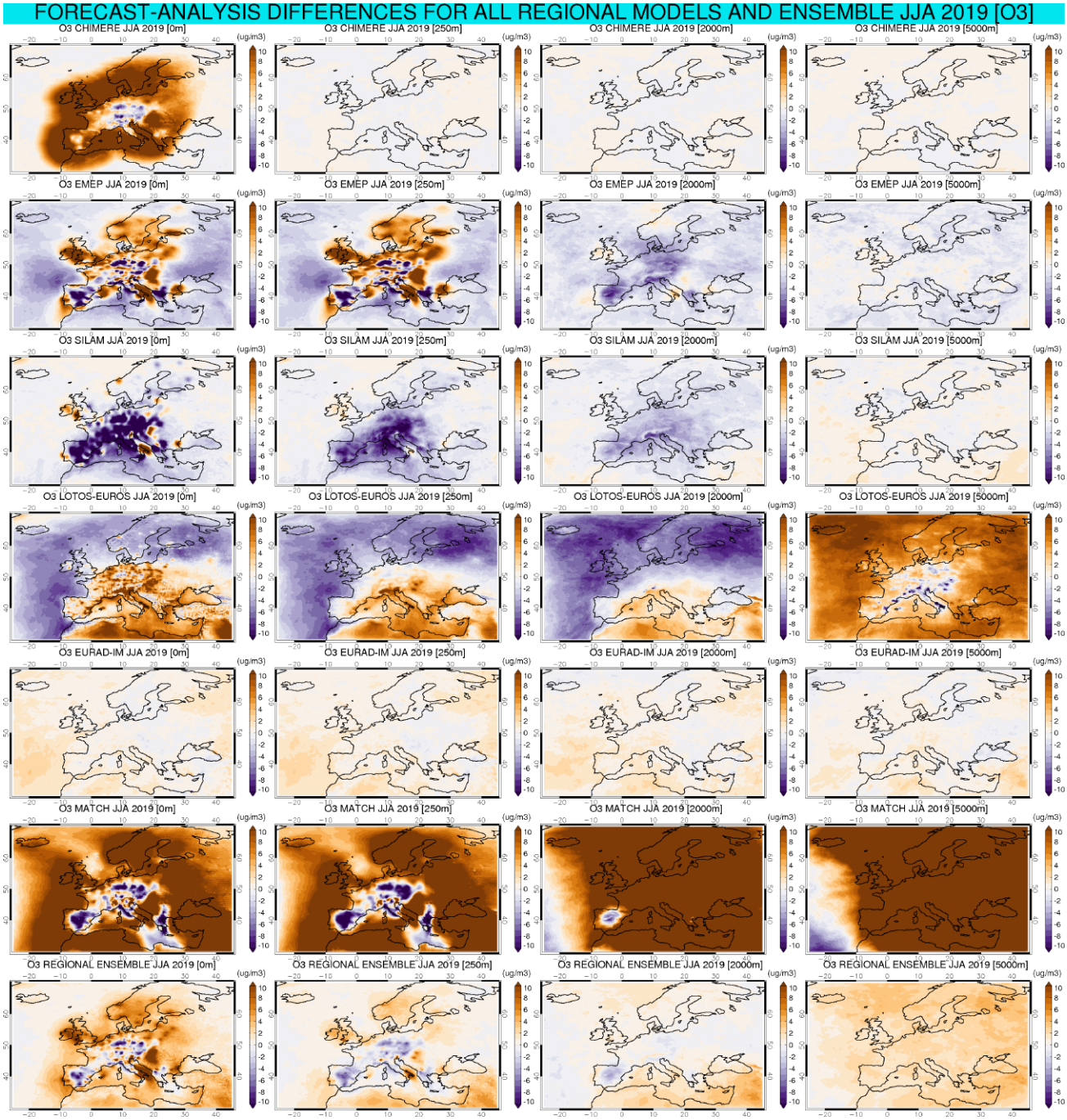

Figure 3.17. Mean regional O_3 differences between analysis and forecast for JJA2019 for four different vertical layers (0, 250, 2000, 5000 m) from regional ensemble and individual ensemble members (top to bottom: CHIMERE, EMEP, SILAM, LOTOS-EUROS, MOCAGE, EURAD-IM, MATCH and ENSEMBLE).

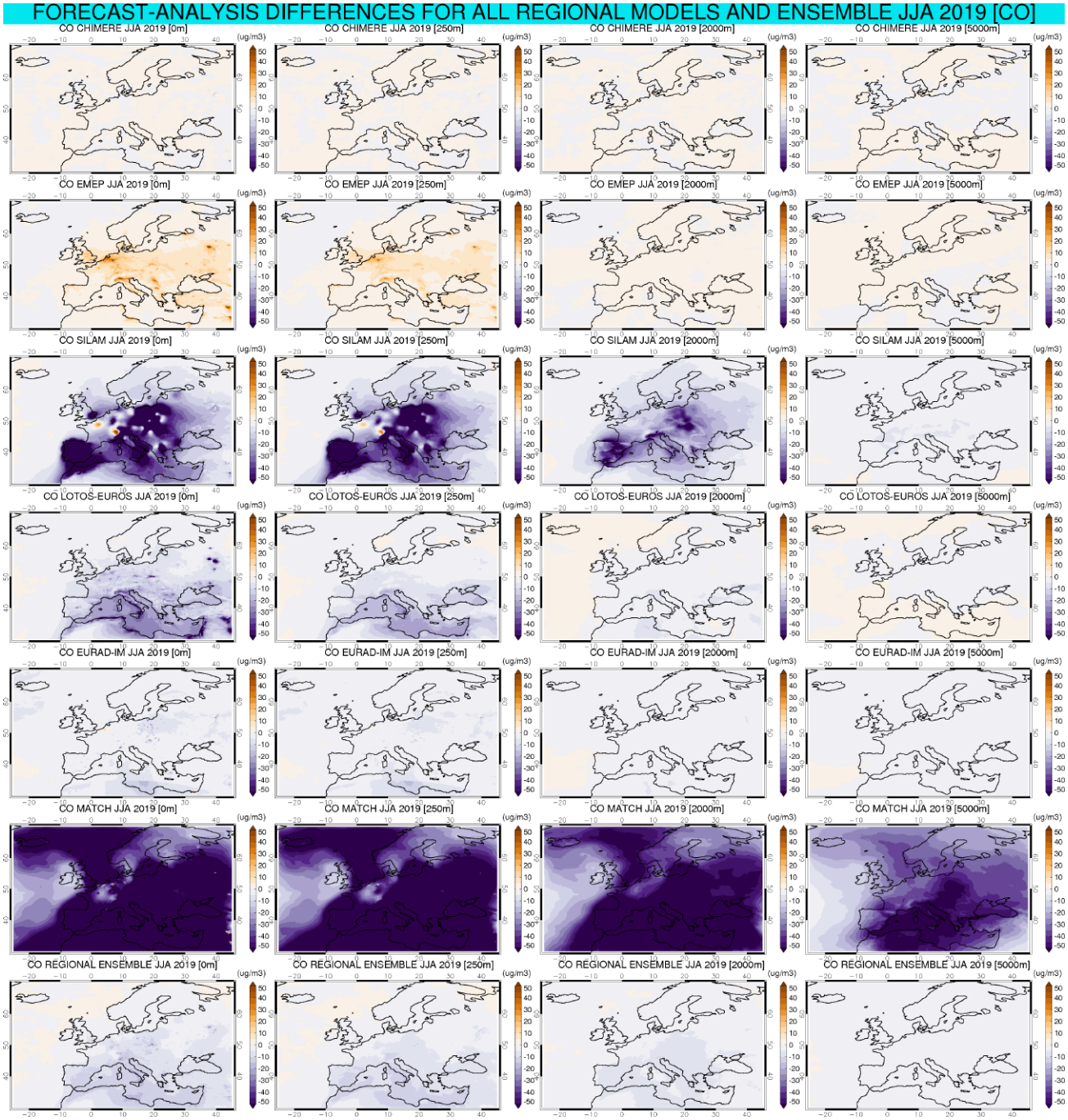

Figure 3.18. Mean regional CO differences between analysis and forecast for JJA2019 for four different vertical layers (0, 250, 2000, 5000 m) from regional ensemble and individual ensemble members (top to bottom: CHIMERE, EMEP, SILAM, LOTOS-EUROS, MOCAGE, EURAD-IM, MATCH and ENSEMBLE).

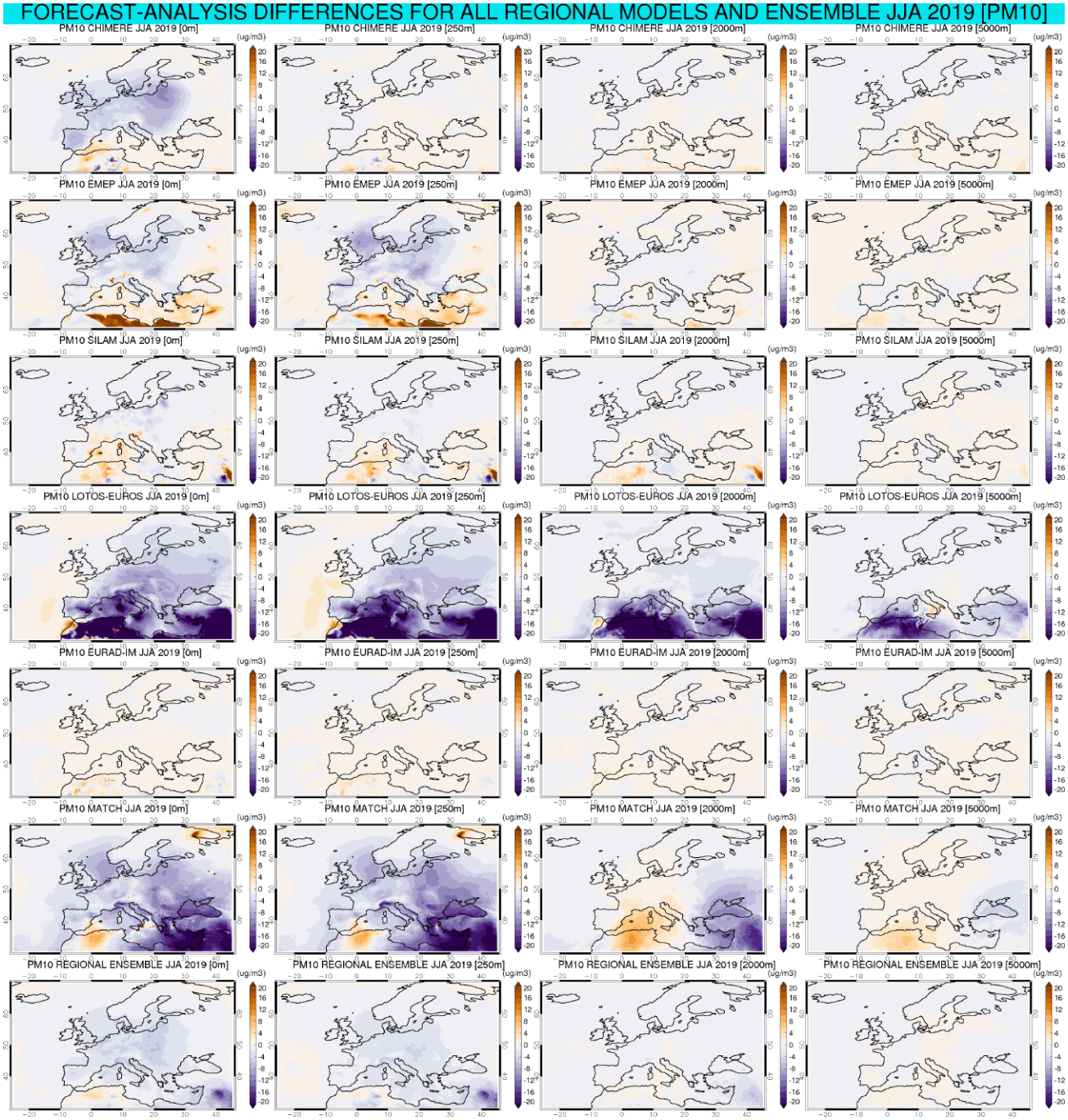

Figure 3.19. Mean regional PM10 differences between analysis and forecast for JJA2019 for four different vertical layers (0, 250, 2000, 5000 m) from regional ensemble and individual ensemble members (top to bottom: CHIMERE, EMEP, SILAM, LOTOS-EUROS, MOCAGE, EURAD-IM, MATCH and ENSEMBLE).

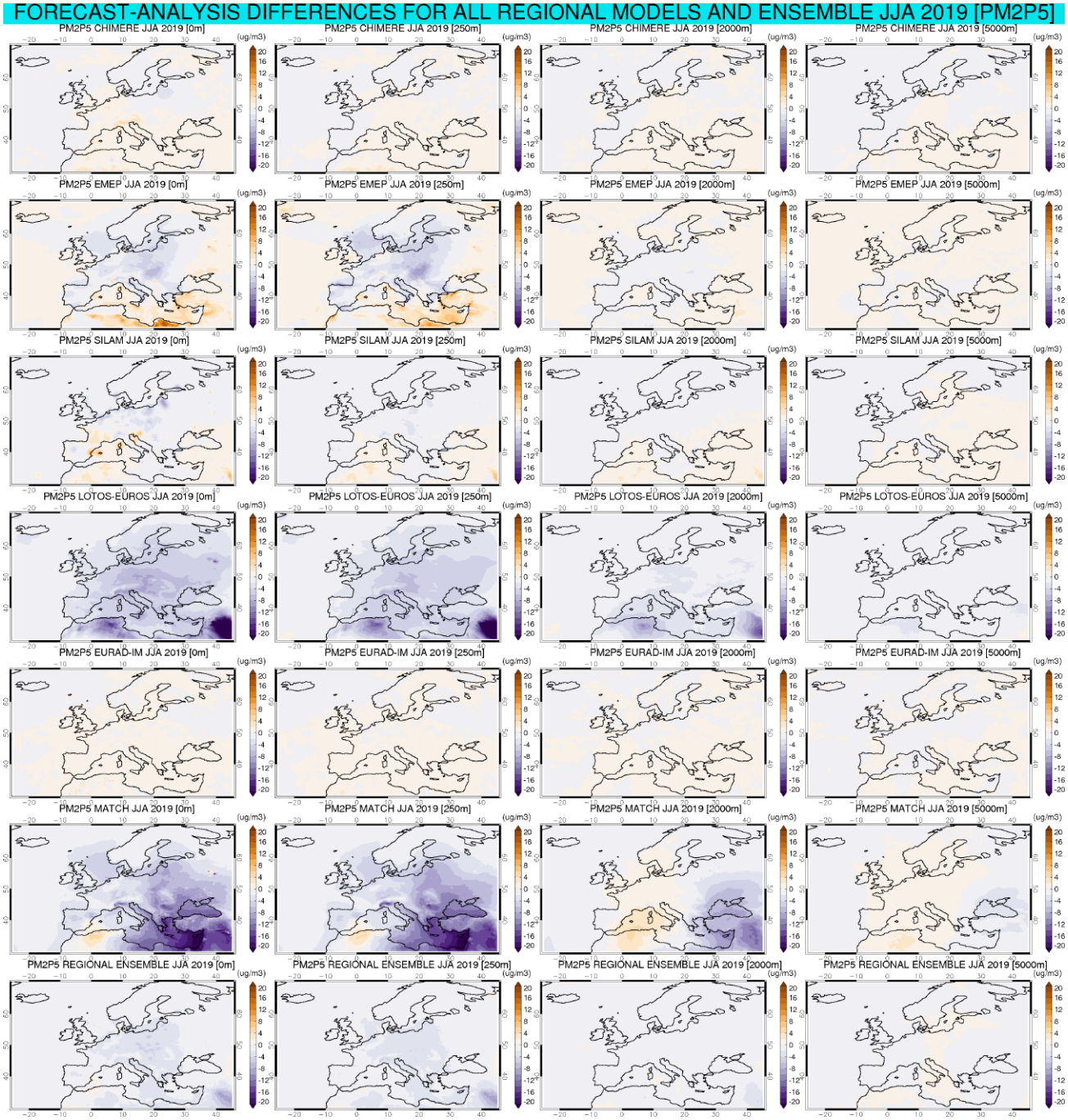

Figure 3.20. Mean regional PM2.5 differences between analysis and forecast for JJA2019 for four different vertical layers (0, 250, 2000, 5000 m) from regional ensemble and individual ensemble members (top to bottom: CHIMERE, EMEP, SILAM, LOTOS-EUROS, MOCAGE, EURAD-IM, MATCH and ENSEMBLE).

3.8 Case study

During the last week of July 2019 several Central European countries (Netherlands, Belgium and Germany) experienced record high temperatures, due to the prevailing heatwave. The CAMS-forecasted implications for air quality, and specifically for near-surface ozone, are presented in Figure 3.21 for both the global and regional systems.

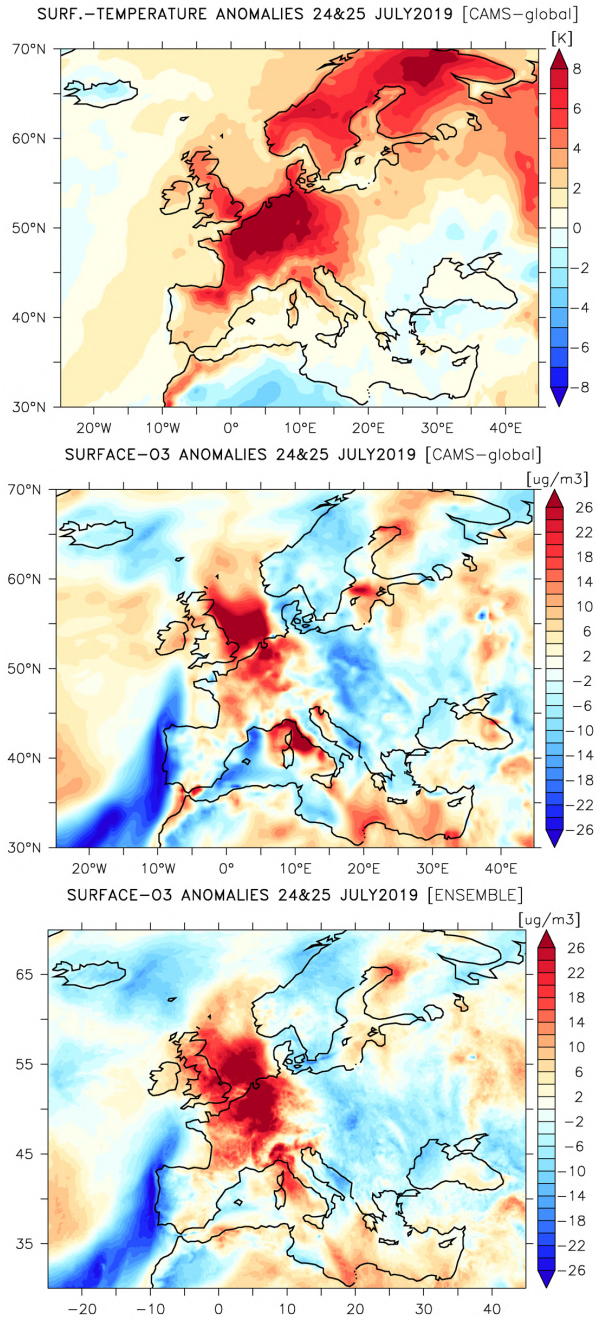

Figure 3.21. Differences between the mean 24th-25th July 2019 and the mean July 2019 for a) CAMS-global surface temperature (°C) b) CAMS-global near-surface ozone concentrations (ug/m3) and c) regional-ENSEMBLE near-surface ozone concentrations (ug/m3).

Figure 3.21 depicts the differences between the mean 24th-25th July 2019 and the mean July 2019 fields for a) CAMS-global surface temperature b) CAMS-global near-surface ozone and c) regional-ENSEMBLE near-surface ozone. A distinct surface warming is seen during the 24th-25th July 2019 period over Central Europe, and especially over the Benelux region, accompanied by an increase of surface ozone, regionally exceeding 26 ug/m3. Noteworthy is the agreement of ozone difference fields, between the CAMS global and regional forecast systems during the heatwave event.

4 Vertical profile and column aerosol comparisons

4.1 Summary for the EARLINET lidar and Aeronet comparisons

The regional models are compared with climatological lidar profiles for each season (EARLINET/ACTRIS data from 2006-2014). Missing information on composition, size and humidity growth of the aerosol in the models introduces considerable uncertainty to the PM derived extinction, which conservatively spans up to a factor 10 for absolute extinction values. Aeronet data are used to calibrate the conversion from modelled mass to optical property aerosol extinction. This way the order of magnitude in extinction is similar between the models and the lidar profiles, but also significant differences appear at some stations in the lowest layers (Granada, Athens). Relative differences in the form of extinction profiles are more certain. We choose the most representative five stations to compare in retrospective the seasonal average aerosol profiles since 2016. The retrospective of the seasonal comparisons since 2016 shows very similar profiles during this season. The respective overestimation or underestimation of the extinction found in 2016 are usually also found in 2017 and 2018 with the ENSEMBLE.

Introduction

The vertical distribution of aerosol reflects processes like atmospheric mixing, removal, and aerosol transport from outside of the domain or formation of secondary aerosol. The vertical mixing processes determine ground concentrations in polluted areas. Long-range transported aerosol, often carried aloft, may contribute to pollution in clean regions. Evaluation of the simulated aerosol column and vertical profiles are thus valuable for the performance characterisation of air quality models.

The 7 regional models provide mass concentration vertical profiles (PM2.5 and PM10) over Europe and may thus be evaluated for their aerosol vertical distribution. However, only very few aircraft campaigns and mountain sites are available to validate aerosol mass at altitude. In contrast frequent measurements of vertical profiles of aerosol backscatter, extinction or its integral, aerosol optical depth, exist. Deriving aerosol optical properties from the mass concentrations is thus needed, assuming lidar ratios and mass extinction coefficients, at least until the models provide more specific output on aerosol composition and optical properties.

In order to assess mass extinction coefficients chosen, the aerosol optical depth derived from the model mass profiles is first compared to AERONET AOD measurements. Secondly, we document a comparison of the extinction profiles derived from modelled mass concentration with climatological extinction profiles derived from European EARLINET/ACTRIS lidars for June-August for the period 2006-2019.

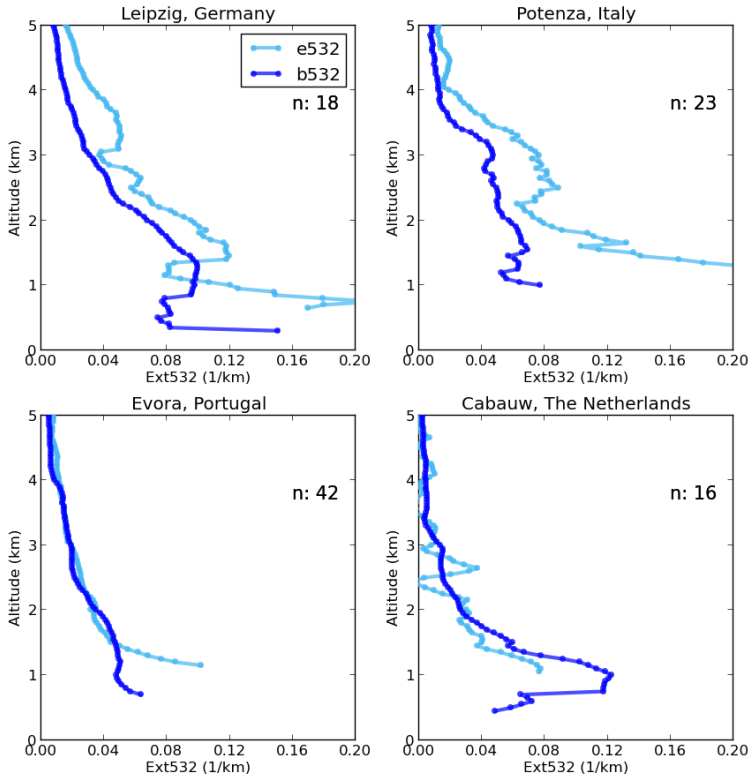

Figure 4.1. Comparison of mean profiles of two aerosol optical properties derived from the same Earlinet Raman lidar at the same time: a) aerosol extinction @532nm (light blue line) and b) extinction @532nm derived from the aerosol backscatter coefficient (dark blue) using a lidar ratio of 50 sr. The profiles use data taken at simultaneous times at each station; number of profiles given as n: x.

4.2 Methodology

AERONET data

The AERONET sun-photometers measure in non-cloudy conditions the aerosol optical depth at several wavelength and in near real time. The spatial distribution of the instruments allows a good coverage of aerosol observations over Europe. The version 3 level 1.5 data has been used in the reporting period presented here. This version and quality level ensures an efficient filtering of the residual clouds (mainly cirrus) for data in near real time. Daily AERONET aerosol optical depth, measured at 550 nm, has been averaged over summer for the European sites available in CAMS model output.

Lidar data

The EARLINET/ACTRIS Lidars are distributed over several locations in Europe and allow comparison across different climates in Europe (Pappalardo et al., 2014). Yet, up to now, there are no near-real-time data available. Regular measurements in EARLINET are sparse and often acquired once per week, with gaps due to maintenance or funding restrictions.

Table.4.1: Number of backscatter profiles (532 nm) available in EARLINET database used to compute seasonal (JJA) climatology. An issue has been discovered with the files from 2015 for the Evora station, thus for this station the previous climatology is still used.

Station	**N (2006-2014)**	**N (2006-2018)**
Ispra	337	337
Cabauw	14	14
Leipzig	76	121
Bucharest	143	181
Evora	69	69
Granada	152	188
Barcelona	45	59
Potenza	49	76
Athens	1	31

The previously computed climatology using available measurement between 2006 and 2014 has been updated in order to include measurements performed up to 2018. This also provides revised data for the earlier period. The number of profiles has increased significantly over some locations (e.g: Bucharest, Barcelona, Athens) making the climatology more statistically robust (Table 4.1).

The backscatter coefficient and extinction profiles at 532 nm have been extracted from the EARLINET database. The more frequently measured backscatter profiles are considered here with priority. An aerosol extinction coefficient profile is computed from the backscatter coefficient using a range of plausible lidar ratios. This latter parameter depends on the aerosol type and is more likely decreasing with the size of the aerosol. Minimum values are observed for sea salt aerosol (below 30 sr at 550 nm, [Ackermann et al., 1998, Omar et al., 2009]), while larger values are related to urban particles (55 sr in [Muller et al., 2007], 70 sr in [Cattrall et al., 2005]). Desert dust is associated with intermediate lidar ratios, ranging from 30 sr to 60 sr depending on the sources and the transport regime. A climatology of aerosols in West Africa published in Mortier et al. [2016] revealed an average lidar ratio (over 9 years) of about 30±15 sr. Due to the location of the stations involved in this study, both dust and urban aerosols and any a mix of them might occur. In order to represent the uncertainty on the nature of aerosols, we show the range in likely mean extinction using a lidar ratio extending from 30 to 70 sr.

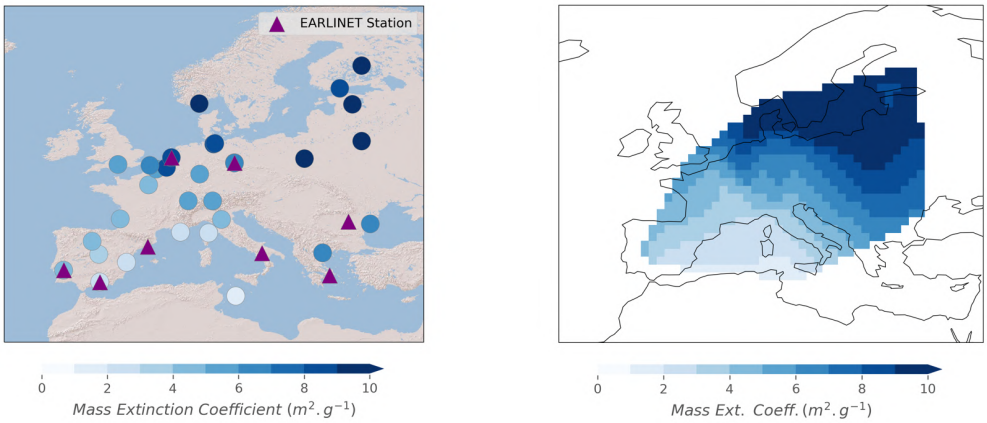

Figure 4.2. Mass extinction coefficient estimated at AERONET location sites (blue dotes) and EARLINET stations (triangles) for JJA2019 (left). A European map of the Mass Extinction Coefficient has been constructed with cubic interpolation in the inner part of the region covered by AERONET on the model grid (right), and with the nearest neighbours in the outer part of this region (not shown).

As a test, the conversion of lidar backscatter to extinction coefficient is performed assuming a constant average lidar ratio of 50 sr at locations where both backscatter and extinction coefficients are measured in EARLINET. This allows consistent comparison and visualization of some of the error associated to our simplified constant lidar ratio assumption. We have excluded from this comparison cases where local extinction coefficient was above 0.5 km^{-1} in order to avoid outliers. The profiles shown in Figure 4.1 from 4 stations reveal an error in the mean profile of 0-30% in extinction, which is small compared to the model spread documented below. The extinction profiles derived from the backscatter coefficients look vertically smoother. We have excluded from this comparison cases where local extinction coefficient was above 0.5 km^{-1} in order to avoid outliers.

In addition to this aerosol typing uncertainty, a sampling error should be accounted for. The observations are sporadic, while the models predict the aerosol concentration continuously. Therefore, seasonal averages are not computed with the same coverage in model and observation. Our earlier model-based bootstrap studies revealed, that, depending on the station, a set of ca. 30 daily observations allows reproducing the seasonal average with an error of about 10% [ACTRIS Deliverable WP6/D6.21]. In our case, this error might be larger since the synoptic situation is very different between our EARLINET climatological dataset, covering 2006-2014, and the season covered in this report. An overall uncertainty of about 20% has been chosen to represent the sampling error.

Model data

The ensemble mean and the underlying 7 regional CAMS models are investigated. For each of these models, the hourly PM10 and PM2.5 vertical profiles are extracted at the EARLINET station locations from the first day of each daily forecast at levels 0, 50, 250, 500, 1000, 2000, 3000, 5000 m.

The conversion of PM10 mass concentration to extinction requires a mass extinction coefficient (MEC). MEC depends on the size distribution, refractive index and density of the particles. This information is not yet available from the models. For different kind of aerosols, MEC values can vary

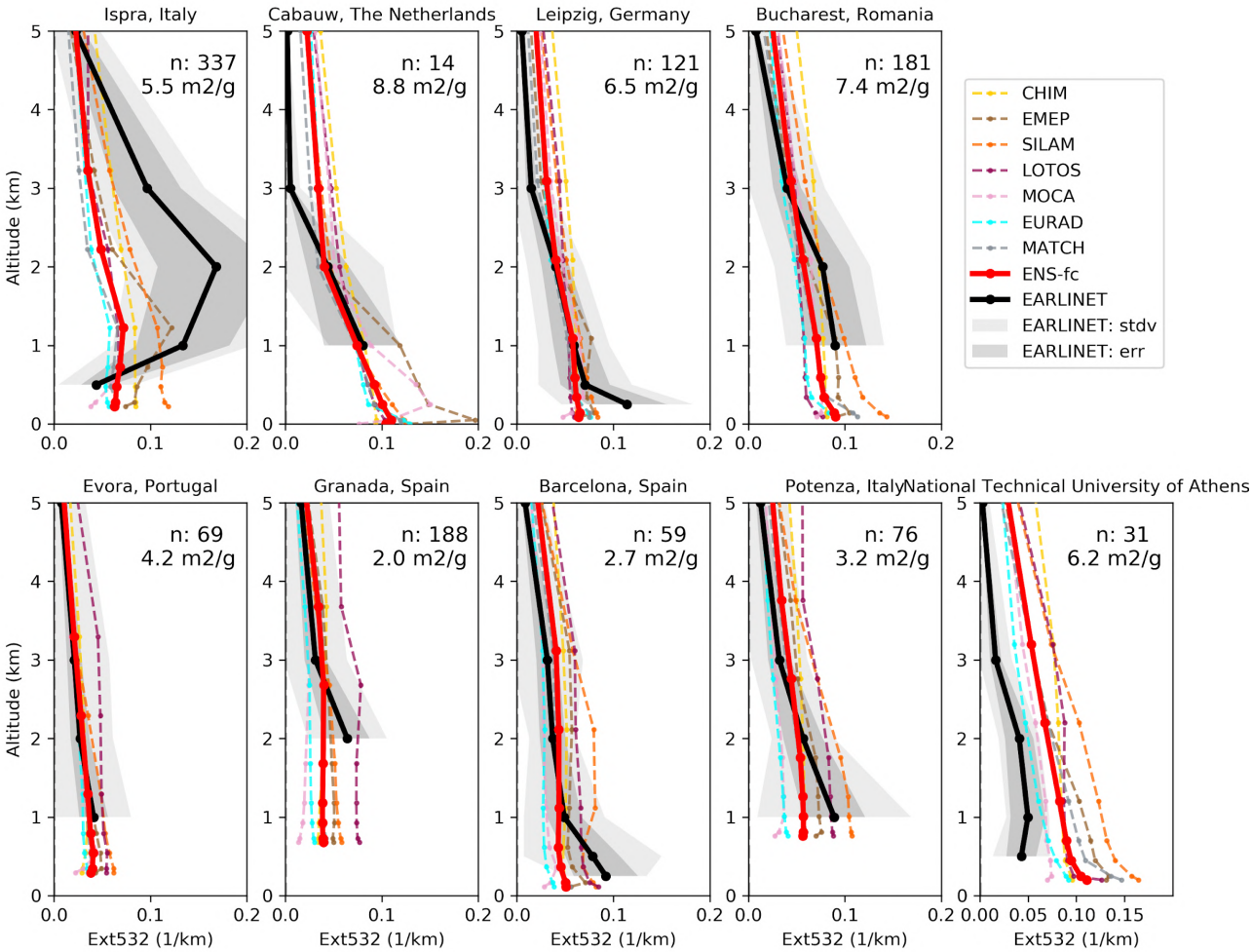

Fig 4.3. Extinction profiles June - August 2019 derived from the ENSEMBLE forecast mass concentration profiles (red envelope) and from EARLINET (climatology) backscatter profiles (grey envelope: lidar ratio uncertainty, light grey: including sampling error). "n: XX means number of individual EARLINET profiles assembled (June - August 2006-2019). The EMC used for the calculation of the extinction from the concentration profiles is indicated for each station below the number of EARLINET profiles "n" used for the calculation of the climatology.

from about 0.5 m^2g^{-1} in the case of desert dust aerosols up to 8 m^2g^{-1} for urban particles [Chin et al., 2002]. No variation with height or aerosol type is taken into account, mainly because the models provide no further info on aerosol speciation. We derive the MEC value to convert the model profile data to extinction profiles from a combination of the modelled mass column load and consistent Aeronet AOD data.

For the Aeronet based computation of the MEC, the model data are picked at the location and on the day when sun photometer observations were available. The CAMS-regional mass concentrations have been averaged for coincident days (with the measurements) and averages are converted, with a seasonal and site dependent mass extinction coefficient estimated with AERONET retrievals, into extinction profiles. A seasonal and site dependent mass extinction coefficient is obtained when combining it with AERONET AOD retrievals. Values of MEC are ranging from 1 m^2g^{-1} in South-West of Europe to more than 10 m^2g^{-1} in the North-East. Since some of the EARLINET stations are not co-

located with Sun photometers, a European map of MEC has been constructed, for each season, by interpolating (cubic interpolation) and extrapolating (nearest neighbour) the available AERONET based MEC calculations on the grid of the model (Figure 4.2). One can notice a gradient with the longitude with lower values found in the Western part while the highest values are observed in the Eastern part of Europe. Also, the values are generally lower as compared to last year, which might reveal a higher concentration in coarse particles (dust). The seasonal AERONET-based MEC is then used at each EARLINET station to calculate the model extinction from concentration profiles. The uncertainty on the MEC being removed allows more accurate comparisons with the observed vertical profiles than using an average MEC over whole Europe.

4.3 Results

4.3.1 Comparison of extinction profiles

The extinction profiles estimated from the 7 CAMS models and the ENSEMBLE and EARLINET measurements are compared for JJA2019 (Figure 4.3).

One observes generally a good agreement between the two datasets. Disparities occur once again in Ispra, as the number of profiles used for computing the climatology has remained identical, as compared to JJA 2018. The EARLINET climatology computed with a higher number of profiles, by averaging seasonal profiles between 2004 and 2018, implies more robust statistical averages and then lower uncertainties. In Leipzig, models were overestimating extinction values along the whole profiles in summer 2018. In 2019, this overestimation persists above the altitude of 3 km but has been diminished below. Under 500 m, models still underestimate the extinction values, similarly to the previous year. The biggest change in the EARLINET climatology is noticed in Athens (1 observation in 2018 Vs 31 observations in 2019). The new climatology is much smoother and the associated uncertainty has been significantly reduced. However, with a EMC of 6.2 m2/g, three times larger than the one in 2018, the models are overestimating the extinction profiles in an homogeneous way vertically by a factor 2.

In Evora, while the EARLINET climatology did not change as compared to last year, as well as the EMC (4.3 m2/g in 2018 Vs 4.2 m2/g in 2019), the agreement with the regional profiles has greatly improved.

4.3.2 Seasonal variability

In order to investigate the performance of the model in reproducing the vertical profiles, it is interesting to observe the inter-annual variability for the different seasons. This will be of use for the development of a score providing an assessment of the models skills, and is also useful to investigate the models synoptic variability. The seasonal profiles have been reported since 2016 at 5 stations (Leipzig, Barcelona, Potenza, Evora and Bucharest) in Figure 4.4, using the new EARLINET climatology. As discussed previously, summer profiles in 2019 present a better agreement in Evora than in 2018 as similar EMC values were used for the two years. In Barcelona, although a lower EMC value was used in 2019 as compared to 2018, which might explain the greater underestimation of the extinction values in the lowest layers, one observe an increase of the extinction above 3 km of altitude. This increases the bias with respect to the climatology computed from EARLINET.

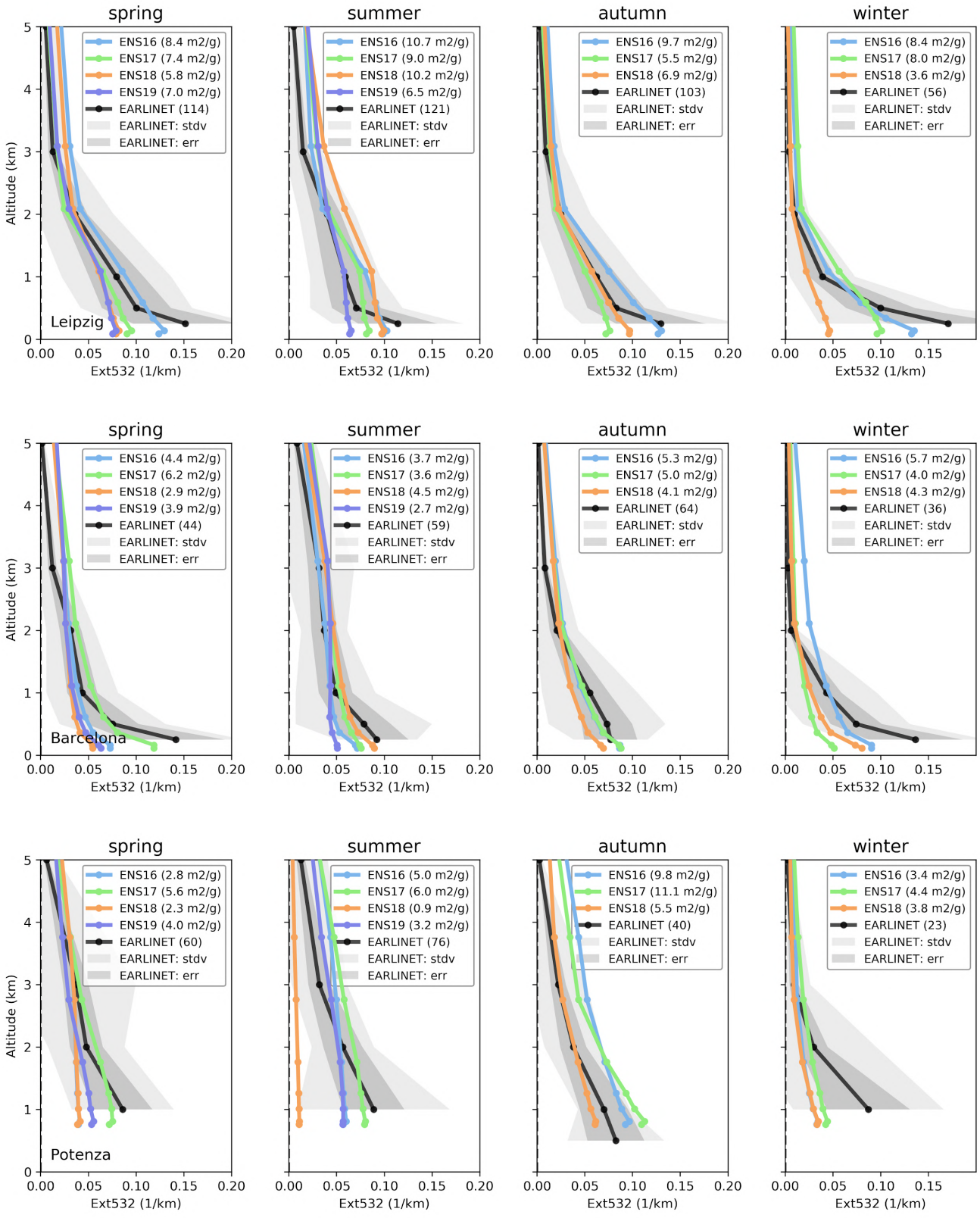
spring
ENS16 (8.4 m2/g)
ENS17 (7.4 m2/g)
ENS18 (5.8 m2/g)
ENS19 (7.0 m2/g)
EARLINET (114)
EARLINET: stdv
EARLINET: err
Leipzig
summer
ENS16 (10.7 m2/g)
ENS17 (9.0 m2/g)
ENS18 (10.2 m2/g)
ENS19 (6.5 m2/g)
EARLINET (121)
EARLINET: stdv
EARLINET: err
autumn
ENS16 (9.7 m2/g)
ENS17 (5.5 m2/g)
ENS18 (6.9 m2/g)
EARLINET (103)
EARLINET: stdv
EARLINET: err
winter
ENS16 (8.4 m2/g)
ENS17 (8.0 m2/g)
ENS18 (3.6 m2/g)
EARLINET (56)
EARLINET: stdv
EARLINET: err
spring
ENS16 (4.4 m2/g)
ENS17 (6.2 m2/g)
ENS18 (2.9 m2/g)
ENS19 (3.9 m2/g)
EARLINET (44)
EARLINET: stdv
EARLINET: err
Barcelona
summer
ENS16 (3.7 m2/g)
ENS17 (3.6 m2/g)
ENS18 (4.5 m2/g)
ENS19 (2.7 m2/g)
EARLINET (59)
EARLINET: stdv
EARLINET: err
autumn
ENS16 (5.3 m2/g)
ENS17 (5.0 m2/g)
ENS18 (4.1 m2/g)
EARLINET (64)
EARLINET: stdv
EARLINET: err
winter
ENS16 (5.7 m2/g)
ENS17 (4.0 m2/g)
ENS18 (4.3 m2/g)
EARLINET (36)
EARLINET: stdv
EARLINET: err
spring
ENS16 (2.8 m2/g)
ENS17 (5.6 m2/g)
ENS18 (2.3 m2/g)
ENS19 (4.0 m2/g)
EARLINET (60)
EARLINET: stdv
EARLINET: err
Potenza
summer
ENS16 (5.0 m2/g)
ENS17 (6.0 m2/g)
ENS18 (0.9 m2/g)
ENS19 (3.2 m2/g)
EARLINET (76)
EARLINET: stdv
EARLINET: err
autumn
ENS16 (9.8 m2/g)
ENS17 (11.1 m2/g)
ENS18 (5.5 m2/g)
EARLINET (40)
EARLINET: stdv
EARLINET: err
winter
ENS16 (3.4 m2/g)
ENS17 (4.4 m2/g)
ENS18 (3.8 m2/g)
EARLINET (23)
EARLINET: stdv
EARLINET: err
Altitude (km)
Ext532 (1/km)

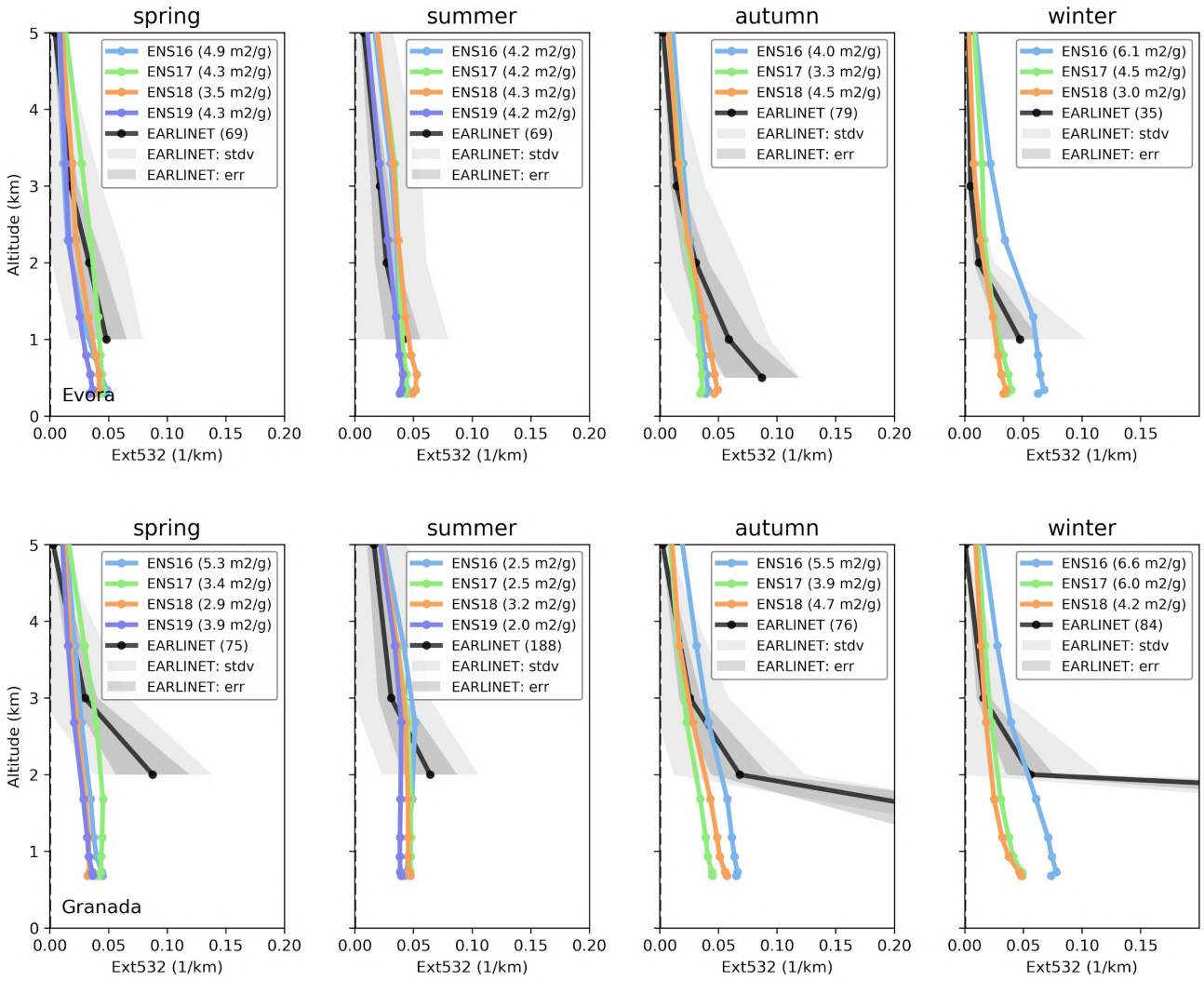

Fig 4.4: Seasonal extinction profiles derived from ENSEMBLE forecast mass concentration profiles for 2016 (ENS16), 2017 (ENS17), 2018 (ENS18), 2019 (ENS19) and EARLINET climatology. The parenthesis indicates for the CAMS profiles, the MEC used for the extinction estimation, and for the EARLINET, the number of profiles used for constructing the climatology.

5 IAGOS aircraft CO and O_3 profile comparisons

5.1 Summary

Routine observations of ozone and CO over European airports are available from the IAGOS fleet. Take-off and landing profiles were sampled from the hourly model 3D forecasts along the flight tracks.

Ozone in-situ: Ozone is well represented by both the regional ensemble the CAMS-global during the heat wave periods with slightly better results from the regional ensemble. Large differences are found when ozone observation levels are low which might be partly explained by a negative bias in IAGOS observations.

Carbon monoxide: In the lowest layers, CO is mostly underestimated by all models which present similar behaviour especially before the CAMS global upgrade. After the upgrade, CAMS global is improved in the surface and boundary layer and presents smaller bias than the regional ensemble in some cases. In the free troposphere CAMS-global performs well while the regional ensemble underestimates CO.

5.2 IAGOS Validation Method

Validation is possible at the European airports visited by the IAGOS fleet. For the European-based carriers, there are regular profiles at the home airports. There are two aircraft operated by Lufthansa, one operated by Air France. Thus, when the fleet is fully operational, there are daily profiles Frankfurt and Paris (CDG). IAGOS is also installed on two aircraft operated by the Asian-based carrier China Airlines. Aircraft fly regularly from Taipei to Amsterdam or Vienna and sometimes to Rome. Other airports may be visited depending on the operational schedules of the airlines. During this period, in Europe only the airport of Frankfurt has been visited as shown in Figure 5.1.

We download the daily latitude-longitude datasets for the 7 regional models and the ensemble for two species (carbon monoxide and ozone) on 8 vertical levels (surface, 50m, 250m, 500m, 1000m, 2000m, 3000m, 5000m). The aircraft takes about 10 minutes to climb or descend the 5000m vertical extent covered by the regional models. During this time and travelling at up to 166 m s^{-1}, it covers about 120km and therefore traverses many grid-boxes of resolution 10km. We perform a spatial interpolation from the grid of the regional models to the aircraft's trajectory. The IAGOS measurements in ppbv are converted to µg m^{-3} using the temperatures measured by IAGOS. The data are validated by the PI but are not yet calibrated. Calibration takes place after an operational period of about 6 months.

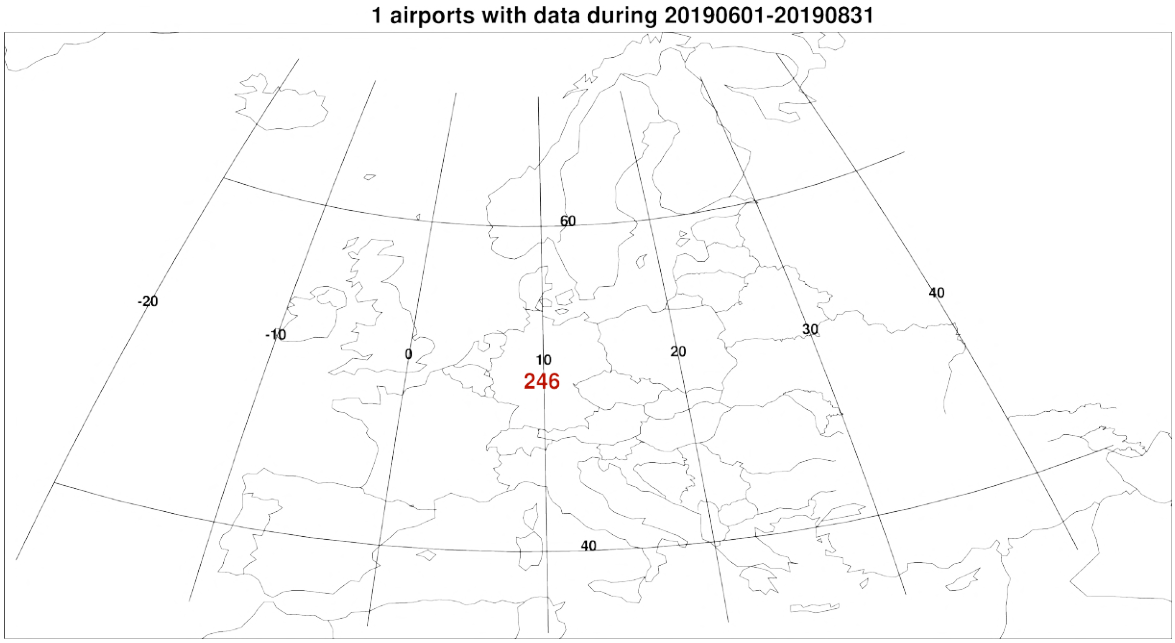

Figure 5.1. Map showing the number of profiles available in the period June - August 2019.

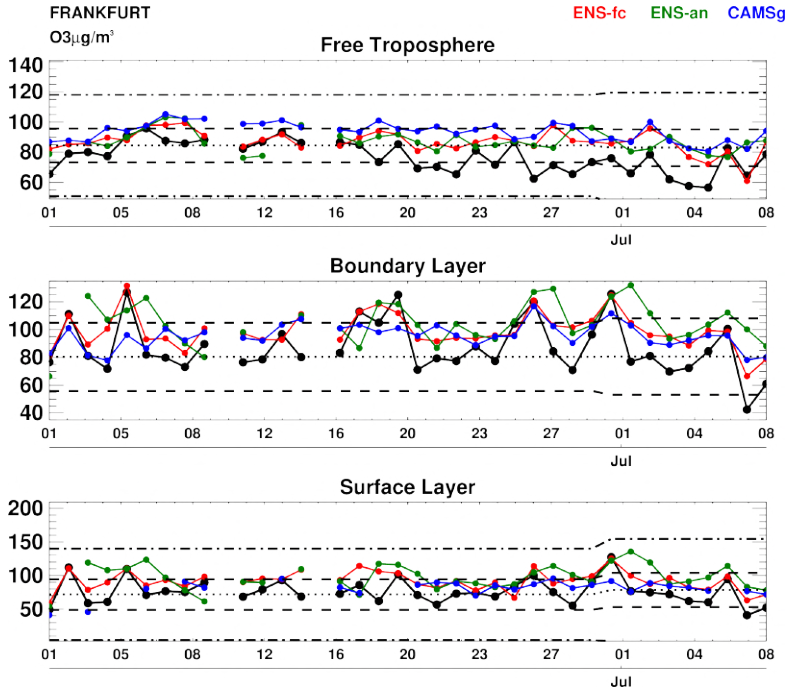

Figure 5.2.a Daily time series of ozone at Frankfurt for the period 1st June to 8 July 2019. The regional ensemble and associated analysis is shown in red and green respectively, and CAMS-global is shown in blue. The black dotted line is the monthly mean of the observations (IAGOS/MOZAIC) over the period 2003-2016 (Level 2 data), the black dashed line shows 1 standard deviation from the monthly mean and the black doted-dashed line shows 3 standard deviations from the monthly mean.

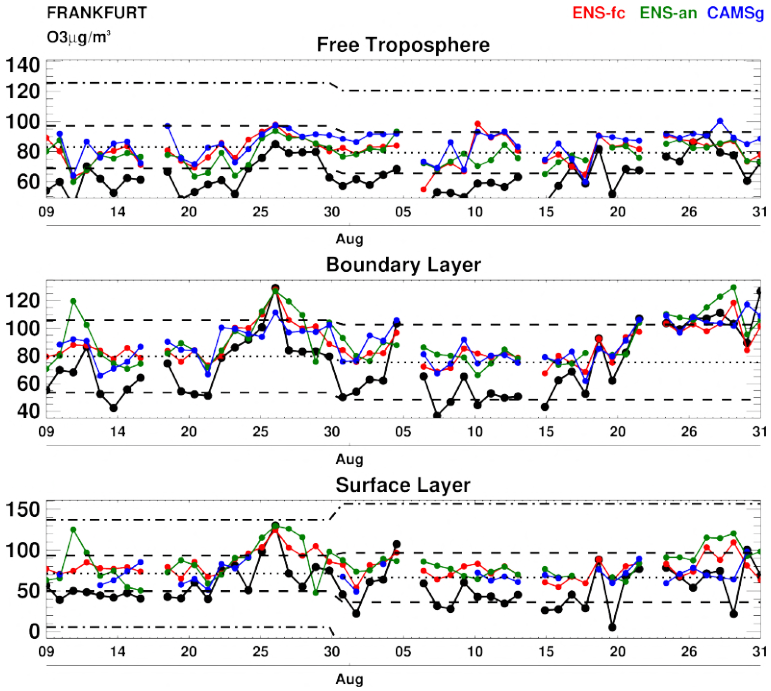

Figure 5.2.b. Same as Fig. 5.2.a. for the period from 9 July to 31 August 2019.

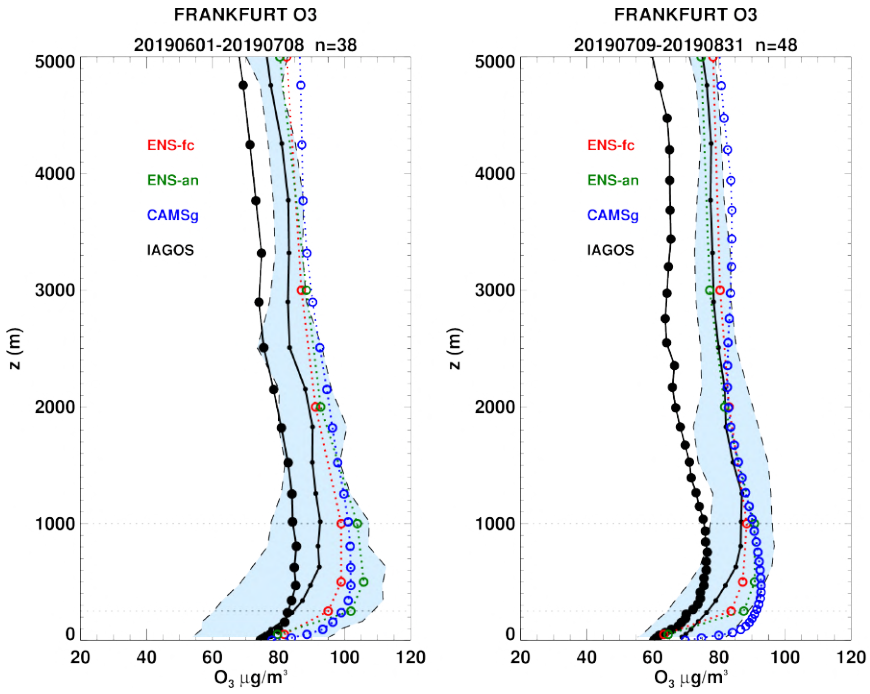

Figure 5.3. Mean profile of ozone at Frankfurt for the period JJA 2019 (left: between 1st June and 8 July, right: between 9 July and 31 August). The regional ensemble and associated analysis are shown in red and green respectively, and the global o-suite is shown in blue. The shaded area indicates the range of the mean climatology of the observations plus/minus one standard deviation during the same period for all years between 2003 and 2016 (level 2 data).

5.3 IAGOS Ozone

For the period June 2019 - August 2019, observations are available only at Frankfurt, the daily time series are presented in two Figures corresponding to two sub-periods before and after the upgrade of CAMS global in Fig. 5.2.a and 5.2.b. The associated averaged profiles at Frankfurt are presented in Fig. 5.3.a and 5.3.b. In all plots, the forecast and analysis of the regional ensemble is shown in red and green respectively, and CAMS-global is shown in blue. These figures show that the models behave rather similarly in all layers, with some slight difference in the surface and boundary layer and in particular during the ozone episodes. The regional model performs better than CAMS global during ozone episodes. Moreover, the results from the regional analysis often present larger ozone values than the forecast. In the Free troposphere, all the models overestimate similarly.

The time series show that there is a good agreement in the surface and boundary layer between the models and IAGOS during the different ozone episodes of this period especially in the last week of June and the last week of July corresponding to the heat wave periods over Europe. The results from both regional and CAMS global present similar results with a better performance from the regional model. However, when ozone is low, the differences between the models and IAGOS are large and IAGOS values are much lower than the model results. The averaged profiles for the corresponding periods also show that IAGOS observations for this period are lower than the climatological values. This is unexpected given the strong ozone episodes that occurred in both June and July this year. An increase of the bias in IAGOS comparisons has already been mentioned in MAM 2019 reports as well and in CAMS Reanalysis report. This new evaluation period gives more evidence to support the idea of a possible bias in IAGOS data which could partly explain the increase of the bias attributed to the model. This might be further checked with the availability of Level 2. In addition, it must be mentioned that on 16 august, one of the instrument suspected to measure less ozone has been replaced, and after a quick check on the observations for the second half of August it seems that ozone values measured by this instrument are now more reliable (not shown here). This will be confirmed in the coming months with the availability of longer time periods from the new instrument.

Several of the individual profiles obtained at Frankfurt during this JJA period are presented in Fig. 5.4a-c. Most profiles selected here show ozone values beyond the climatological values especially on 26 and 30 June for the first heat wave (Fig. 5.4.a-b) period and on 22, 23 and 26 July (Fig. 5.4.b-c) with concentration reaching a maximum of 150 µg/m^3 near the surface (near 3 standard deviation from the mean) and in the boundary layer (above one standard deviation) as also shown in Fig. 5.2.a-b. For most profiles during the two heat waves, the regional ensemble agrees well with the observations. The results from the different forecast times discrepancies only during these episodes, where the closest forecast times give better results.

Outside the heat wave period high ozone values are also observed in the boundary layer at several periods during JJA 2019: first around 6 June, then between 17-19 June and also at the end of August. The profiles for days 5, 17 and 19 June are presented in Fig. 5.4.a, and time series show that ozone reached values above one standard deviation on these days (Fig.5.2.a). In general, the regional ensemble performs well for these days. On 19 June the sharp peak of about 140 µg/m^3 in the boundary layer is not reproduced by the regional ensemble which provides a smoother profile

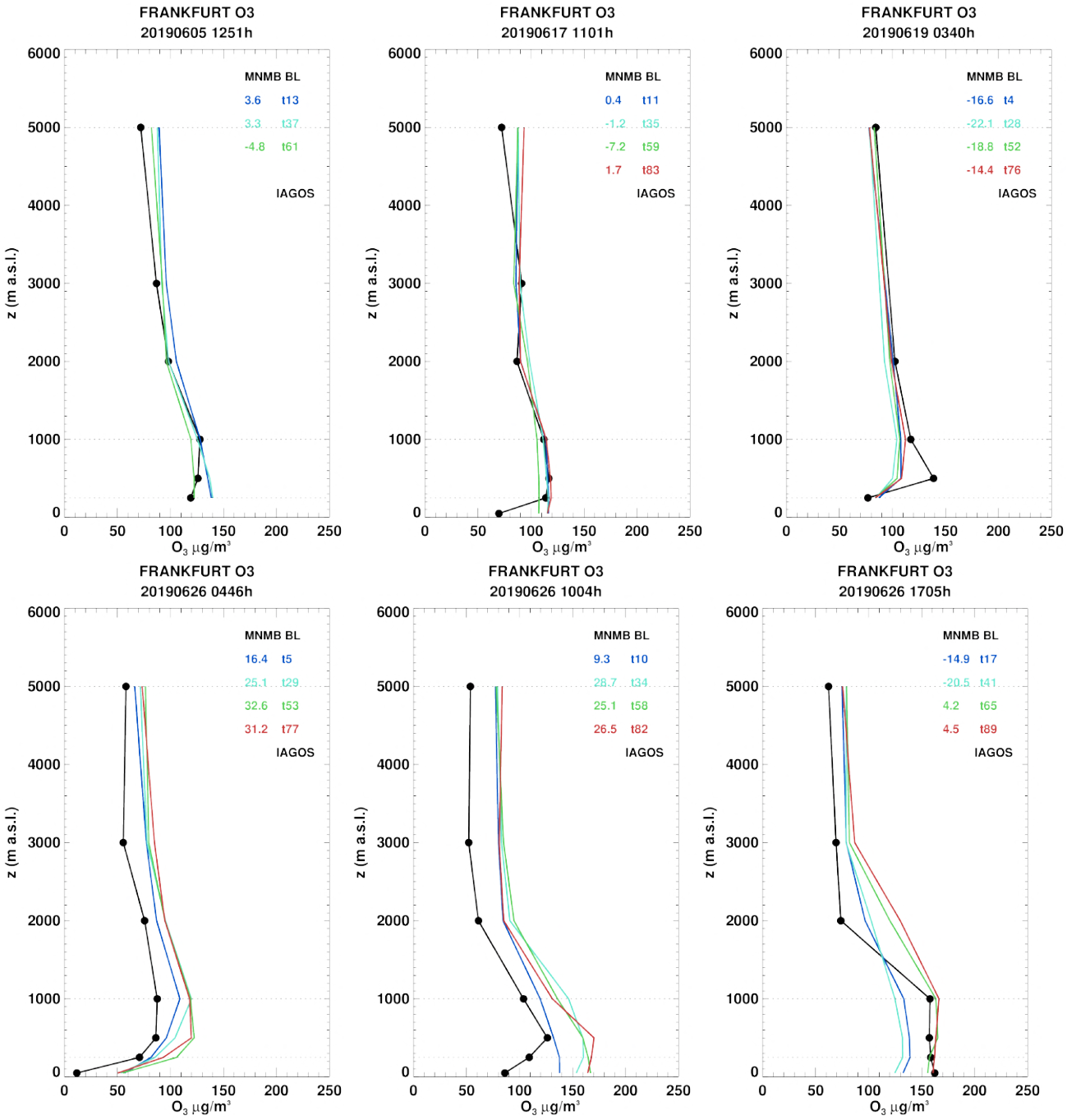

Figure 5.4.a. Selection of ozone profiles at Frankfurt during the period JJA 2019. The ensemble is shown at 4 forecast times (blue: 1-day; cyan: 2-day; green: 3-day; red: 4-day).

with a value of 110 µg/m^3 in this layer. At the end of August, high ozone values are also found in the boundary layer with nearly 110 µg/m^3 (around one standard deviation, Fig. 5.2.b). Like during the heat wave periods, the regional ensemble agrees well with observations although surface values are often overestimated during this period of August as shown on both time series (Fig. 5.2.b) and individual profiles of 28, 29 and 31 August (Fig. 5.4.c).

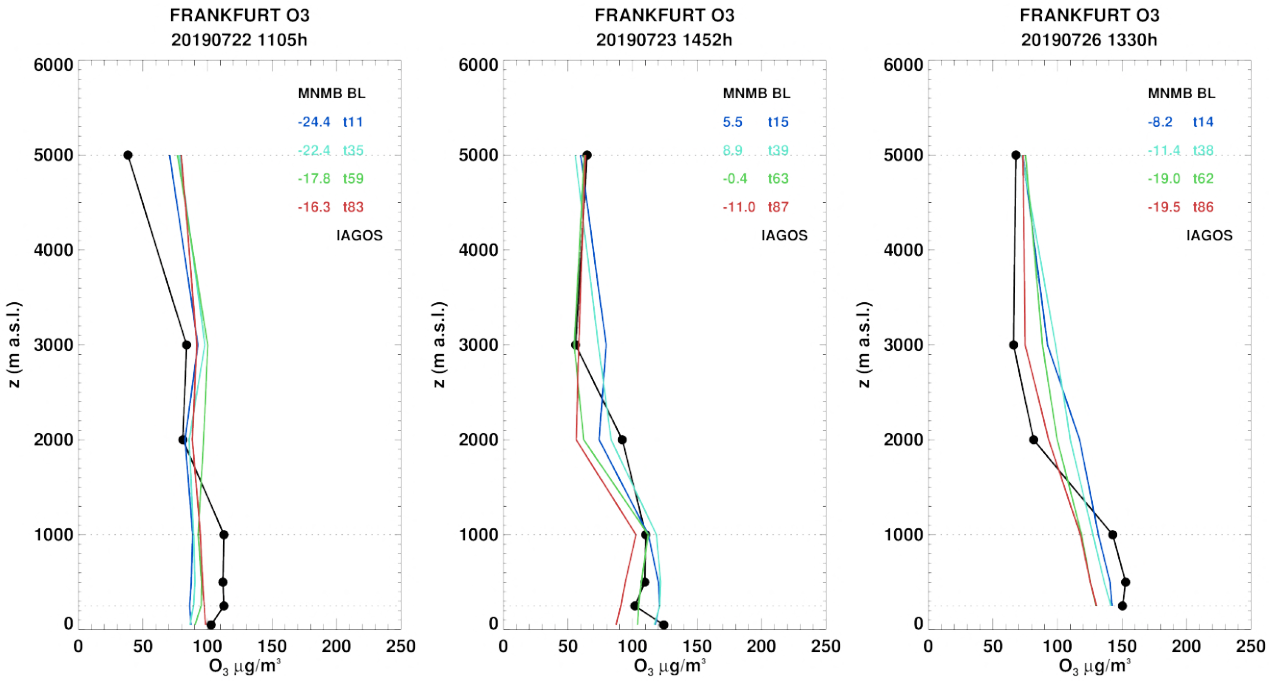

Figure 5.4.b. Selection of ozone profiles at Frankfurt during the period JJA 2019. The ensemble is shown at 4 forecast times (blue: 1-day; cyan: 2-day; green: 3-day; red: 4-day).

Some profiles obtained with all individual models of the ensemble are presented in Fig. 5.5.a-e (chronological order). On these profiles it can be seen that the MOCAGE model usually presents large overestimations in the surface and boundary layer as compared to other models, although sometimes the agreement is better with this model during the high ozone episodes described above but not always (e.g. see profiles of 26 June and 26 July). For the free troposphere the results of the different models are very similar except for some profiles showing for the EMEP model ozone overestimation is larger than those of other models as shown on 27 and 28 July.

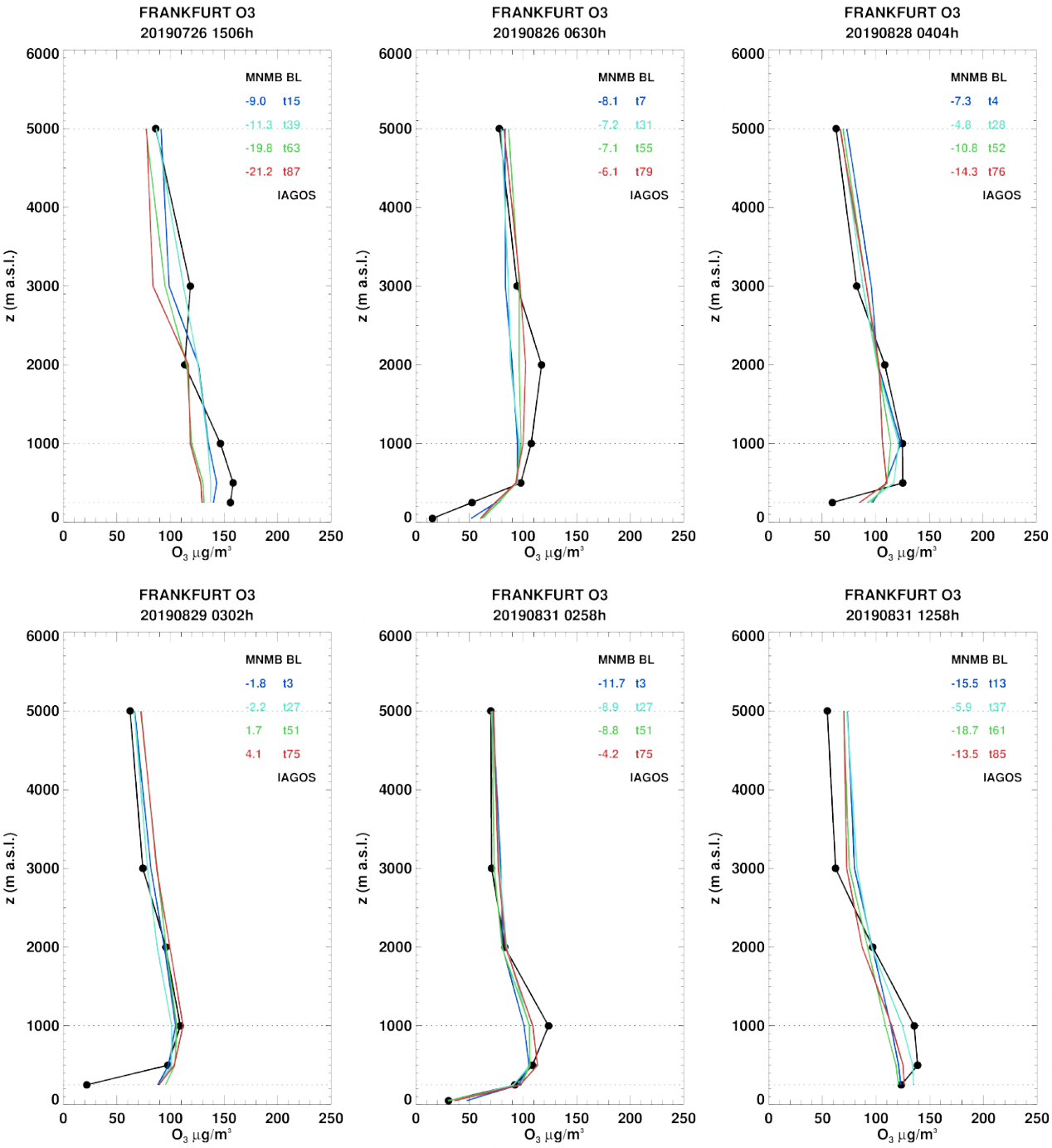

Figure 5.4.c. Selection of ozone profiles at Frankfurt during the period JJA 2019. The ensemble is shown at 4 forecast times (blue: 1-day; cyan: 2-day; green: 3-day; red: 4-day).

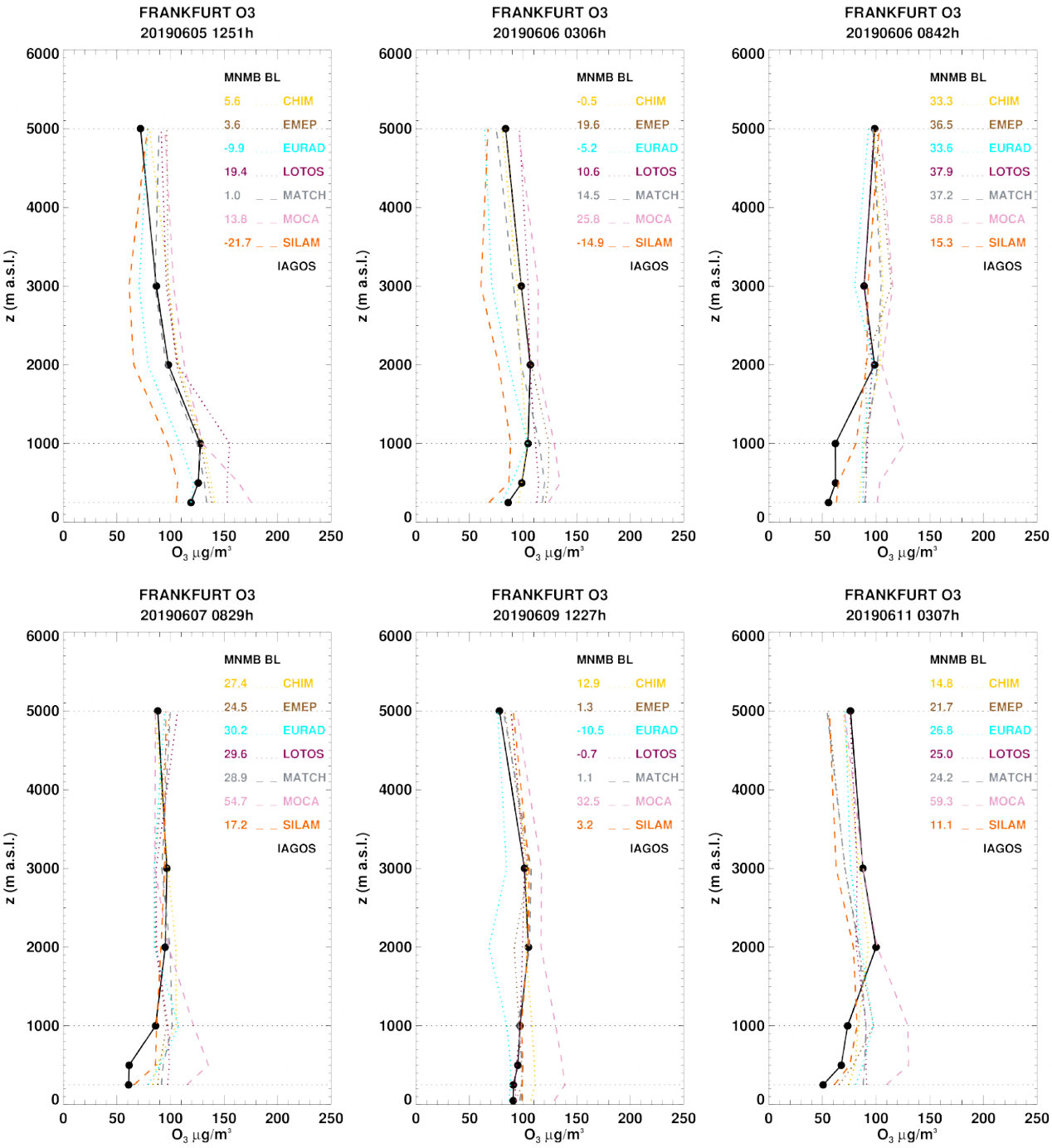

Figure 5.5.a: Ozone profiles at Frankfurt during the period JJA 2019. Each color/ Line style corresponds to one of the 7 models for the ensemble. In the legend, the models are CHIM=CHIMERE, EMEP=EMEP, SILAM=SILAM, LOTOS=LOTOS-EUROS, MOCA=MOCAGE, EURAD=EURAD, MATCH=MATCH.

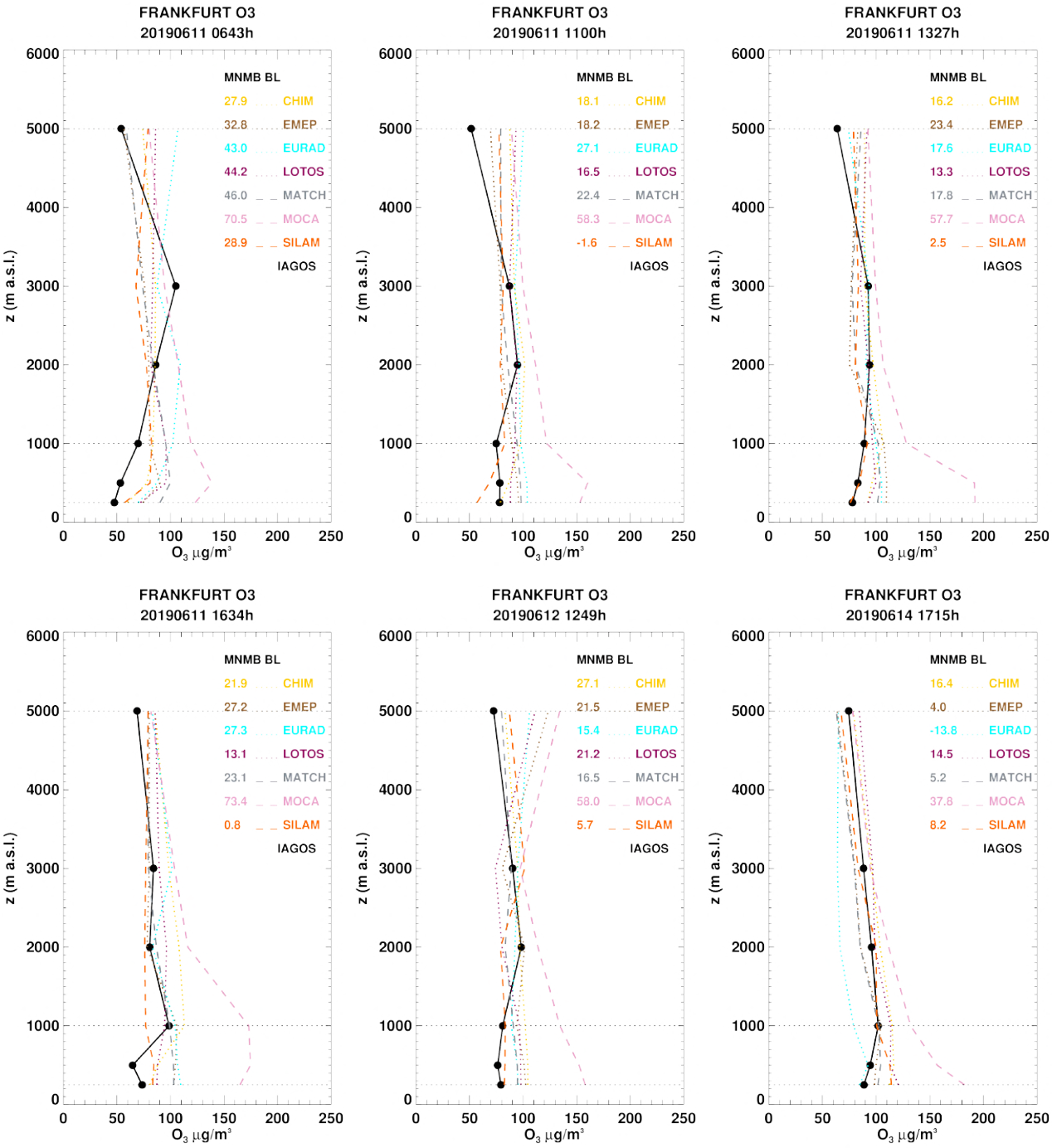

Figure 5.5.b: Ozone profiles at Frankfurt during the period JJA 2019. Each color/ Line style corresponds to one of the 7 models for the ensemble. In the legend, the models are C

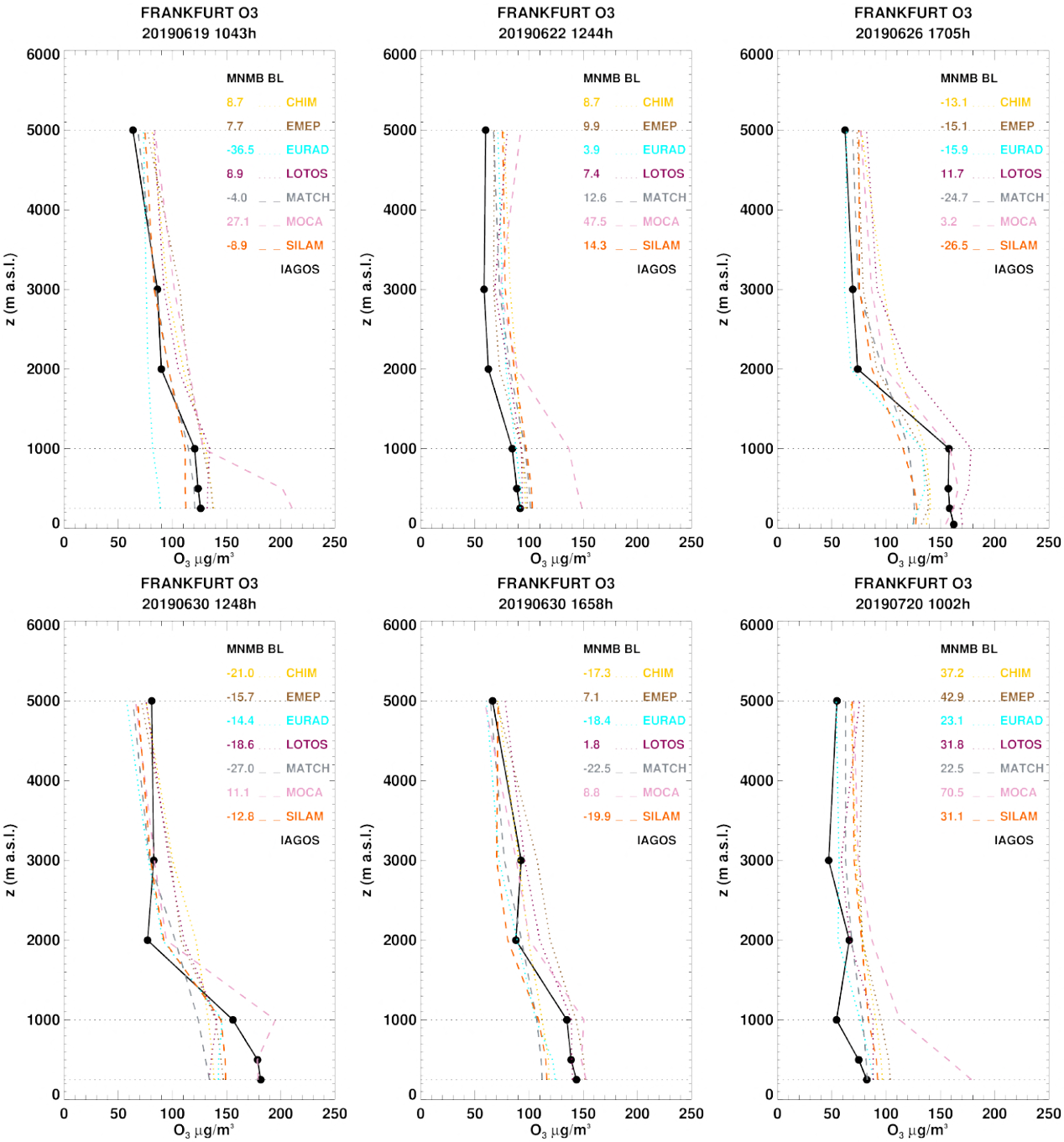

Figure 5.5.c: Ozone profiles at Frankfurt during the period JJA 2019. Each color/ Line style corresponds to one of the 7 models for the ensemble. In the legend, the models are CHIM=CHIMERE, EMEP=EMEP, SILAM=SILAM, LOTOS=LOTOS-EUROS, MOCA=MOCAGE, EURAD=EURAD, MATCH=MATCH.

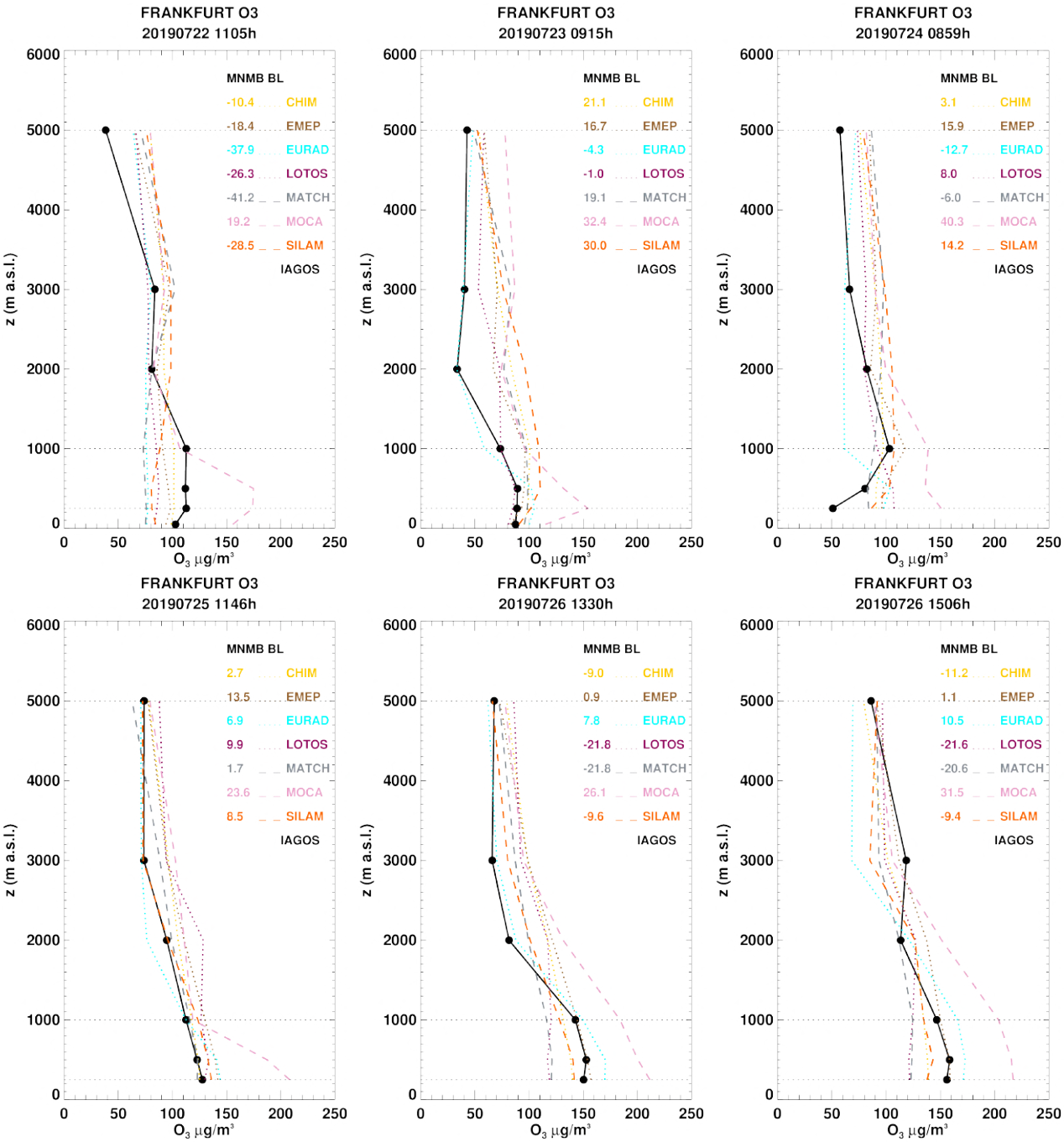

Figure 5.5.d: Ozone profiles at Frankfurt during the period JJA 2019. Each color/ Line style corresponds to one of the 7 models for the ensemble. In the legend, the models are CHIM=CHIMERE, EMEP=EMEP, SILAM=SILAM, LOTOS=LOTOS-EUROS, MOCA=MOCAGE, EURAD=EURAD, MATCH=MATCH.

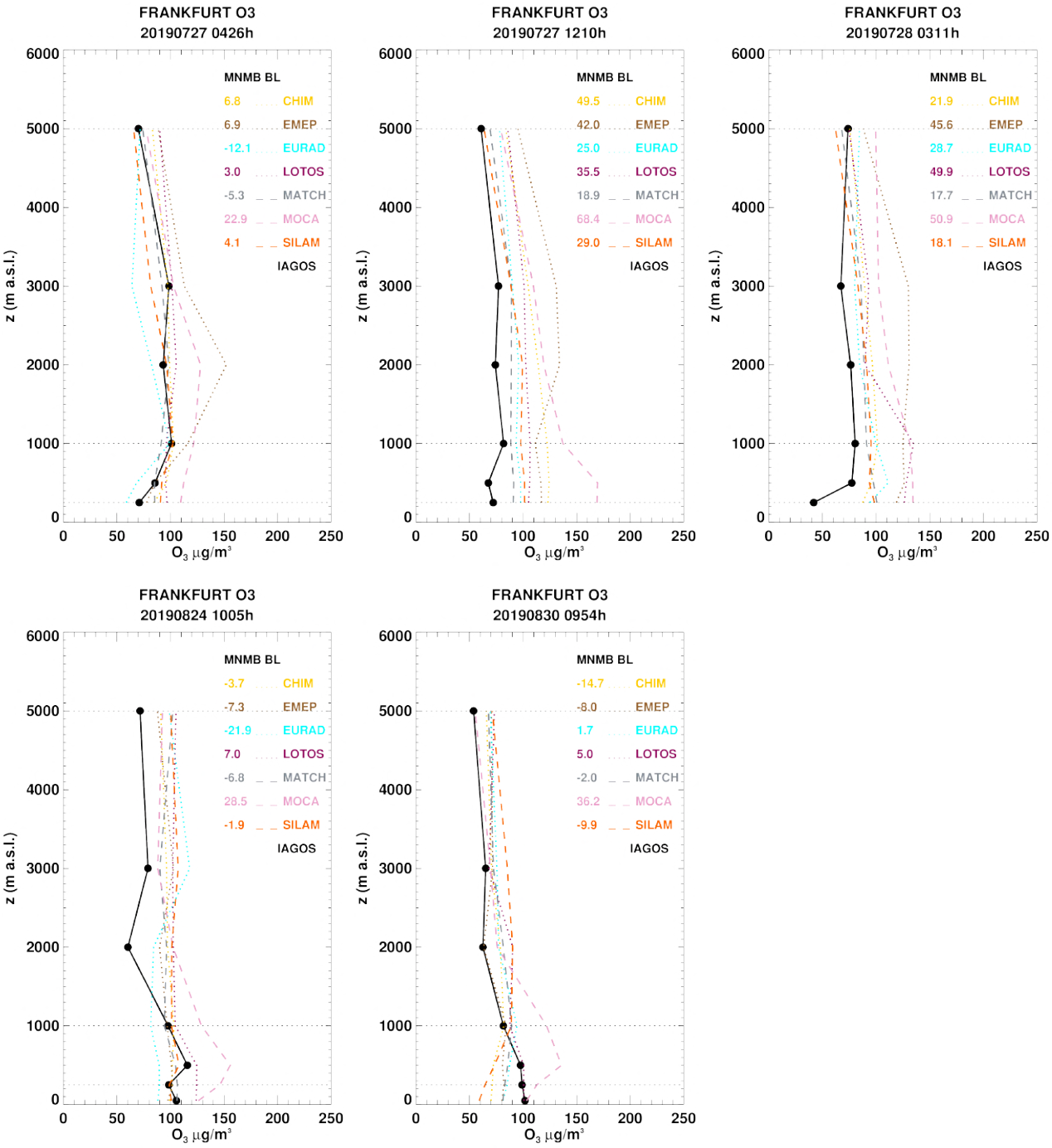

Figure 5.5.e: Ozone profiles at Frankfurt during the period JJA 2019. Each color/ Line style corresponds to one of the 7 models for the ensemble. In the legend, the models are CHIM=CHIMERE, EMEP=EMEP, SILAM=SILAM, LOTOS=LOTOS-EUROS, MOCA=MOCAGE, EURAD=EURAD, MATCH=MATCH.

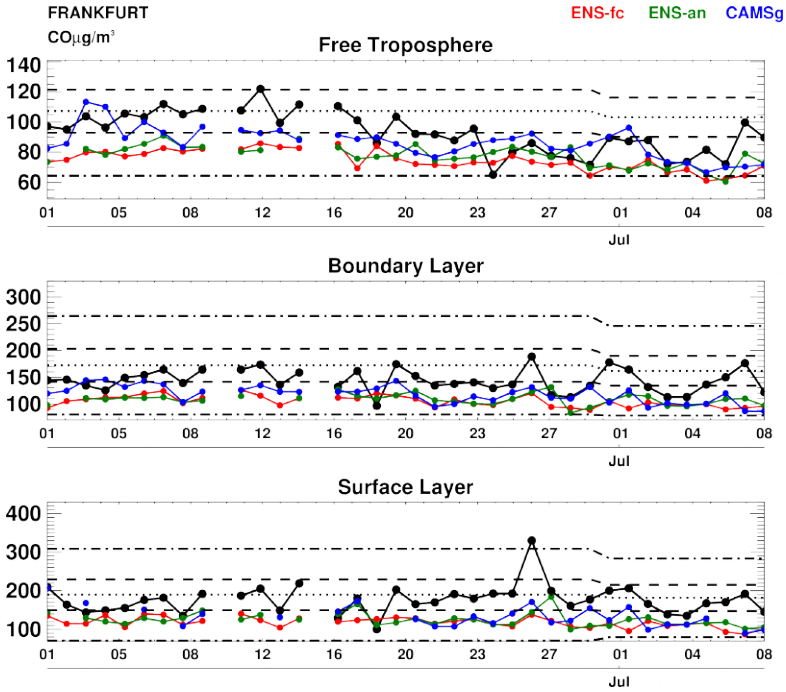

Figure 5.6.a. Daily time series of CO at Frankfurt for the period between 1st June to 8 July 2019. The regional ensemble and associated analysis is shown in red and green respectively, and CAMS-global is shown in blue. The black dotted line is the monthly mean of the observations (IAGOS/MOZAIC) over the period 2003-2016 (Level 2 data), the black dashed line shows 1 standard deviation from the monthly mean and the black doted-dashed line shows 3 standard deviations from the monthly mean.

5.4 IAGOS Carbon Monoxide

Like for the ozone section, the daily time series of CO and associated averaged profile at Frankfurt are presented in two sub-periods related to the upgrade of CAMS global Fig. 5.6.a-b and 5.7.a-b.The forecast and analysis of the regional ensemble is shown in red and green respectively, and CAMS-global is shown in blue. In the surface and boundary layers CO is always underestimated by the models, but the results obtained for the first and the second period differ. In the first period (i.e. before the upgrade), the results of the regional ensemble and CAMS-global are in general very similar with an underestimation of CO values (Fig. 5.6.a). After the last upgrade of CAMS global, as clearly shown on the time series (Fig. 5.6.b) the performance of CAMS global often appears better than that of the regional in both surface and boundary layers. In the free troposphere, the results are similar for both sub-periods, CO is also underestimated for the regional ensemble (forecast and analysis) while CAMS-global often shows a good performance. Meanwhile, on average the results from all models are similar for both periods when looking at the mean profile in Fig. 5.7.

During the first period, a major peak of CO slightly above 3 standard deviations is observed in the surface layer during the last week of June with a maximum of about 300 µg/m^3 in the surface layer. This peak is correlated with the high episode of ozone during the first heat wave of summer 2019 over Europe (see ozone section 5.3). Two secondary peaks are also observed in both surface and boundary layer around the 1st and 7 July (near one standard deviation). For all these days, the regional ensemble is largely underestimating CO values from the surface to an altitude of about

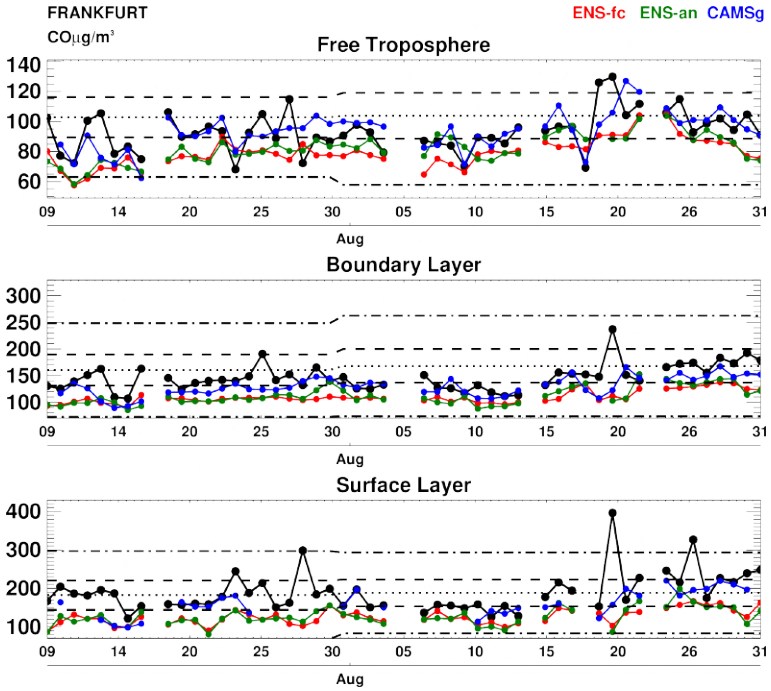

Figure 5.6.b. Same as Fig. 5.6.a. for the period from 9 July to 31 August 2019.

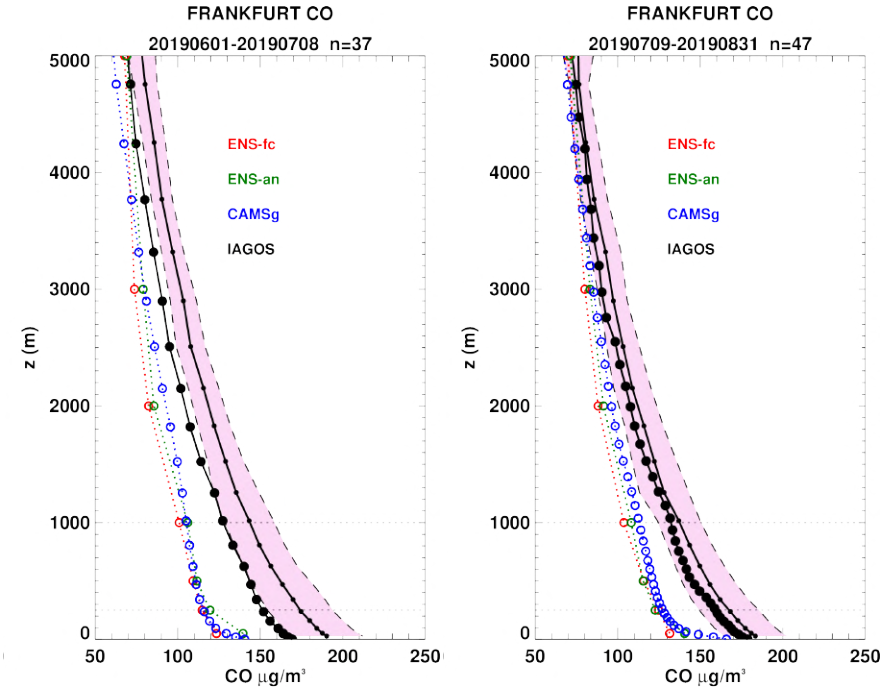

Figure 5.7. Profile of CO at Frankfurt for the period JJA 2019. The regional ensemble and associated analysis are shown in red and green respectively, and the global o-suite is shown in blue. The shaded area indicates the range of the mean climatology of the observations plus/minus one standard deviation during the same period for all years between 2003 and 2016 (level 2 data).

3000 m as shown on the individual profiles of Figure 5.8.a-b for days of 26, 27 and 30 June, 1st and 7 July. The results of CAMS global appear very similar to those of the regional ensemble for these 3 episodes.

During this first period, in the free troposphere a small anomaly of ozone is also observed on 12 June (one standard deviation) with 120-400 µg/m^3 (Fig. 5.6.a). This anomaly is not captured by any of the models (Fig. 5.6.a and 5.8.a).

In the second sub-period between 9 July and 31 August, 3 high peaks of CO are observed in the surface layer all reaching at least 3 standard deviations. The most important one occurs around 20 August with nearly 400 µg/m^3, and the two other secondary peaks take place on 28 July and 26 August with concentrations of about 300 µg/m^3 respectively. Preceding the peaks of 28 July, day 23 and 25 July also present high CO near one standard deviation. Indeed, this last week of July corresponds to the second heat wave period over Europe previously mentioned in the ozone section. Daily values of CO in the surface layer often remain high as well (near one standard deviation) during the period from 20 to 31 august (Fig. 5.6.b). Individual profiles for all these episodes are presented in Fig. 5.8.b-d. Like for the CO episodes of June, ozone is largely underestimated by the regional ensemble and CAMS global, with slightly better performance from CAMS global as shown on the time series (Fig. 5.6.b). This better performance of CAMS global is more obvious at the end of August between day 20 and 31.

On 20 August, high values of ozone are also observed in the other layers up to the Free Troposphere with 240 µg/m^3 and 130 µg/m^3 in the boundary layer and free troposphere respectively. The day before (19 August) also present an similar anomaly in the free troposphere only (Fig. 5.8.c and 5.6.b). In the lowest layers the regional ensemble largely underestimated ozone as well as CAMS global. However, CAMS global performs well in the free troposphere while ozone remains underestimated by the regional ensemble.

As regards the results of the individual models, some profiles are presented in Fig. 5.9.a-c showing examples related to the episodes described above and also example of cases with where individual models present different behaviours. In general the results of the models are very similar with most differences in the lowest layers. On many profiles, the EURAD model presents larger values of CO than the other models, and in these cases is often in better agreement with observations than the other models (0620, 0626, 0629, 0630). This behaviour is not systematically related to the high CO episodes, as shown when comparing profiles for 26 June, 28 July and 20 August. The SILAM model sometimes also presents much larger values of CO in the low troposphere as compared to other models, but this occurs rarely (0606 and 0624).

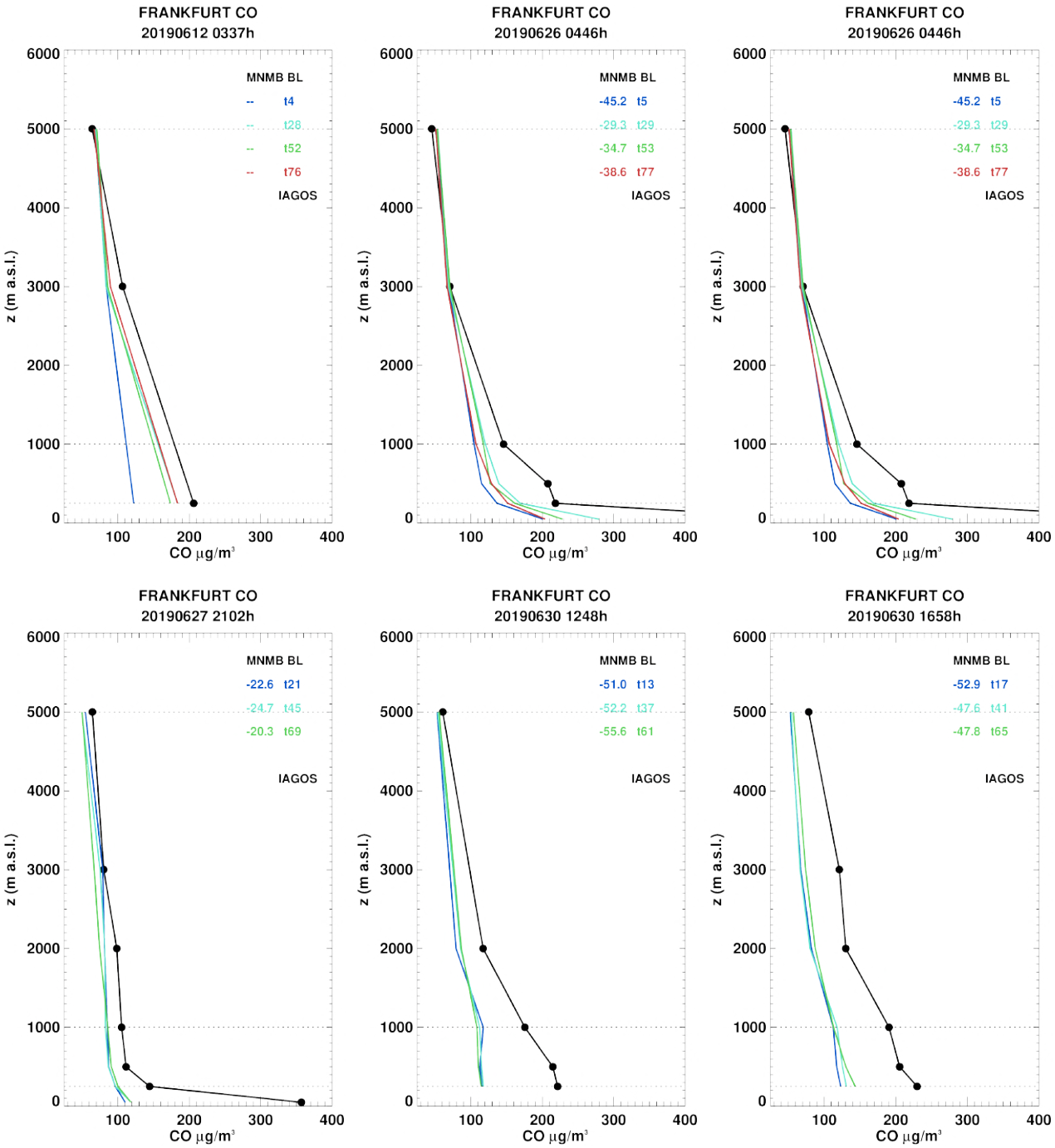

Figure 5.8.a. Selection of CO profiles at Frankfurt during the period JJA 2019. The ensemble is shown at 4 forecast times (blue: 1-day; cyan: 2-day; green: 3-day; red: 4-day).

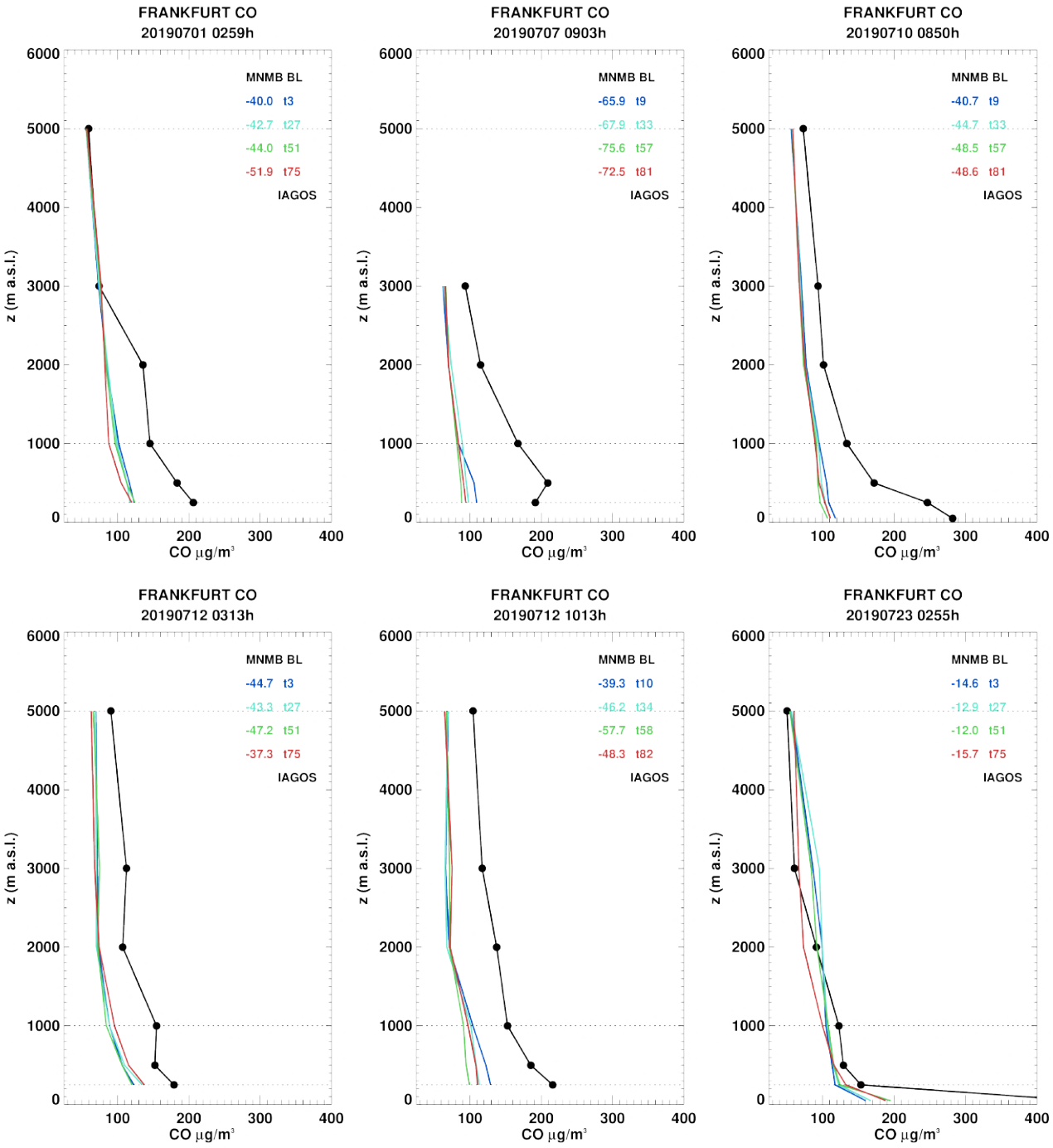

Figure 5.8.b. Selection of CO profiles at Frankfurt during the period JJA 2019. The ensemble is shown at 4 forecast times (blue: 1-day; cyan: 2-day; green: 3-day; red: 4-day).

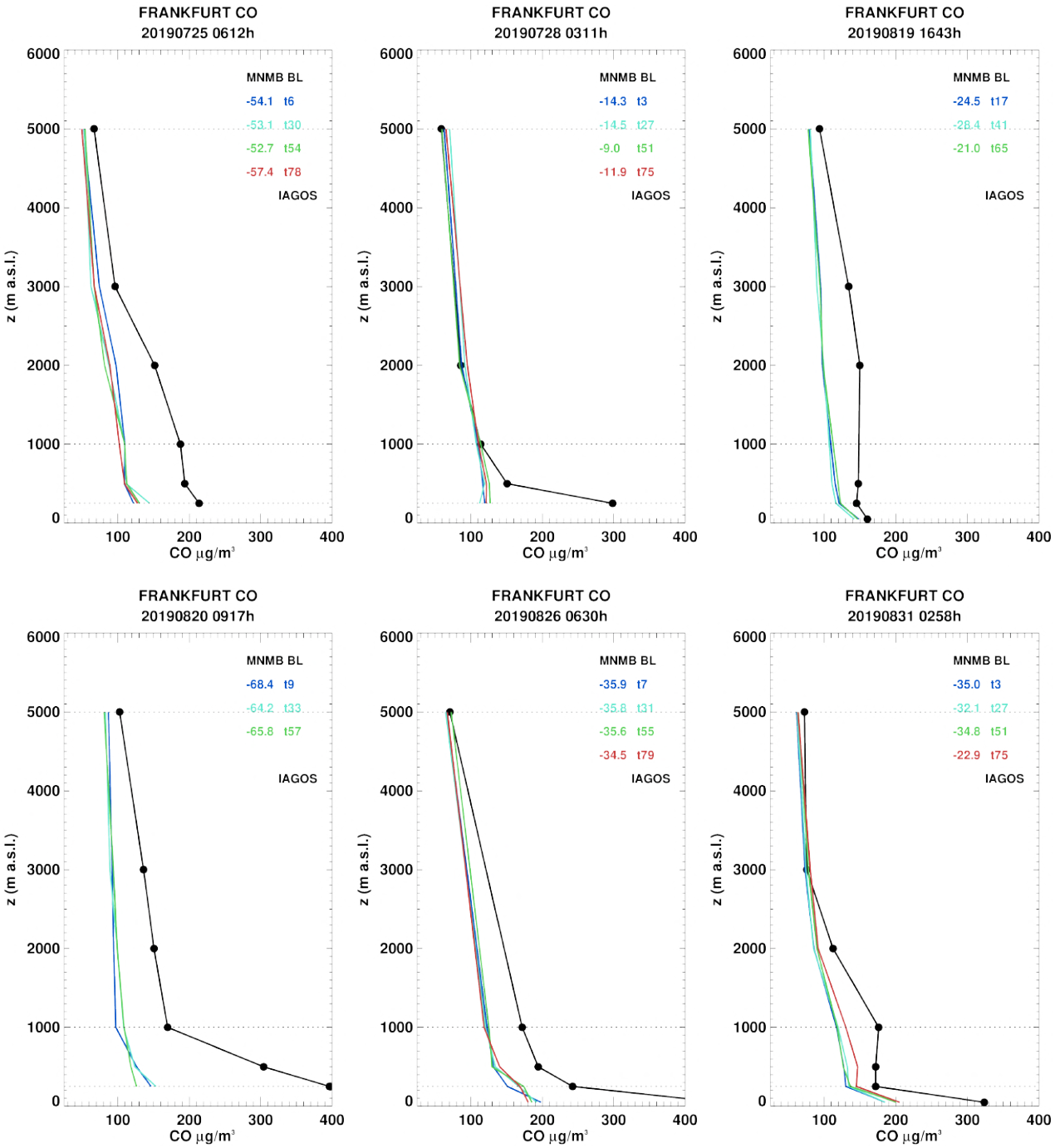

Figure 5.8.c. Selection of CO profiles at Frankfurt during the period JJA 2019. The ensemble is shown at 4 forecast times (blue: 1-day; cyan: 2-day; green: 3-day; red: 4-day).

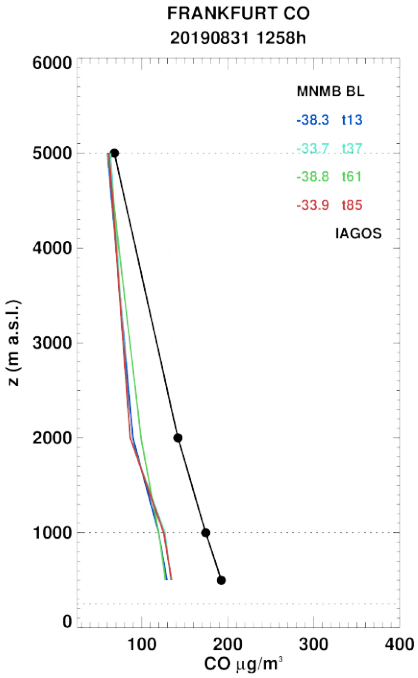

Figure 5.8.d. Selection of CO profiles at Frankfurt during the period JJA 2019. The ensemble is shown at 4 forecast times (blue: 1-day; cyan: 2-day; green: 3-day; red: 4-day).

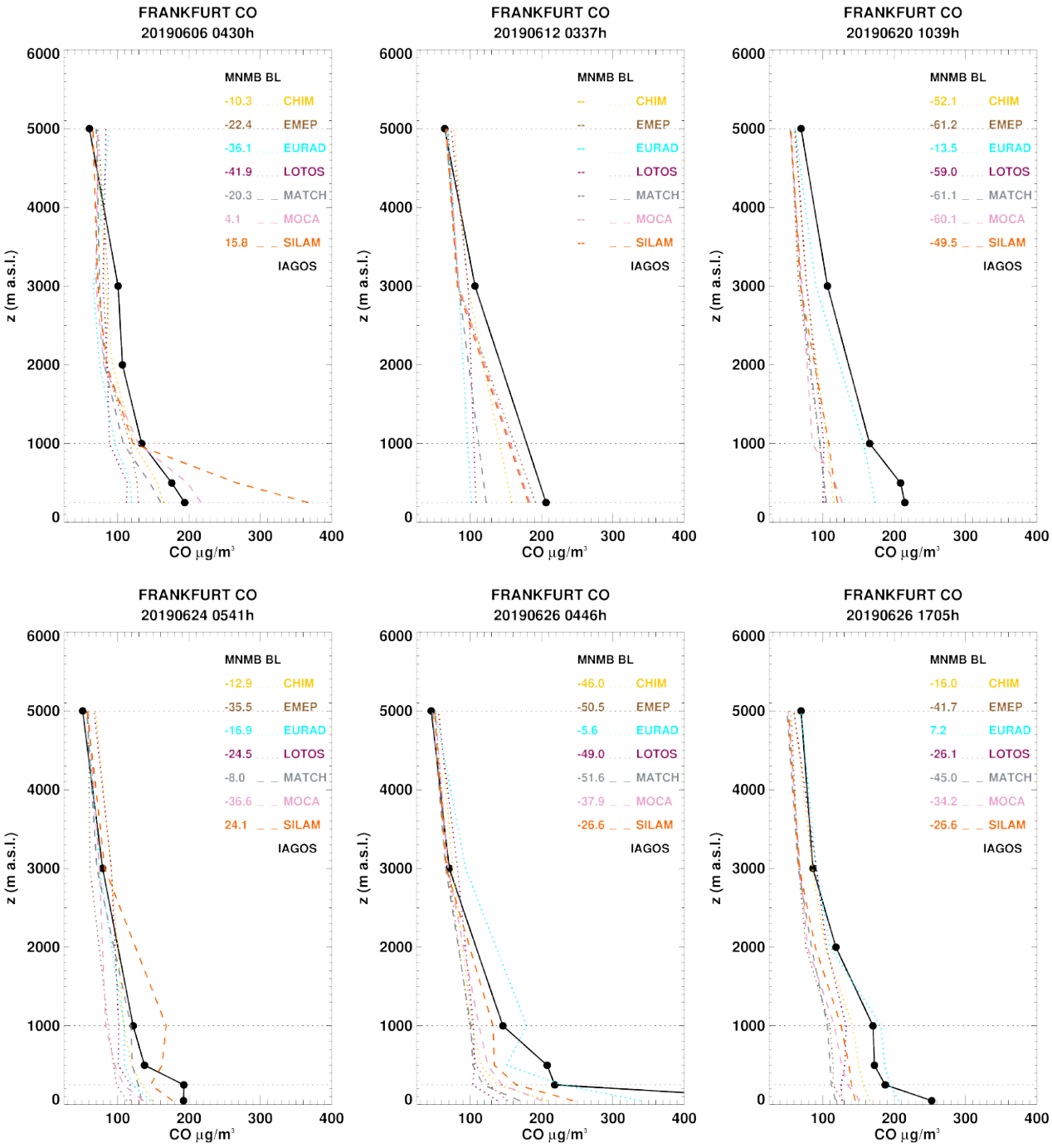

Figure 5.9.a: CO profiles at Frankfurt during the period JJA 2019. Each color/ Line style corresponds to one of the 7 models for the ensemble. In the legend, the models are CHIM=CHIMERE, EMEP=EMEP, SILAM=SILAM, LOTOS=LOTOS-EUROS, MOCA=MOCAGE, EURAD=EURAD, MATCH=MATCH.

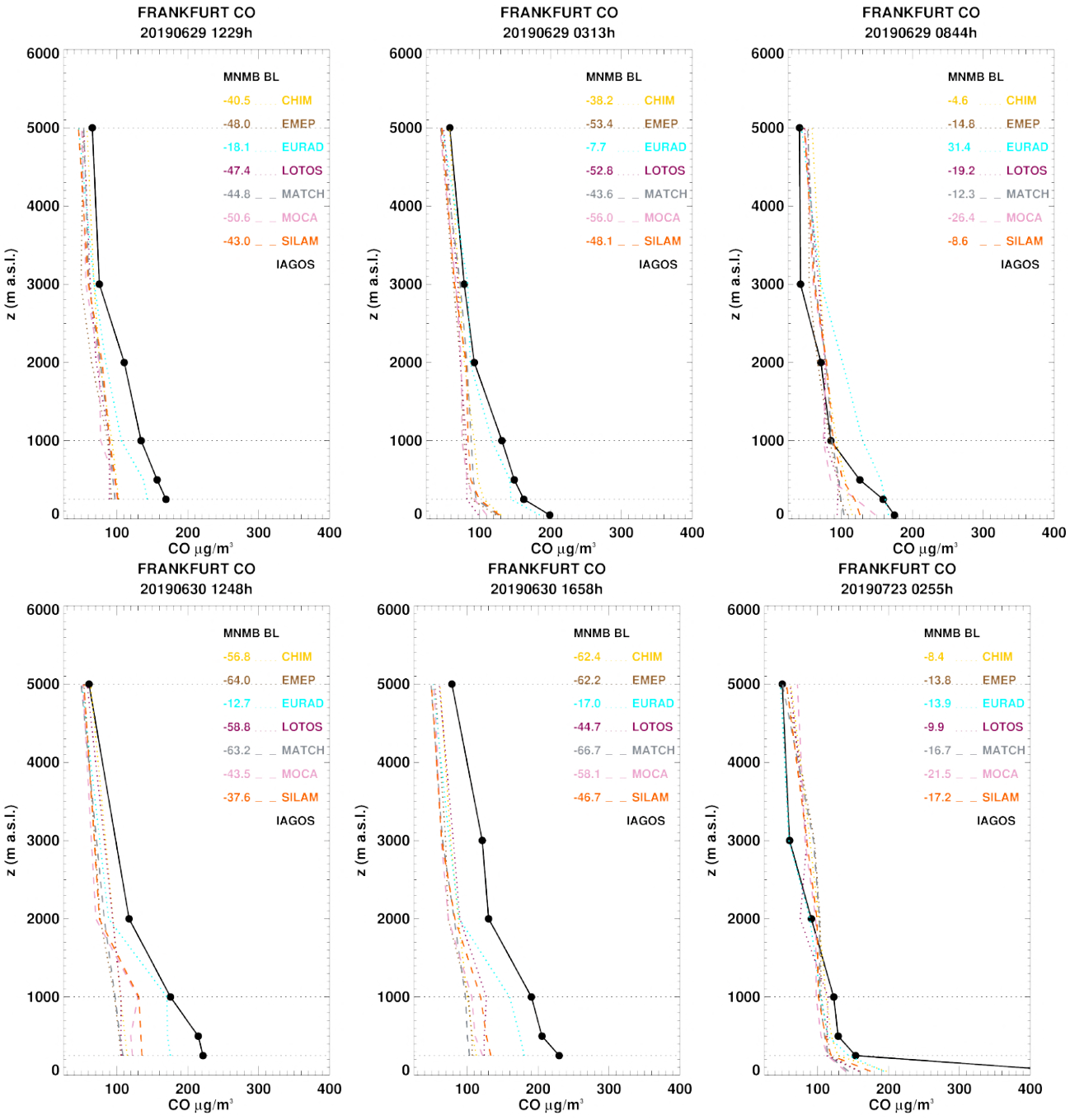

Figure 5.9.b: CO profiles at Frankfurt during the period JJA 2019. Each color/ Line style corresponds to one of the 7 models for the ensemble. In the legend, the models are CHIM=CHIMERE, EMEP=EMEP, SILAM=SILAM, LOTOS=LOTOS-EUROS, MOCA=MOCAGE, EURAD=EURAD, MATCH=MATCH.

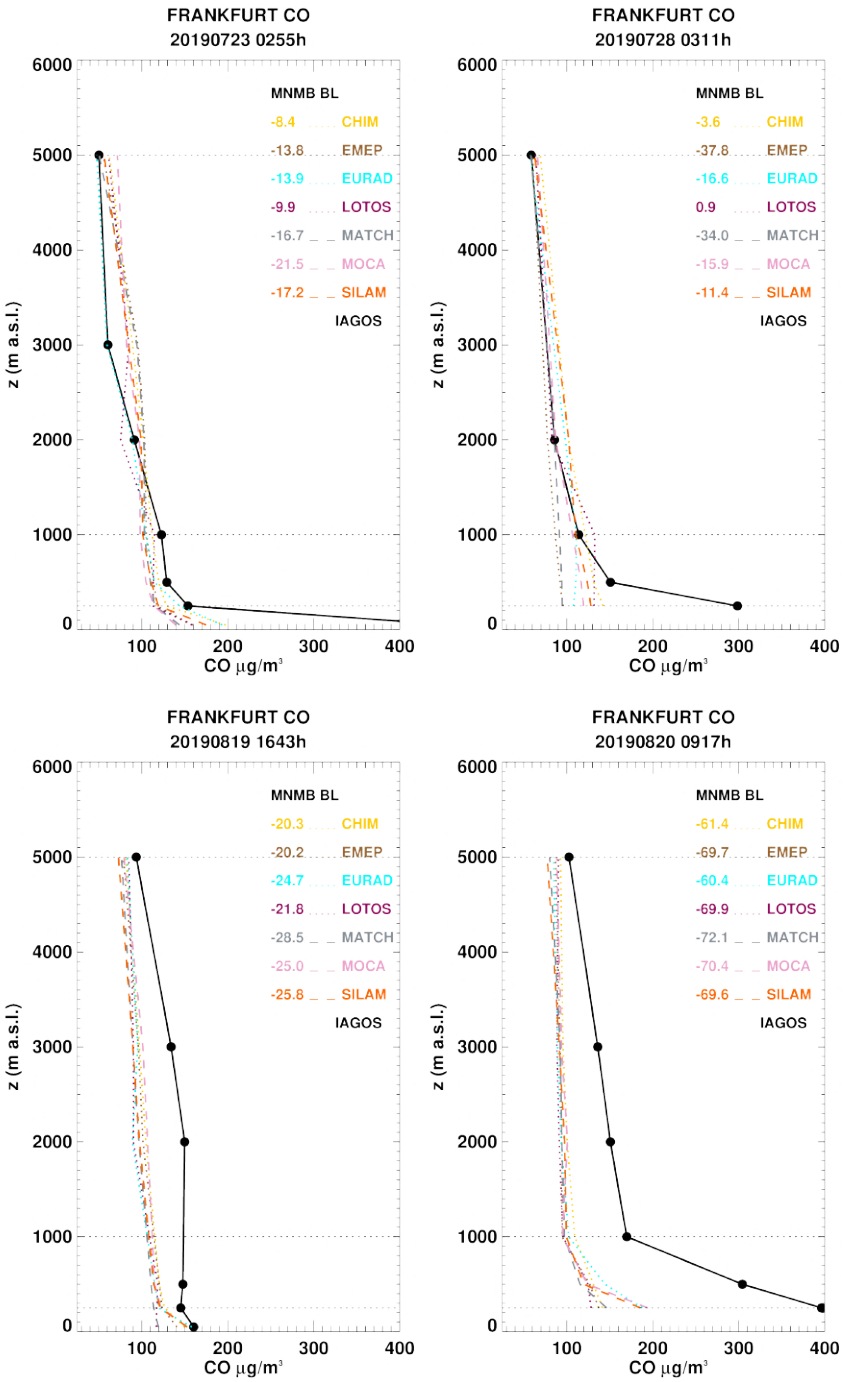

Figure 5.9.c: CO profiles at Frankfurt during the period JJA 2019. Each color/ Line style corresponds to one of the 7 models for the ensemble. In the legend, the models are CHIM=CHIMERE, EMEP=EMEP, SILAM=SILAM, LOTOS=LOTOS-EUROS, MOCA=MOCAGE, EURAD=EURAD, MATCH=MATCH.

6 Validation of regional model tropospheric NO_2 using MAX-DOAS

6.1 Summary

MAX-DOAS surface remote sensing observations provide tropospheric columns of NO_2, with the largest sensitivity in the boundary layer. The magnitude of VCDs derived from the measurements for the three urban stations De Bilt, Uccle and Bremen are reproduced rather well by the models. Although many of the model simulated values probably fall within the uncertainty range of MAX-DOAS retrievals, the latter alone cannot explain differences between retrievals and simulations, especially those found for variations in time. Moderate correlations on the order of 30-70 % are found for each station. The regional model ensemble performs significantly better than the global model in terms of correlation at each station. However, some of the larger NO_2 values inside individual pollution plumes are underestimated by the models.

6.2 Introduction

MAX-DOAS observations of atmospheric composition are performed by taking measurements of the scattered sunlight at different elevation (and sometimes also azimuthal) angles. Depending on the viewing angle and solar position, the light path through the atmosphere is different, with the observation in the zenith direction usually providing the shortest light path through the lower troposphere. Therefore, using the zenith measurement as intensity of incident radiation and the observations in other angles as intensity of transmitted radiation, the total amount of molecules of a certain species along the light path difference, the so-called slant column densities, can be determined using Lambert Beer's law. Using radiative transfer modelling and Optimal Estimation techniques, this can be inverted to tropospheric columns and even lower altitude tropospheric profiles.

The advantage of MAX-DOAS measurements is their ability to observe several pollution related species at the same time (e.g. NO_2, HCHO, CHOCHO, SO_2, aerosols, potentially also O_3) and to provide data which is virtually free of interferences from other species such as PAN or NO_y for NO_2. Also, the fact that the observations integrate over a comparatively large volume can be an advantage for satellite and model validation as the observed quantity is relatively close to the modelled one. On the other hand, the uncertainty of the retrievals is considerable (on the order of 30% for NO_2 tropospheric columns and larger for individual layers) and depends on cloud occurrence and aerosol loading.

In this report, regional air quality model forecasts of tropospheric NO_2 columns are compared to MAX-DOAS retrievals from 3 urban stations (De Bilt– KNMI, Bremen – IUP-UB, Uccle - BIRA-IASB). The reader is referred to previous reports for comparisons from the rural station OHP (BIRA-IASB) (which showed in general an underestimation by the model ensemble and an overall better performance for the o-suite here) as the instrument at this site stopped working in March 2017. Profile retrieval and averaging kernel data are available for Bremen and Uccle, but not for De Bilt, where a block profile is assumed in the MAX-DOAS retrieval and where column averaging kernels are estimated based on the box air mass factor for each observation layer. An overview of the station data is given by Table 6.1.

6.3 Intercomparison Method

Model VCDs (vertical column densities) have been calculated based on regional model data interpolated to MAX-DOAS output altitudes. Column averaging kernels (AVKs) from the measurements were applied to model NO_2 partial columns before summing up NO_2 values in the vertical:

$$VCD_{method2}^{model} = \sum_{i=1}^{Nobs} AVK_i \cdot VCD_i^{model}$$

The averaging kernels are part of the profiling output and represent the sensitivity of the retrieved column to the NO_2 amount at different altitudes. As the sensitivity of MAX-DOAS retrievals is largest in the boundary layer, the application of averaging kernels from the measurements to model simulations can have a crucial influence on validation results.

Only those model values closest to the measurement time are used below. As the model output is given in hourly time steps, the maximum possible time difference between measurements and simulations shown here is 30 minutes.

6.4 Results

Figure 6.1 shows time series of tropospheric NO_2 VCDs derived from MAX-DOAS for the model ensemble. The magnitude of VCDs from the measurements for the three urban stations is reproduced by the models, retrievals show a larger variability of values compared to the models. Measurements and simulations don't agree very well for some of the time steps investigated. The models underestimate some of the larger NO_2 values inside individual pollution plumes. Models may fail to reproduce these peaks due to errors in NOx emissions, transport of NO_2 towards the stations and chemistry.

Vertical profiles of NO_2 partial columns are shown in Figure 6.2. Although all regional models overestimate values at lower altitudes for Uccle, the overall shape shows higher concentrations near the surface compared to higher altitudes for both, models and retrievals. CAMS-global shows an underestimation compared to MAX-DOAS at most levels for Uccle, the ensemble overestimates values at the lowest observation levels at this station. Note that the number of vertical levels shown in Figure 6.2 corresponds to the number of MAX-DOAS output levels and that the real number of independent vertical levels of the retrievals is generally lower (about 2 to 3 degrees of freedom). MAX-DOAS observations are most sensitive in the boundary layer, whereas for uppermost output levels retrievals do not differ much from the a-priori assumed within the retrievals.

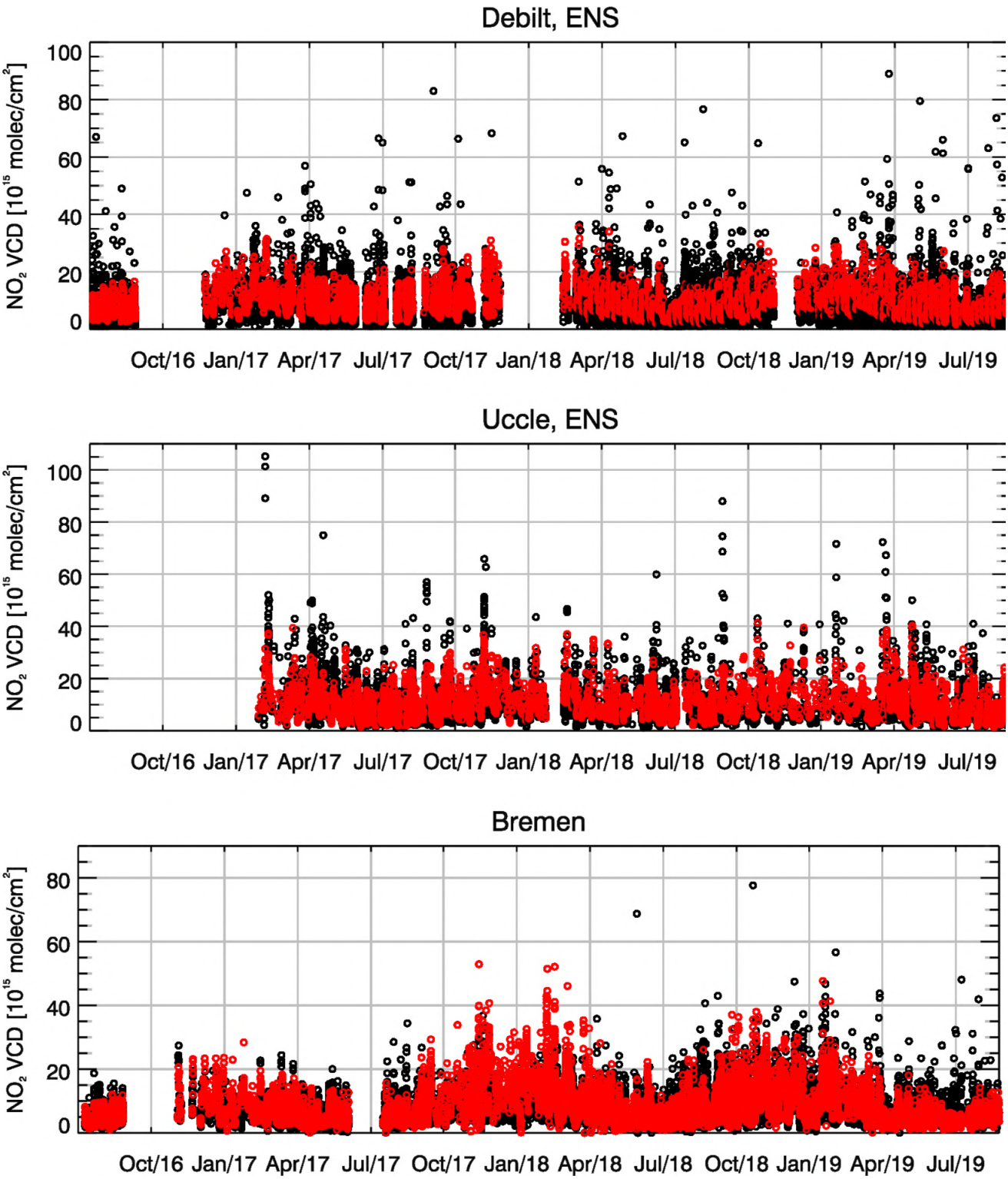

Figure 6.1. Time series of tropospheric NO_2 VCDs [10^{15} molec. cm^{-2}] from (black circles) MAX-DOAS and (red circles) the model ensemble for different stations. Model results were calculated by multiplying NO_2 partial columns with averaging kernels for each observation layer followed by summing up resulting values in the vertical. Model data was interpolated to observation layer altitudes prior to calculation of VCDs.

Table 6.1. Overview of MAX-DOAS station data used for validation of regional air quality model simulations. The time period covered in this report is July 2016 to August 2019. MAX-DOAS retrievals for De Bilt and Bremen are not available for August to October as well as large parts of November 2016 due to the CINDI-2 measurement campaign. Data from the instrument at Uccle is available since January 2017.

Station	Latitude, longitude	Altitude above sea level	Institution	Quantity	Character
Bremen (Germany)	53.106°N, 8.86°E	21 m	IUP-UB	column/ profile	urban
De Bilt (Netherlands)	52.1° N, 5.18° E	23 m	KNMI	column	urban
Uccle (Belgium)	50.8° N, 4.32° E	120 m	BIRA-IASB	column/ profile	urban

Figure 6.3 shows comparisons of diurnal cycles. Mean column amounts are comparable for urban stations. Regional models perform significantly better than CAMS-global for De Bilt and Uccle, where CAMS-global is negatively biased. Some regional models show different variations from one hour to another especially during the morning for Bremen, where rush hour peaks simulated by the models are not confirmed by the retrievals. This may be related to different photochemistry, scaling of emissions in time or vertical distribution of NO_2 and errors in simulating pollution transport towards the station. With respect to the ENSEMBLE, the simulation of diurnal cycles of tropospheric NO_2 columns depends on the location, with good to moderate results at urban stations.

Comparisons of weekly cycles are shown in Figure 6.4. Weekly cycles are underestimated by all models, with a stronger decrease of NO_2 columns from workdays towards the weekend retrieved by MAX-DOAS for all urban stations. Note that some variations of values from one day to another may just be coincidence due to data sampling.

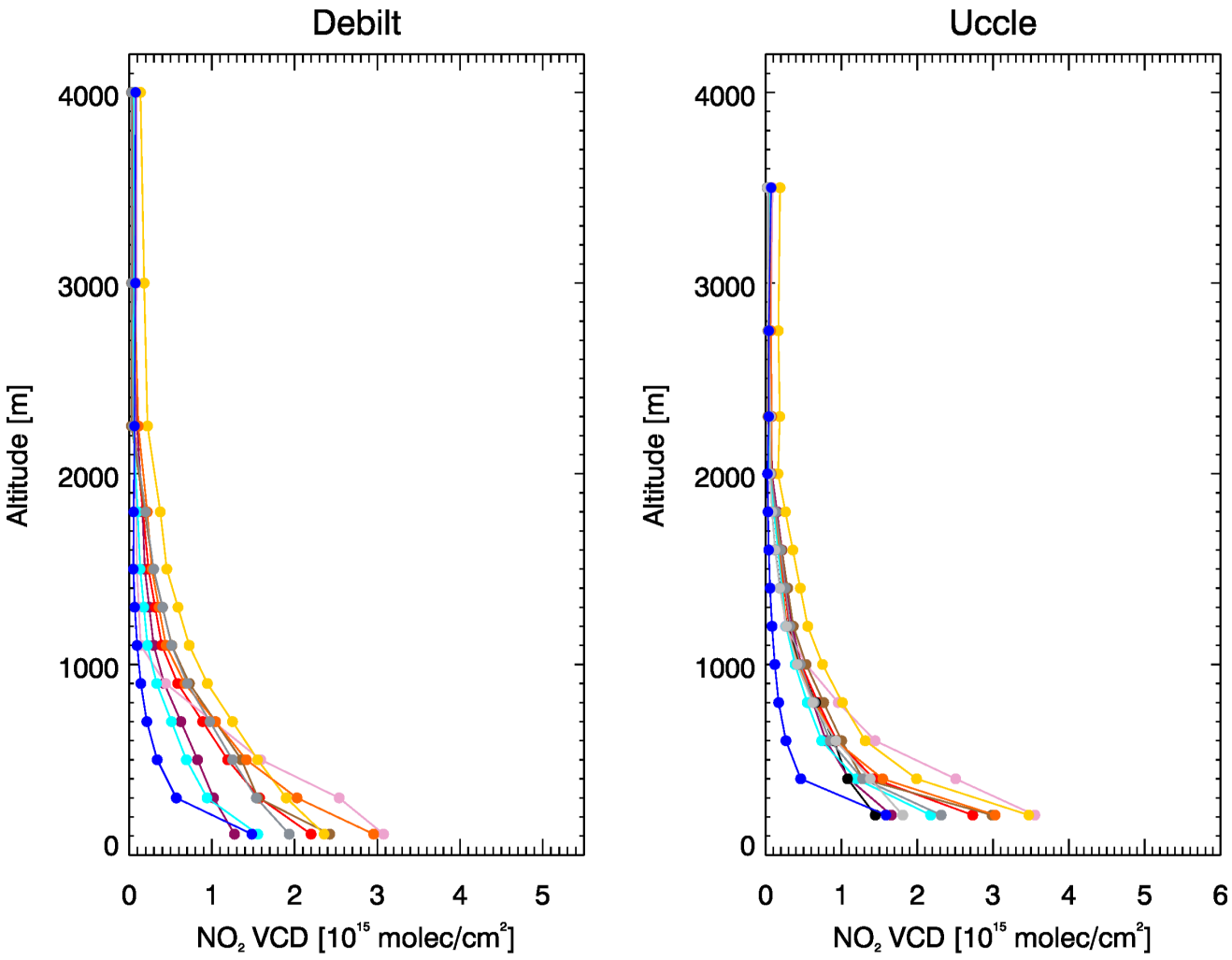

Figure 6.2. Vertical profiles of tropospheric NO_2 partial columns [10^{15} molec. cm^{-2}] for (left) De Bilt and (right) Uccle for the time period after the recent upgrade of CAMS-global 10 Jul - 31 Aug 2019. The black and light grey lines show the MAX-DOAS retrievals and a priori used for MAX-DOAS retrieval, respectively. All other lines refer to model data: (red) ensemble, (yellow) CHIMERE, (brown) EMEP, (orange) SILAM, (purple) LOTOS-EUROS, (cyan) EURAD-IM, (pink) MOCAGE, (grey) MATCH and (blue) CAMS-global. Model data was interpolated to observation layer altitudes. MAX-DOAS vertical profiles are not available for De Bilt for the investigated time period and only model results are shown for these stations accordingly. Profile plots for Bremen are currently not shown due to computational issues.

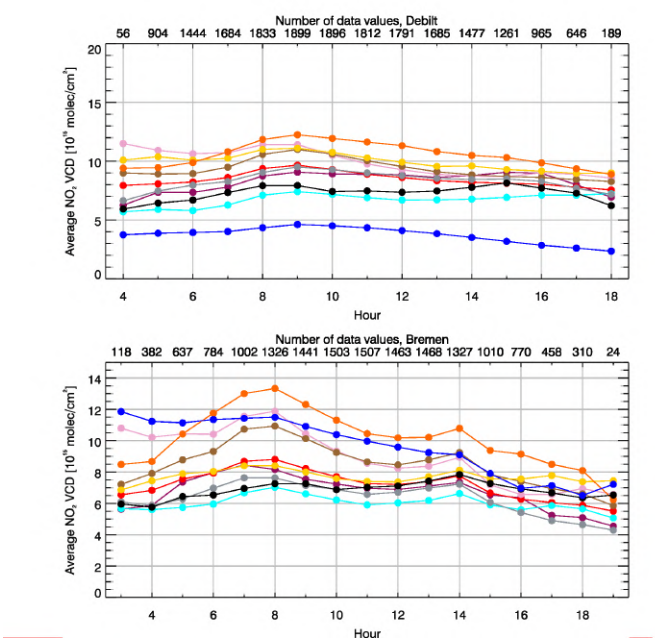

Figure 6.3. Diurnal cycles (averages over hourly bins) of tropospheric NO_2 VCDs [10^{15} molec. cm^{-2}] for (top left) De Bilt, (top right) Uccle and (lower left) Bremen. The black lines show the MAX-DOAS retrievals for JJA2019. All other lines refer to model data: (red) ensemble, (yellow) CHIMERE, (brown) EMEP, (orange) SILAM, (purple-blue) LOTOS-EUROS, (cyan) EURAD-IM, (pink) MOCAGE, (grey) MATCH and (blue) CAMS-global.

Scatter density plots or heat maps of tropospheric NO_2 VCDs from MAX-DOAS against model ensemble values corresponding to the time series displayed in Figure 6.1 as well as statistical values (root mean squared error, bias, correlation) are given in Figure 6.5. Corresponding statistical values for all individual models are given in Table 6.2. Moderate correlations on the order of 30-70 % are found for each station for all models, with the ENSEMBLE reaching the highest correlation of about 68 % at Uccle. Models tend to overestimate lower and underestimate higher NO_2 VCDs for the three urban stations. While the spread of values is quite large for individual data points, there is a good agreement between models and retrievals for the majority of measurements for urban stations (as shown by the high percentage of values close to the reference line). The ensemble performs significantly better than CAMS-global in terms of correlation for all stations. In contrast to the ENSEMBLE, CAMS-global has a strong negative bias at De Bilt and Uccle.

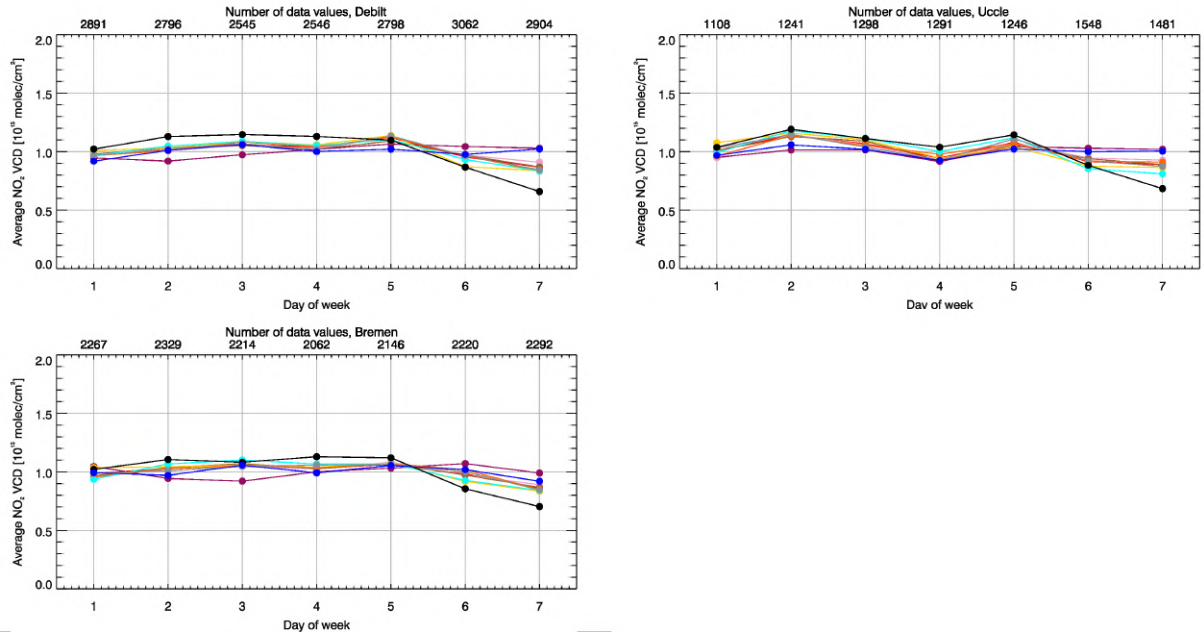

Figure 6.4. Weekly cycles (averages over daily bins divided by mean over whole week) of tropospheric NO_2 VCDs [10^{15} molec cm^{-2}] for (top left) De Bilt, (top right) Uccle and (lower left) Bremen averaged over JJA2019. The black lines show the MAX-DOAS retrievals. All other lines refer to model data: (red) ensemble, (yellow) CHIMERE, (brown) EMEP, (orange) SILAM, (purple) LOTOS-EUROS, (cyan) EURAD-IM, (pink) MOCAGE, (grey) MATCH and (blue) CAMS-global.

Table 6.2: Statistics on how tropospheric NO_2 VCDs [10^{15} molec. cm^{-2}] from models compare to MAX-DOAS retrievals at the four stations. Each column entry shows from left to right: root mean squared error [10^{15} molec. cm^{-2}], bias [10^{15} molec. cm^{-2}] and correlation coefficient (cor).

	De Bilt	Uccle	Bremen
ENS	6.233/1.189/0.447	5.560/1.199/0.684	4.809/0.481/0.548
CHIMERE	7.133/2.655/0.394	7.426/3.393/0.559	4.854/0.727/0.520
EMEP	7.068/2.126/0.407	6.664/2.620/0.625	6.248/1.957/0.505
SILAM	8.052/3.493/0.401	6.877/2.655/0.640	8.869/3.798/0.504
LOTOS-EUROS	6.914/1.054/0.325	6.218/0.152/0.564	5.860/0.097/0.408
EURAD-IM	7.367/2.527/0.369	7.573/3.266/0.563	6.793/2.155/0.483
MOCAGE	6.109/-0.697/0.432	5.643/-0.892/0.661	4.628/-0.852/0.509
MATCH	6.537/1.149/0.429	5.771/0.868/0.653	5.082/-0.335/0.521
OSUITE	7.298/-3.534/0.298	8.093/-4.408/0.418	8.173/2.804/0.350

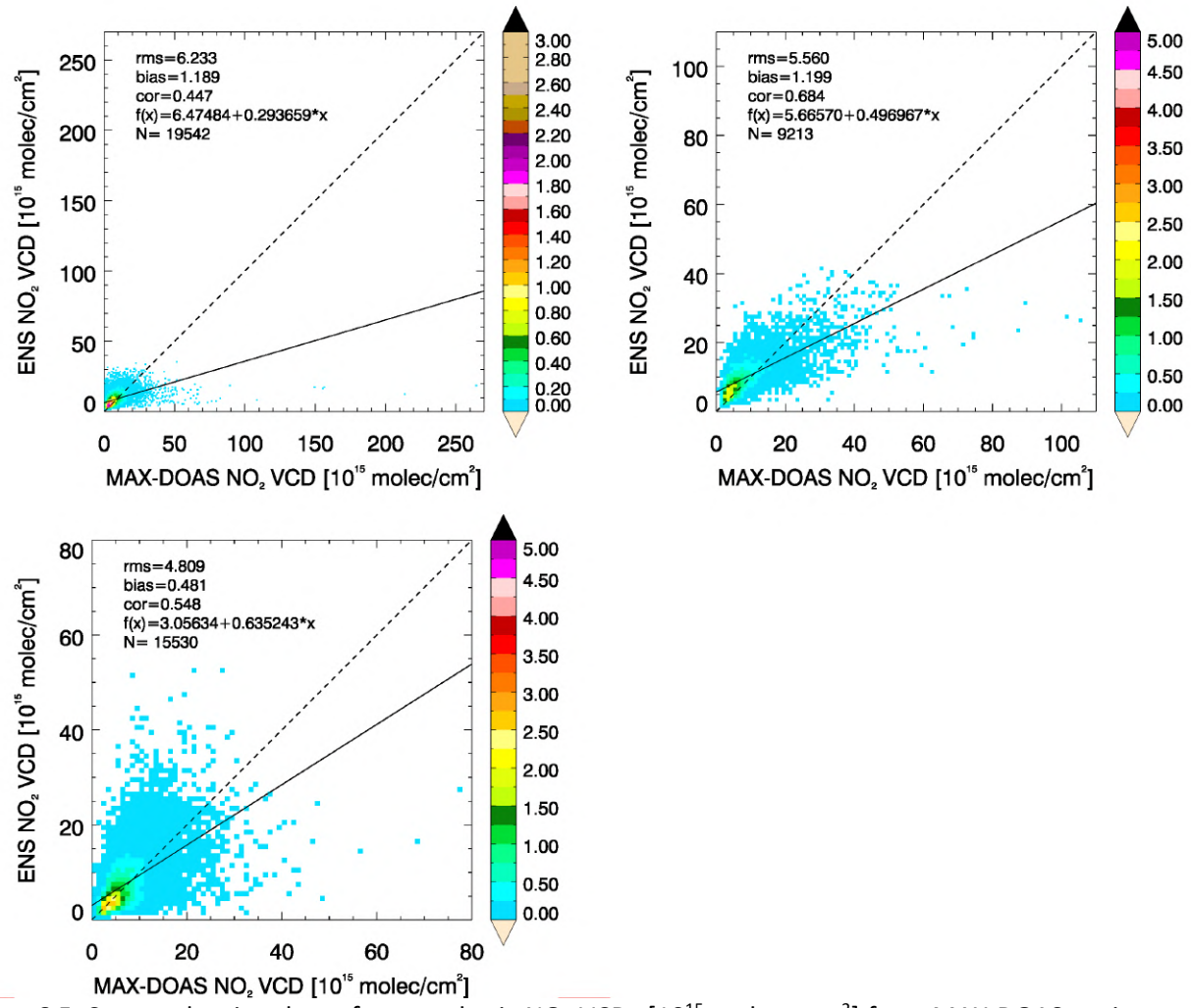

Figure 6.5. Scatter density plots of tropospheric NO_2 VCDs [10^{15} molec. cm^{-2}] from MAX-DOAS against model ensemble hourly data for (top left) De Bilt, (top right) Uccle and (lower left) Bremen for JJA2019. The data is shown with a bin size of 1 x 10^{15} molec. cm^{-2} and colour according to the number of data points per bin [%]. The dashed line is the reference line (f (x)=x). The solid line is the regression line (see top left of each plot for f(x) of this line). The root mean squared error (rms) [10^{15} molec. cm^{-2}], bias [10^{15} molec. cm^{-2}], pearson correlation coefficient (cor) as well as the number of data points N are given at the top left of each plot.

7 Validation of tropospheric NO_2 columns against satellite retrievals

7.1 Summary

Regional air quality model columns of tropospheric NO_2, derived from the output provided on 8 levels with a top at 5km, are compared to 9:30 local time GOME-2/MetOp-A NO_2 satellite retrievals (IUP-UB v1.0 product). The overall spatial distribution of tropospheric NO_2 is reproduced by the ensemble, but values over central European emission hotspots are significantly underestimated by the majority of the models during winter, which results in a strong underestimation over these regions and of the seasonal cycle for the ensemble. There are stronger shipping signals compared to the satellite data. As a result of a major regional model upgrade in June (2019), which includes the use of an updated European emissions inventory with improved estimates for North African and Middle Eastern anthropogenic emissions, enhanced tropospheric columns of NO_2 are now reproduced over these regions by all models. Differences between models and satellite observations may result from errors in anthropogenic emissions, photochemistry during winter months and from chemical processing inside ship plumes. In contrast to the analysis, the regional ENSEMBLE forecast shows a negative bias compared to the retrievals which is most pronounced for winter (~2-3 x 10^{15} molec/cm^2) but smaller during the rest of the year (overall ~0.5 x 10^{15} molec/cm^2). The negative bias is even larger for CAMS-global, which is in agreement with the stronger underestimation of values for European emission hotspots compared to regional models, demonstrating the benefit of running models at higher horizontal resolution. A systematic negative bias is however not present in the analysis for seasons other than winter.

7.2 Comparison with GOME-2 NO_2

In this section, regional air quality model columns of tropospheric NO_2 are compared to GOME-2/MetOp-A NO_2 satellite retrievals (IUP-UB v1.0) [Richter et al., 2011]. This satellite data provides excellent coverage in space and time and very good statistics. However, only integrated tropospheric columns are available, and the satellite data is always taken at 09:30 LT for GOME-2 and at clear sky only. Therefore, model data are vertically integrated, interpolated in time and then sampled to match the satellite data. Uncertainties in NO_2 satellite retrievals are large and depend on the region and season. Winter values in mid and high latitudes are usually associated with larger error margins. As a rough estimate, systematic uncertainties in regions with significant pollution are on the order of 20% – 30%. Conclusions may differ for comparisons to other satellite NO_2 products (e.g. TEMIS GOME-2, http://www.temis.nl shows lower retrieved NO_2 values for January). It should be noted here that model data is only available for altitudes up to 5000 m, meaning that (depending on tropopause height) tropospheric model columns may not be representative of the total amount of NO_2 in the troposphere. Note that since the CAMS-global upgrade of 26 June 2018, GOME-2 observations are assimilated by the global system. This is, however, a different retrieval product than what is used in the validation reported here (University of Bremen retrieval).

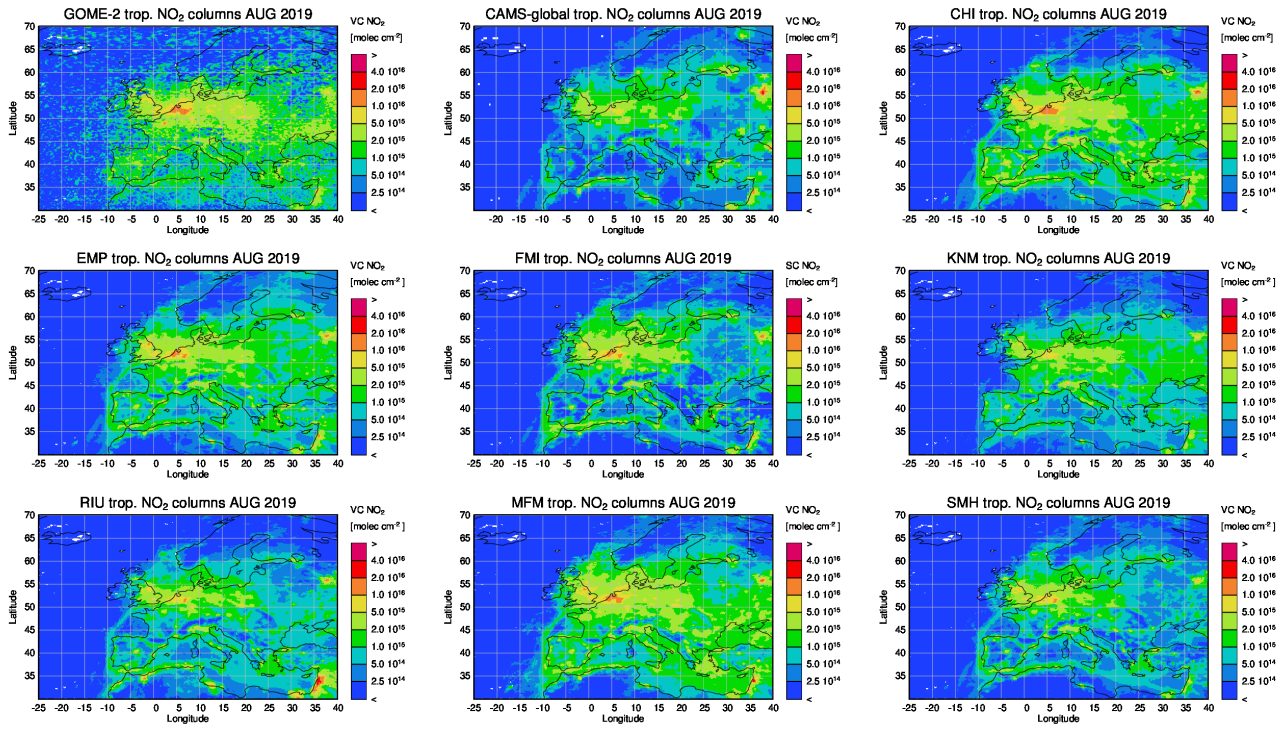

Figure 7.1. Maps of satellite-retrieved and model-simulated tropospheric NO_2 columns [molec cm^{-2}] for August 2019 for from left to right: (top row) GOME-2, CAMS-global and CHIMERE; (middle row) EMEP, SILAM and LOTOS-EUROS; (lower row) EURAD-IM, MOCAGE and MATCH. GOME-2 data were gridded to regional model resolution (i.e. 0.1° x 0.1°). Model data were treated with the same reference sector (25°W - 20°E) subtraction approach as the satellite data and linearly interpolated to the satellite overpass time (9:30 LT).

Figure 7.1 shows maps of monthly mean tropospheric NO_2 columns from GOME-2, regional models and CAMS-global for August 2019. The overall spatial distribution and magnitude of tropospheric NO_2 is reproduced by the regional models in principle. There are stronger shipping signals in all models compared to the satellite data, which may result from errors in anthropogenic emissions or from chemical processing inside the ship exhaust plumes (see e.g. Vinken et al., 2014).

Compared to CAMS-global, regional models perform better for Central European emission hotspots, showing the benefit of higher horizontal resolution runs. Prior to this report, as emissions over Lebanon and Israel were not included in the TNO emission inventory, the majority of the seven regional models failed to reproduce enhanced tropospheric NO_2 columns over these areas in contrast to the o-suite. As a result of a major regional model upgrade in June (2019), which includes the use of an updated European emissions inventory with improved estimates for North African and Middle Eastern anthropogenic emissions, enhanced tropospheric columns of NO_2 are now reproduced over these regions by all models.

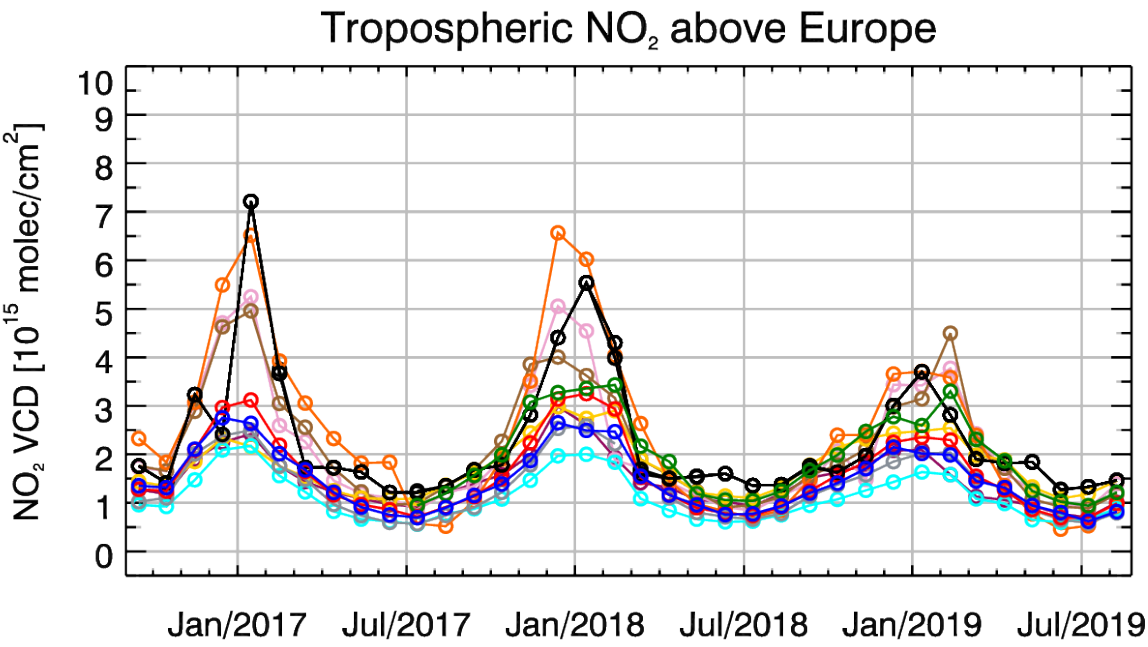

Figure 7.2. Time series of monthly averaged tropospheric NO_2 columns [10^{15} molec cm^{-2}] retrieved by (black) GOME-2 and simulated by (red) ensemble, (yellow) CHIMERE, (brown) EMEP, (orange) SILAM, (purple) LOTOS-EUROS, (cyan) EURAD-IM, (pink) MOCAGE, (grey) MATCH and (blue) CAMS-global. GOME-2 data were gridded to regional model resolution (i.e. 0.1° x 0.1°). Model data were treated with the same reference sector (25°W - 20°E) subtraction approach as the satellite data and linearly interpolated to the satellite overpass time (9:30 LT).

Figure 7.2 shows time series of monthly mean tropospheric NO_2 columns for GOME-2 and the models. The seasonal variation is better reproduced by SILAM, MOCAGE and EMEP than by the other models. The latter clearly underestimate the seasonal cycle over Europe due to the strong underestimation of values in winter described above. The regional ENSEMBLE forecast shows a negative bias compared to the retrievals which is most pronounced during winter (~2-3 x 10^{15} molec/cm^2) but smaller during the rest of the year (overall ~0.5 x 10^{15} molec/cm^2). One of the reasons for this may be that the regional model output is limited to 5 km altitude. Compared to the ensemble, the negative bias of CAMS-global is a bit larger, which is in agreement with the stronger underestimation over European emission hotspots for CAMS-global especially during winter. A systematic negative bias is not present in the regional model ensemble analysis for seasons other than winter. The decrease in retrieved wintertime maxima from 2017 to 2019 is not reproduced by the majority of regional models and CAMS-global.

8 Comparison with high-altitude EEA Air Quality e-reporting surface stations

8.1 Summary

European ozone EA Air Quality e-reporting measurements from high-altitude stations (above 1km) have been used to evaluate the regional models. Differences between the regional model orography and the true altitude of the station were used to select the model altitude level to compare with. The ensemble median mostly overestimates ozone levels during the period June 2019 - August 2019. More specific, depending on the station the observed ozone levels are reproduced to within -10% and 15% by the ensemble median D+0 forecast (1h-24h). Correlations observed were between 0.60 and 0.85 and the ensemble median D+0 forecast has a performance better than any of the individual seven models. Two (namely SILAM and MOCAGE) out of the 7 individual models were deviating significantly from the ensemble median in terms of MNMBs and 2 models (namely EURAD and SILAM) were deviating significantly from the ensemble median in terms of their correlations with observations. Validation metrics are also given for the ENS analysis. The ENS analysis has almost equivalent performance with ENS D+0 forecast in terms of MNMBs but performs better than ENS D+0 forecast in terms of correlations (significantly higher correlations).

8.2 Introduction

The seven models and their ENSEMBLE median (D+0 forecast as well as the analysis) have been compared against Background-Rural EA Air Quality e-reporting measurements for surface stations at elevation greater than 1000 m above mean sea level (http://www.eea.europa.eu/data-and-maps/data/airbase-the-european-air-quality-database-7). Elevated stations were selected to fall within classes 1-2 in the O_3 Joly-Peuch (2012) classification for EA Air Quality e-reporting NRT stations. Table 8.1 shows the stations altitude above mean sea level together with the LOTOS-EUROS model altitude (i.e. from model's topography) pertaining to the nearest to the station grid point. Modelled gas mixing ratios were extracted at the model level, which is closest to the stations altitude as defined from the orography (see column 7 in Table 8.1).

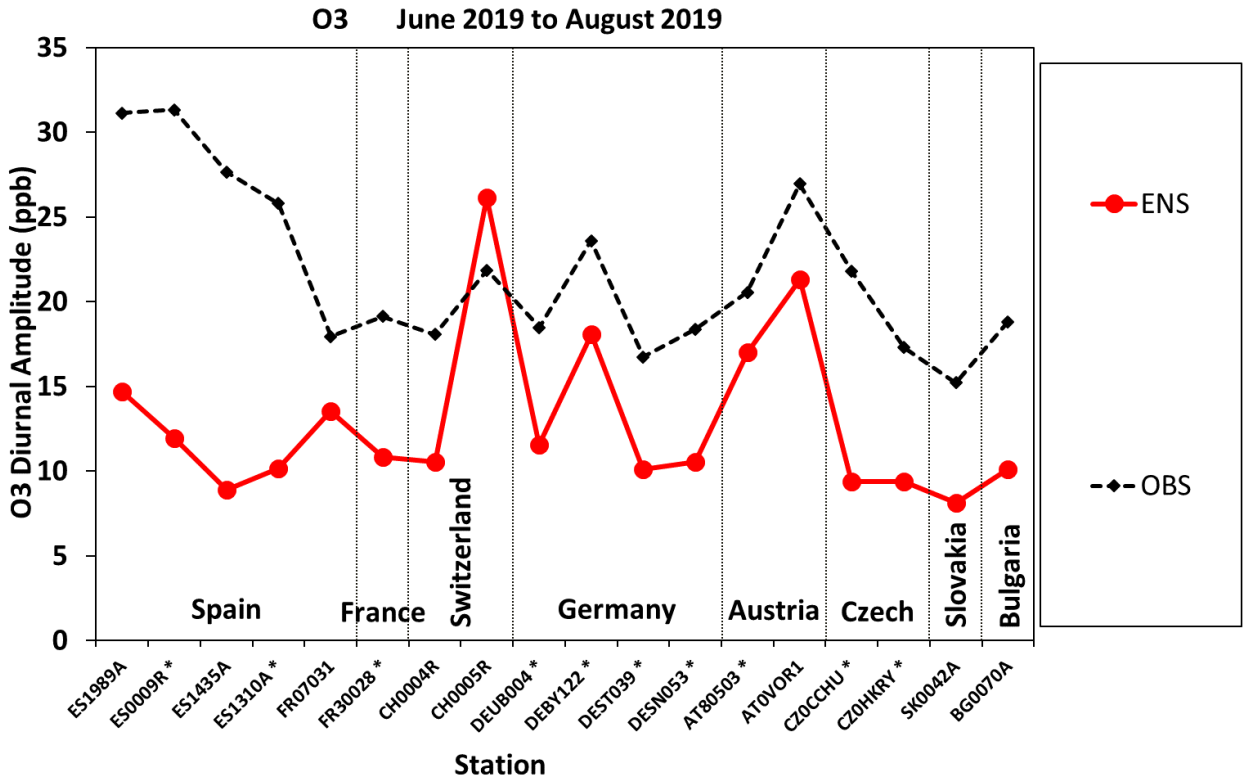

Figure 8.1. Amplitude of the diurnal cycle as measured (ppb) from stations observations (black diamonds) and as calculated from the Ensemble Mean fc D+0 (red circles). With asterisks are denoted stations used in the assimilation process.

Table.8.1: Background-Rural EEA Air Quality e-reporting Stations (with NRT data) with Elevation higher than 1000 m.

Station Name	Stat_id	Longitude	Latitude	real Altitude	model Altitude	nearest Level	use in CAMS50
Lario	ES1989A	-5.09	43.04	1140	1199	0	validation
Capmisabalos	ES0009R	-3.14	41.27	1360	1124	2	assimilation
Vilafranca	ES1435A	-0.25	40.42	1125	907	2	validation
Torrelisa	ES1883A	0.18	42.46	1005	1282	0	validation
Ak- Pardines	ES1310A	2.21	42.31	1226	1117	1	assimilation
Chaumont	CH0004R	6.98	47.05	1136	727	3	-
Rageade	FR07031	3.28	45.11	1040	944	2	validation
Schlucht	FR30028	7.01	48.05	1200	520	3	assimilation
Schauinsland	DEUB004	7.91	47.91	1205	554	3	assimilation
Rigi-Seebodenalp	CH0005R	8.46	47.07	1031	997	1	validation
Sulzberg im Bregenzerwald	AT80503	9.93	47.53	1020	961	1	assimilation
Bad Hindelang/Oberjoch	DEBY122	10.40	47.52	1169	1150	0	assimilation
Brocken	DEST039	10.62	51.80	1130	302	4	assimilation
Fichtelberg	DESN053	12.95	50.43	1214	555	3	assimilation
Vorhegg bei Kötschach-Mauthen	AT0VOR1	12.97	46.68	1020	1427	0	validation
Churanov	CZ0CCHU	13.62	49.07	1118	739	4	assimilation
Krkonose-Rychory	CZ0HKRY	15.85	50.66	1001	530	4	assimilation
Bratislava - Jeséniova	SK0042A	20.99	48.78	1244	445	5	validation
Vitosha mountain	BG0070A	23.24	42.64	1321	863	4	-

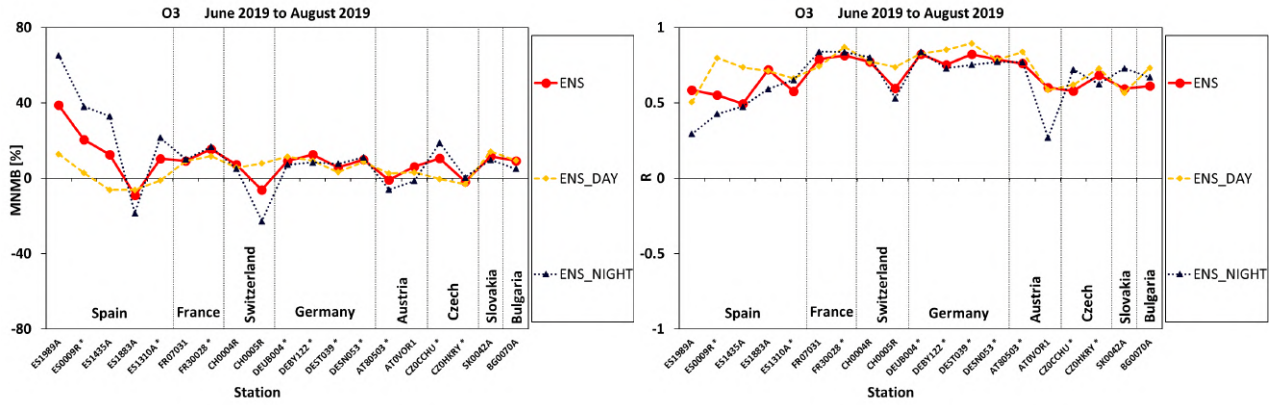

Figure 8.2. MNMBs [%] (left) and temporal correlations (right) calculated for the ENSEMBLE model for during daytime (orange) nighttime (dark blue) as well as for the whole day (red) for the JJA 2019 period. With asterisks are denoted stations used in the assimilation process.

For the validation, hourly O_3 concentration values (µg/m^3) are extracted from the seven models as well as for the Ensemble Mean. It should be noted that, in the EEA Air Quality e-reporting network the O_3 measurements that were made by the instrument in ppb were converted from ppb to µg/m^3, following the EU directive 2008/50, i.e. by multiplying by 2. This conversion is approximately correct for low altitude stations. However, at high altitude stations pressure and temperature should be taken into account when converting from ppb to µg/m^3 and vice versa. As hourly pressure and temperature data were not available for all EEA Air Quality stations the comparison between observed and modelled ozone was done by re-converting both modelled and observed hourly O_3 concentration in ppb. For modelled ozone values the conversion was done by applying the following ideal gas equation with the model's estimates of temperature (T) and pressure (P) (from CAMS global):

$$O3\ (\text{in ppb}) = O3\ (\text{in mg/m3}) * \left(\frac{R * T}{p_m * M_{o3}}\right)$$

8.3 Regional ensemble results

In the previous report it was shown that comparing the observed and modelled amplitude of the diurnal variation of ozone at each high-altitude station could provide a criterion concerning the exposure suitability of the stations. We found out in this report that an additional criterion is needed to differentiate stations as to their suitability in exposure. The additional criterion is the correlation coefficients between the amplitude of the diurnal cycle as observed and modelled to be statistically significant roughly higher than 0.3. Figure 8.1 shows the observed and modelled diurnal amplitude of ozone at each station, moving from Spain to Cyprus. Figure 8.2 shows the MNMBs and the correlation coefficients calculated for the ENSEMBLE model during daytime, at nighttime as well as for the whole day. We can see that the 2 criteria of diurnal amplitude and day and night MNMBs and correlation coefficients differentiate the 2 stations in Spain from all other stations. For the above-mentioned findings these 2 high altitude stations will be excluded from our analysis.

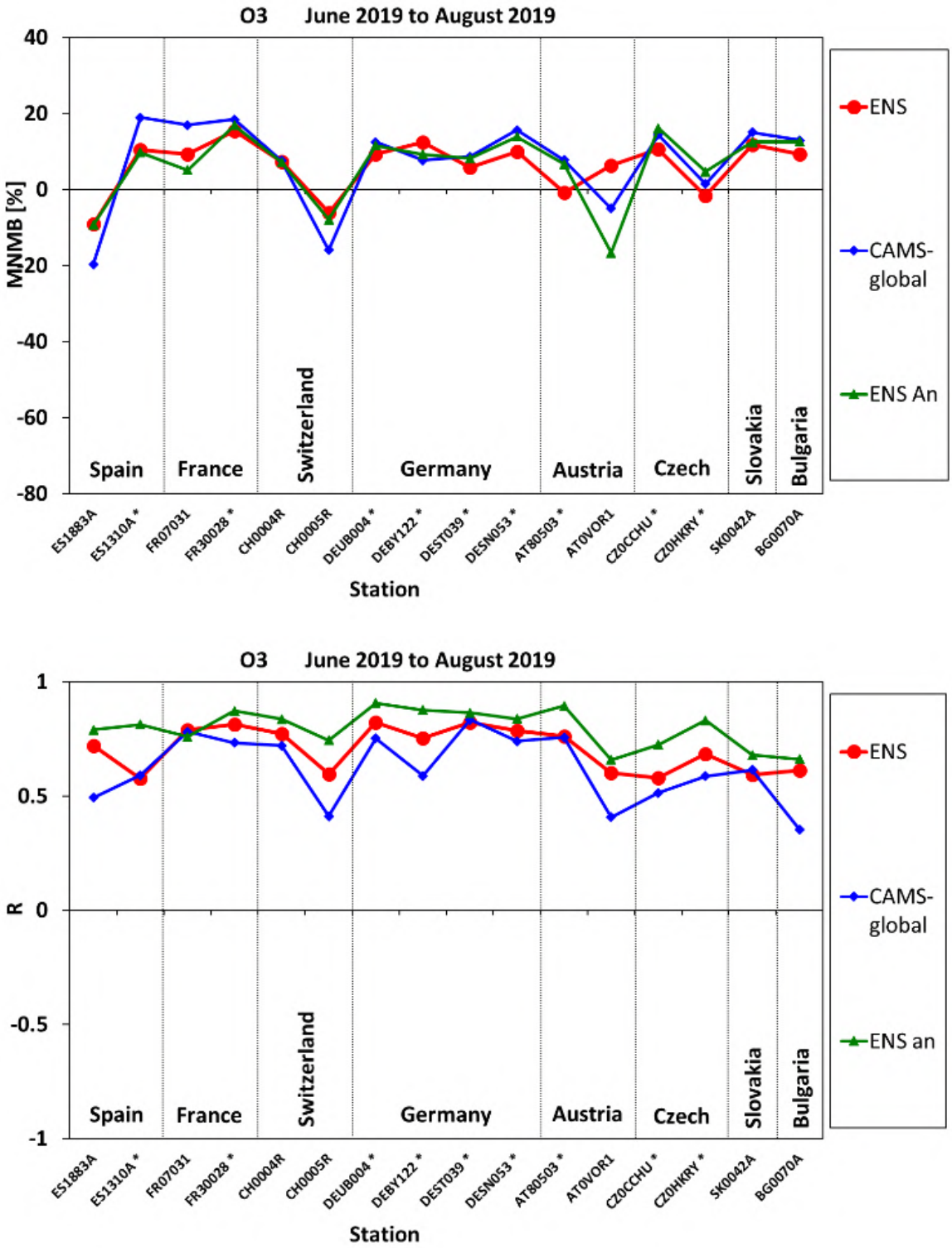

Figure 8.3. O_3 MNMBs [%] (top) and correlation coefficient (bottom) for the Ensemble mean (forecast D+0; red circles and analysis; green triangles) as well as for CAMS-global (forecast D+0; blue diamonds) for the period JJA 2019. With asterisks are denoted stations used in the assimilation process.

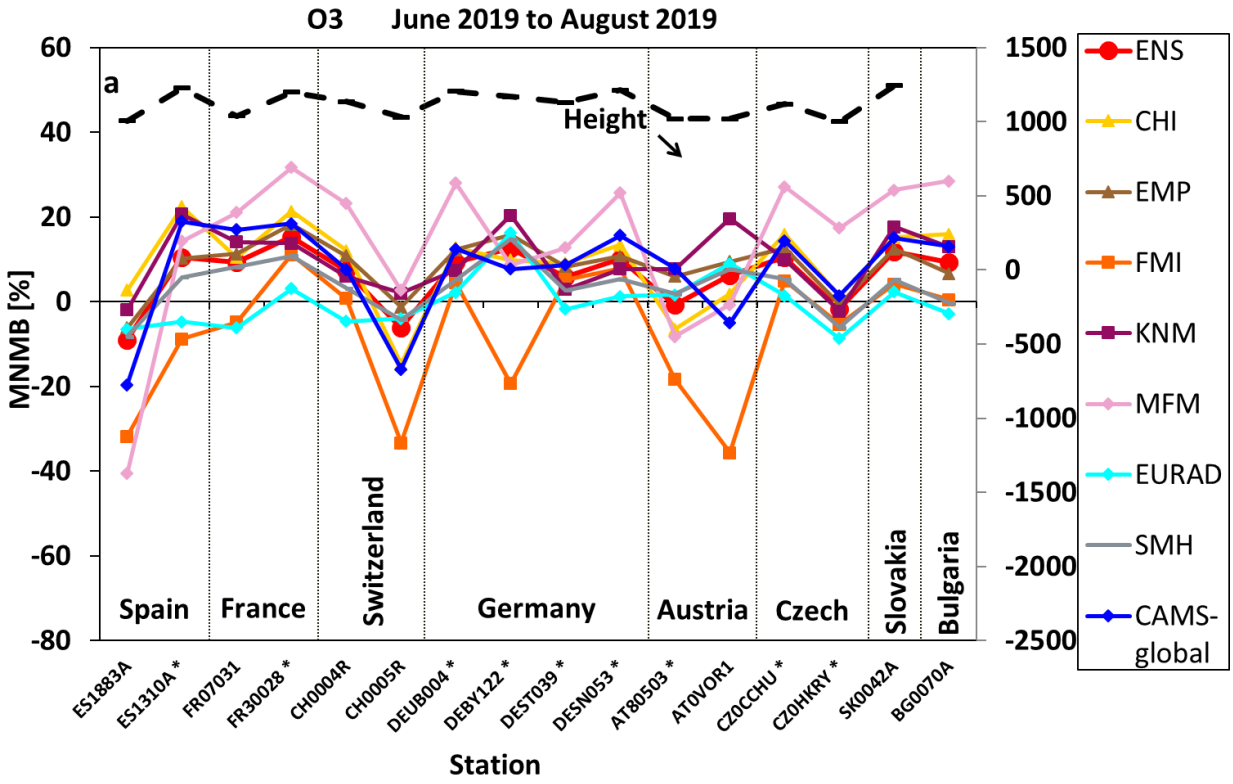

Fig. 8.4. Ozone MNMBs [%] for each one of the 7 models from the Ensemble mean and from CAMS-global (June to August 2019). With asterisks are denoted stations used in the assimilation process.

Figure 8.3 shows the Modified Normalized Mean biases (top) and correlation coefficients (bottom) at each of the remaining stations, moving from Spain to Bulgaria (i.e. from West to East) pertaining to the median of the Ensemble forecast (D+0) and analysis (D+0) as well as CAMS-global (D+0). The ensemble median mostly overestimates ozone levels during the period June to August 2019. Depending on the station the range of MNMB for the ENSEMBLE median D+0 forecast was found to be between -10% up to 15%. From Figure 8.3 (bottom panel) it is clear that the Ensemble Mean reproduces well the ozone variability. As it appears from Figs 8.3 (bottom panel) the correlation coefficients are highly significant ($0.60<r<0.85$). It should be noted that for the period June to August 2019 the ENSEMBLE analysis performs better than the ENSEMBLE D+0 forecast in terms of correlations (significantly higher correlations).

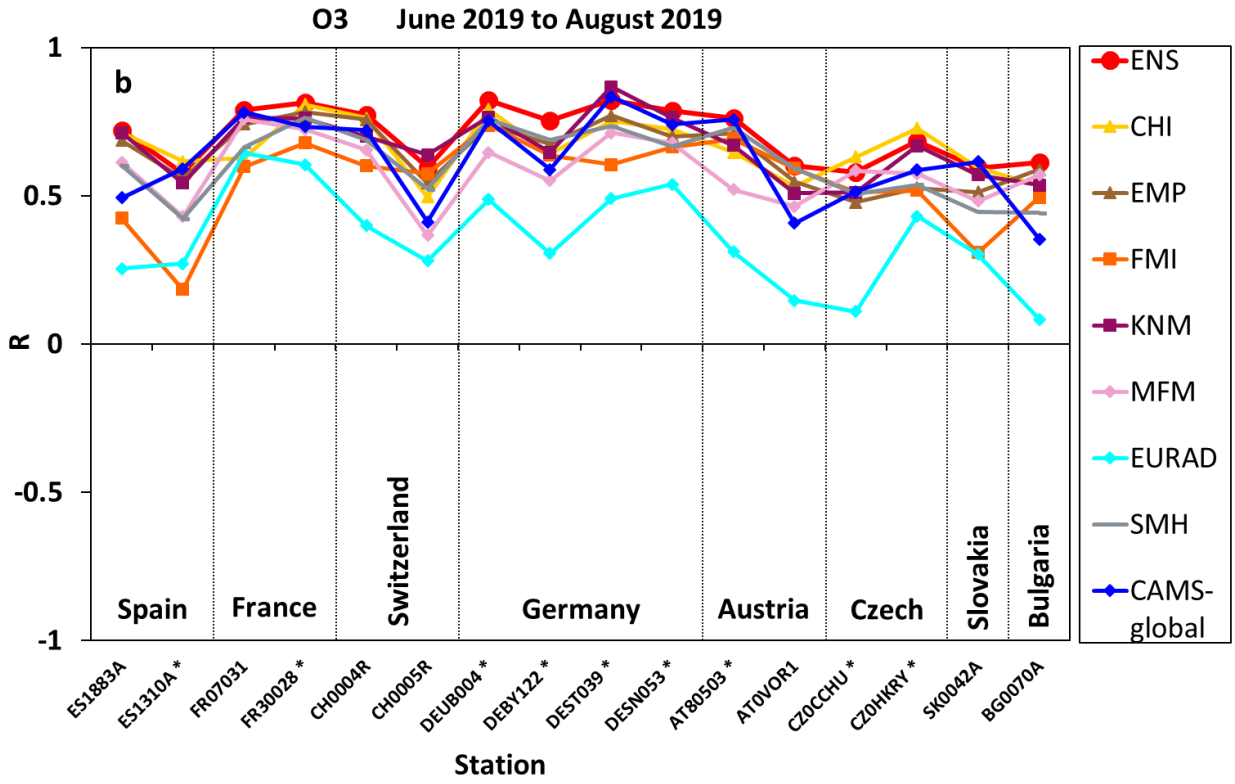

Fig. 8.5: Correlation coefficients (from hourly values) between observed and modelled O_3 from all models of the ensemble and CAMS-global (o-suite) for June to August 2019. With asterisks are denoted stations used in the assimilation process.

8.4 Results for the seven regional models

Figure 8.4 shows Modified Normalized Mean biases at each station with elevation greater than 1000 m above mean sea level, moving from Spain to Bulgaria (from West to East) pertaining to each one of the 7 model calculations, the Ensemble mean as well as CAMS-global. All results are based on the forecast D+0 elevated ozone values. On top of the graph shown is the elevation of the station. Depending on the station the observed ozone levels are reproduced to within -10% and 15% from the Ensemble Median. Figure 8.4 shows that the namely SILAM and MOCAGE models deviate significantly from the ensemble median (strong positive offset up to 30% for MOCAGE; SILAM mostly underestimate ozone values down to -40%) while the remaining models show scores closer to the ENSEMBLE.

Finally, Figure 8.5 shows the correlations between observations and each model. It is clear that the Ensemble Mean reproduces well the ozone variability and has a better score than any of the individual models. The EURAD and SILAM models show lower correlation while the remaining models show scores closer to the ENSEMBLE.

9 Comparison with ozone sonde observations

9.1 Summary

Free tropospheric ozone (<850 hPa) could be reproduced by the ENSEMBLE forecast and analysis with MNMBs between -7% and 10% during JJA 2019. The other models show MNMBs between -12% and 15% (forecasts and analysis). An exception is the MATCH model (SMH), which shows larger negative MNMBs (up to -62%) in the analysis.

9.2 Comparison approach

For the validation, the sonde profiles are compared to the model data closest in time. The model data is provided at the geographical coordinates of the sonde stations, the horizontal drift during the ascend of the sonde is considered negligible.

The model concentrations at the different height levels (0, 50, 250, 500, 1000, 2000, and 5000m above the ground) are matched to the respective sonde observations and are converted to mass mixing ratios. Pressure and temperature values needed for the conversion are taken from the sonde observations. For each station and all individual launches, the differences between observation and model are calculated. In order to be able to compare the profiles of different stations, this is done for fixed altitude levels between 0 and 6000m (interval for the surface 50m, above 100m, interval 100m). The sonde and model values are then aggregated to monthly means for each station and altitude level. For each month mean modified normalized biases (MNMB) are then calculated over all European stations for the free troposphere (<850 hPa).

9.3 Results for the ensemble

For the months June to August 2019, the ENSEMBLE forecast shows MNMBs between -3.4% and 9.6%. The ENSEMBLE analysis shows a similar behaviour with MNMBs between -6.9% and 8.7%., see Fig. 9.1.

Table 9.1: Sonde stations used in the validation for JJA2019

Station/location	Lat	lon	alt [m]
De Bilt	52.1	5.2	4
Hohenpeissenberg	47.8	11.2	976
Jokioinen	60.8	23.5	103
Legionow	52.4	20.97	96
Lerwik	60.14	-1.19	84
Madrid Spain	40.5	-3.8	631
Prag	50	14.4	302
Sodankyla	67	27	180
Uccle Belgium	51	4	100

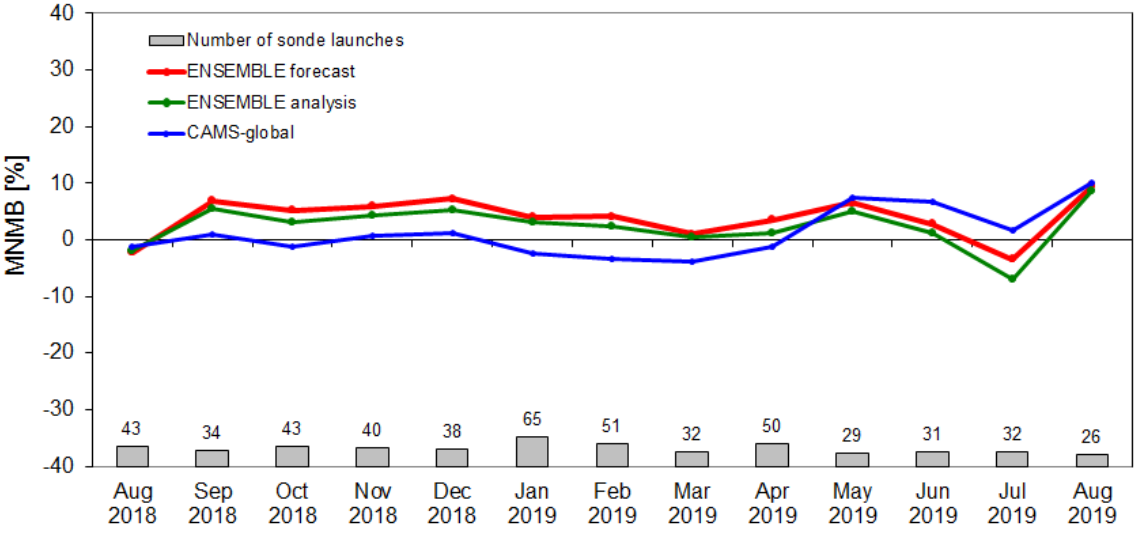

Figure 9.1 - MNMBs for the regional models between June 2019 and August 2019 for the free troposphere region (<850 hPa).

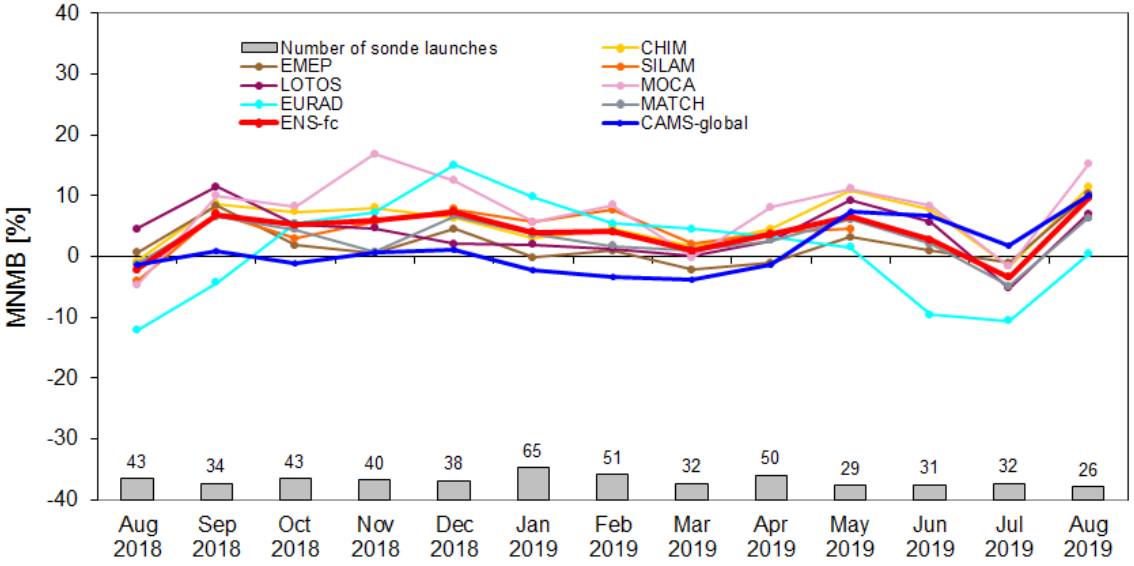

Figure 9.2. MNMBs for the regional models between June 2019 and August 2019 for the free troposphere region (pressure < 850 hPa).

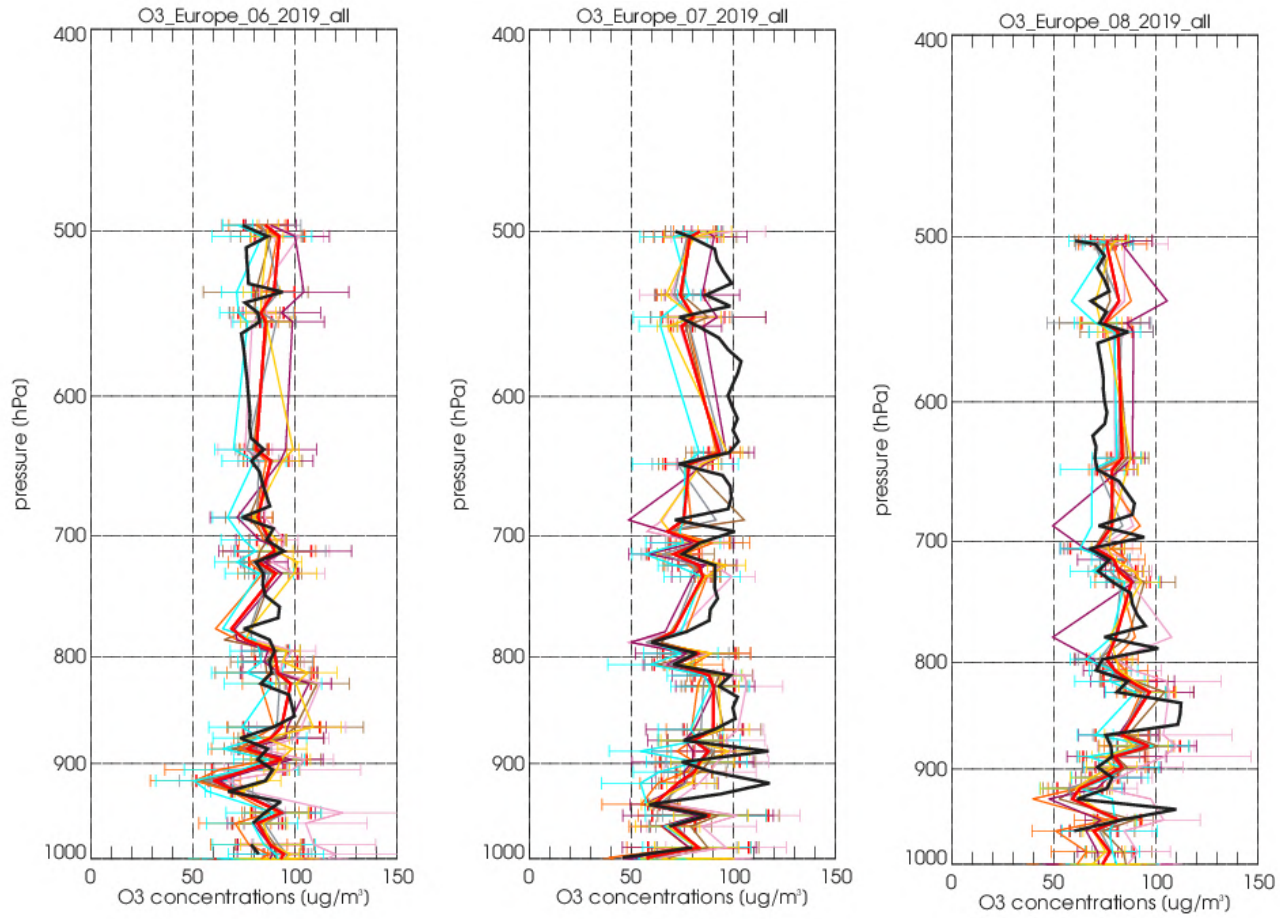

Figure 9.3. Vertical ENSEMBLE forecast and sonde comparison profiles for European sonde stations for June, July and August 2019.

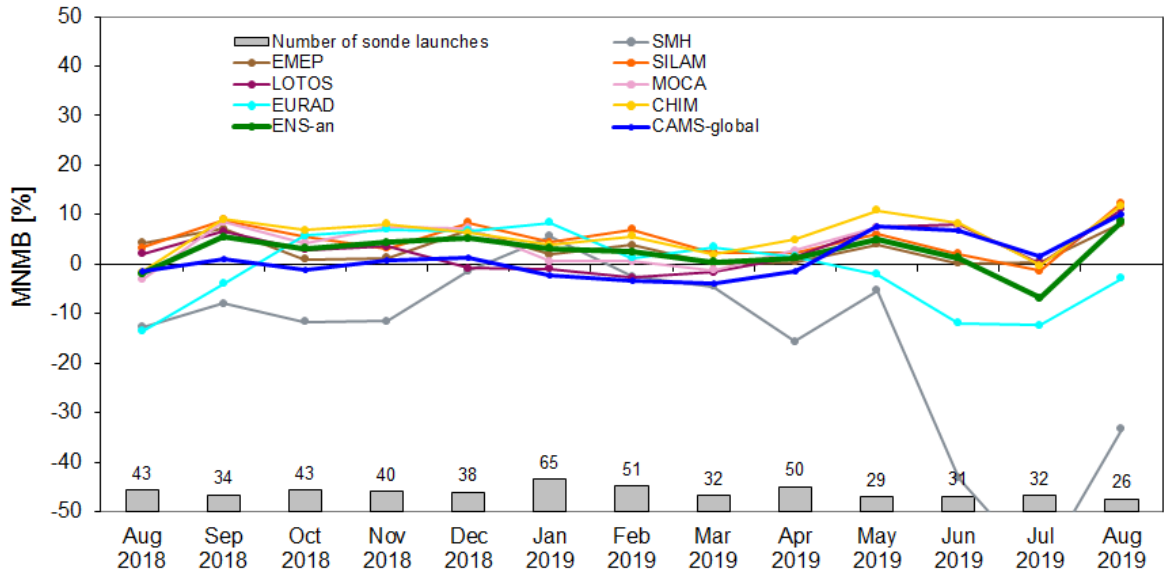

Figure 9.4. MNMBs for the regional models between June 2019 and August 2019 for the free troposphere region (pressure < 850 hPa).

9.4 Results for individual regional models

Between June to August 2019 regional model forecasts show MNMBs in the range of -10.6 % and 15.2%, see Fig. 9.2 and 9.3.

Results for the regional model analyses

Similar to the results of the individual models' forecasts, the analyses show MNMBs between ±12% (Figs. 9.4, 9.5). Only the MATCH model shows larger negative MNMBs up to -62%, which is in contrast to the forecast.

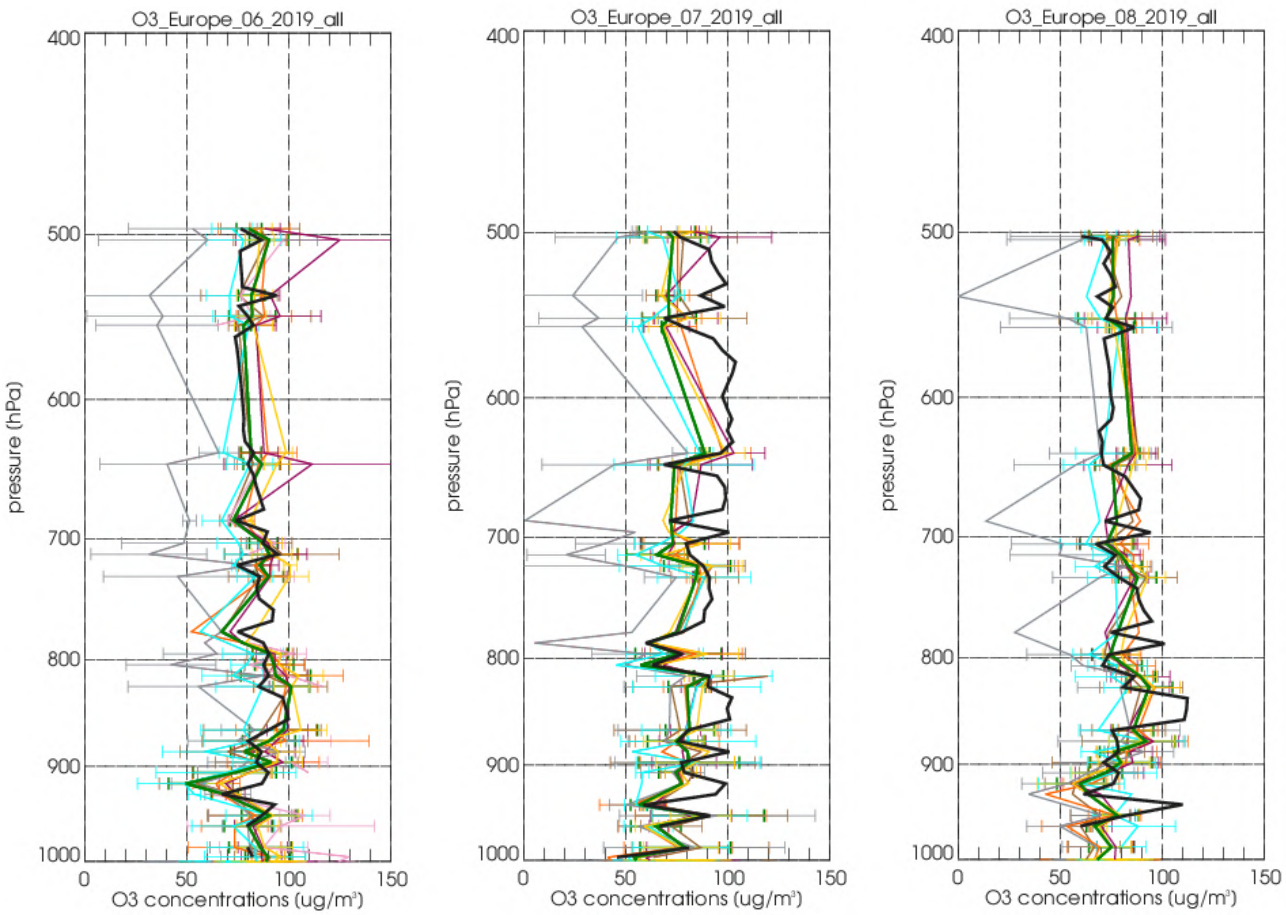

Figure 9.5. Vertical ENSEMBLE analysis and sonde comparison profiles for European sonde stations for June, July and August 2019.

10 Comparison with GAW stations

10.1 Summary

The model concentrations of O_3 and CO at higher model levels were compared with five GAW high-altitude stations in mountainous terrain. As for the EEA air quality e-reporting stations, differences between the regional model orography and the true altitude of the station were used for this model level selection. Good results were obtained for the ENSEMBLE for ozone with small biases and good correlations. The CHIMERE model shows slightly larger MNMBs in both the analysis and the forecast. The MATCH model shows large negative MNMBs in the analysis. For CO, especially the ENSEMBLE corresponds well to the observations, however, small underestimates are found. Like for O_3, the MATCH model behaves differently in the analysis than in the forecast. The time series and correlation coefficients for CO and O_3 show that the ENSEMBLE reproduces for a large part the variability observed.

10.2 Comparison method

Hourly O_3 and CO concentration values in µg/m^3 are extracted from the seven models and are compared to the GAW measurements, which were converted from volume mixing ratios (ppb) into concentrations by using pressure and temperature values at the respective pressure levels from the IFS model.

The altitude of the stations Hohenpeissenberg (HPB), Jungfraujoch (JFJ), Monte Cimone (CMN), Sonnblick (SNB) and Zugspitze in the model has been extracted from the orography as used in the LOTOS-EUROS model, see Table 1. For the level choice, the GAW stations' altitudes together with the best correlation of the corresponding levels were taken into account. Uncertainties due to the choice of level (calculated as mean differences between the chosen level and one up/down for the period JJA for the ENSEMBLE) are up ±30 µg/m^3 for CO and up to ±4 µg/m^3 for O_3.

Table 10.1 - Validation set-up for June - August 2019.

station	altitude station [m]	altitude model [m]	level choice (range 0-7)	altitude at level [m]
HPB	985	813	2	1063
JFJ	3580	1837	5	3837
CMN	2165	602	4	1602
SNB	3105	1687	3	2187

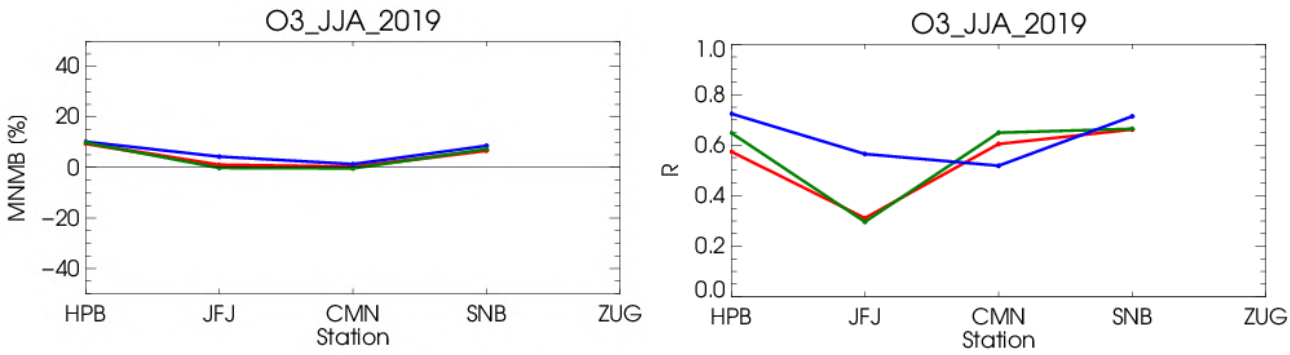

Figure 10.1. MNMBs [%] (left) and correlation coefficients (right) for ozone (red: ENSEMBLE forecast, green: ENSEMBLE analysis, blue: CAMS-global) for the period June to August 2019.

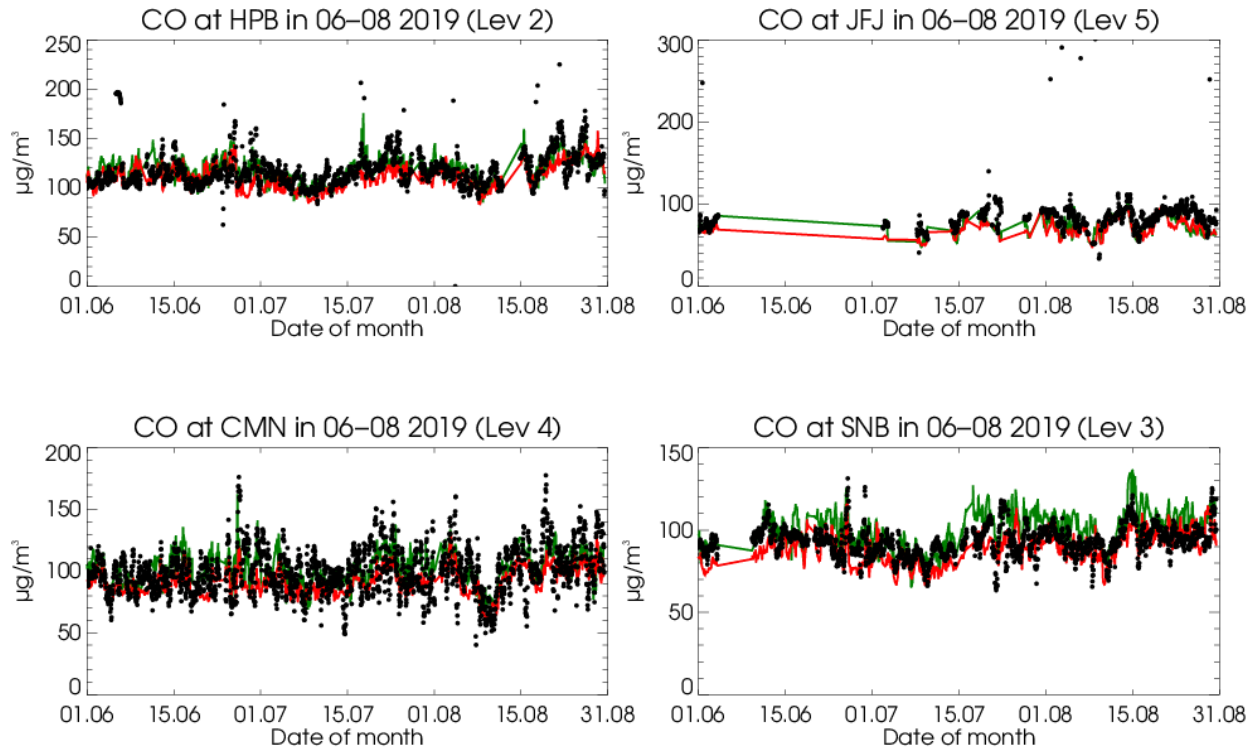

Figure 10.2. Time series plots for the ENSEMBLE forecast (red) and ENSEMBLE analysis (green) for surface O_3 in comparison with high altitude stations.

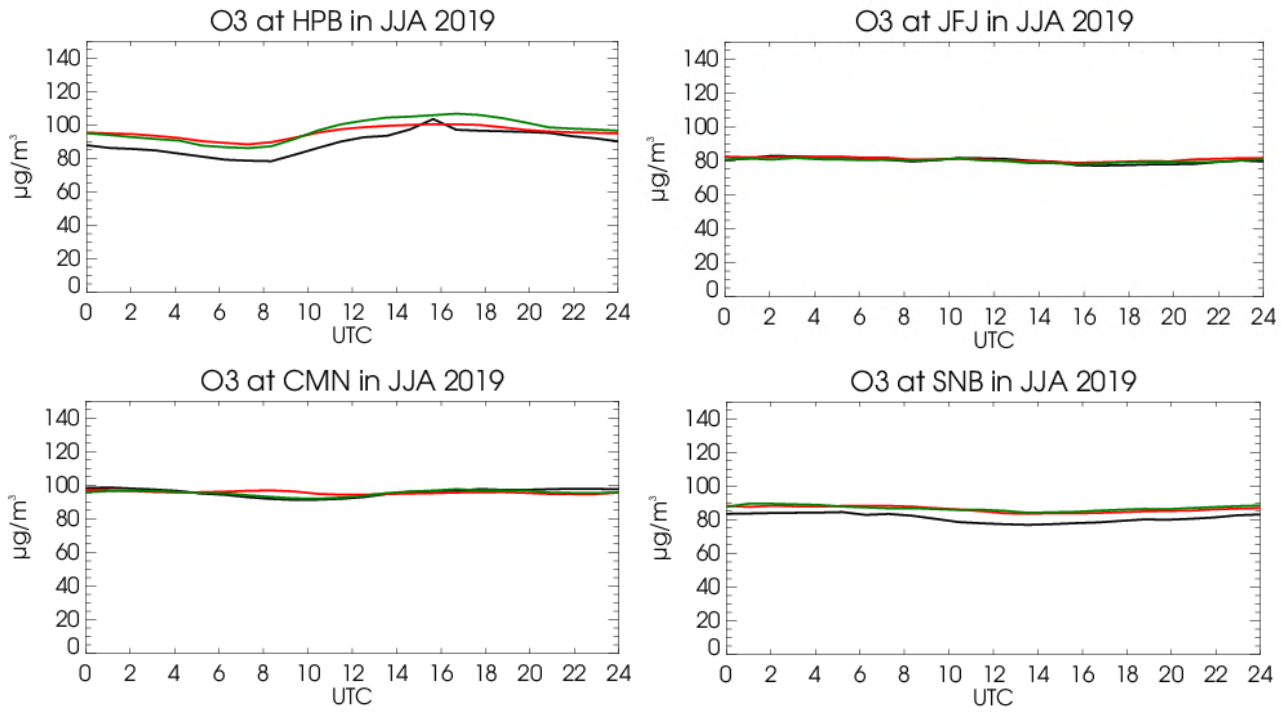

Figure 10.3. Mean diurnal cycle of O_3 for the ENSEMBLE forecast (red) and ENSEMBLE analysis (green) compared to the observations (black) for the period MAM2019.

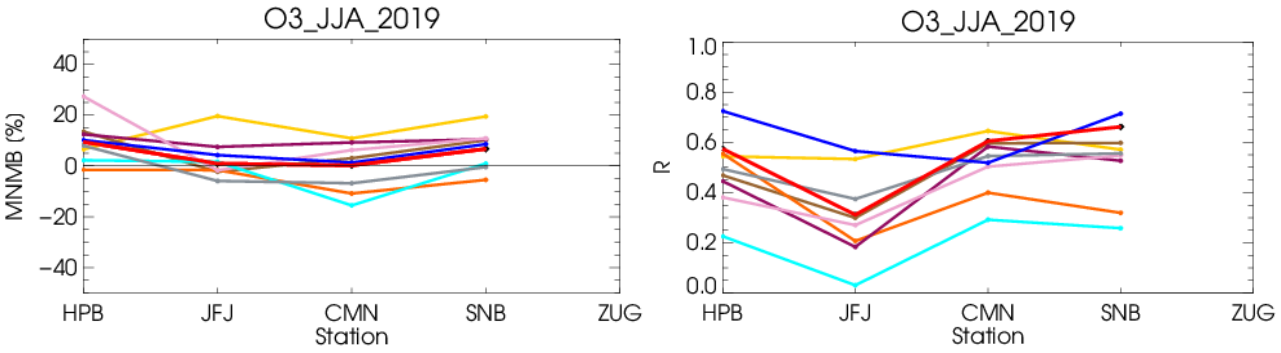

Figure 10.4. MNMBs [%] (left) and correlation coefficients (right) for all model forecasts for ozone (red: ensemble, blue: CAMS-global, yellow: CHIMERE, brown: EMEP, orange: SILAM, purple: LOTOS-EUROS, cyan: EURAD-IM, pink: MOCAGE, grey: MATCH). Altitudes are listed in Table 10.1.

10.3 Ozone

The ensemble forecast shows positive MNMBs between 0% and 9% and correlation coefficients ranging between 0.31 and 0.66 for the period June to August 2019. The ENSEMBLE analysis shows the same MNMBs (between 0% and 9%) and partly slightly better correlation coefficients ranging from 0.29 and 0.66 (see Fig. 10.1).

The time series plots show a good correspondence between model and observations.

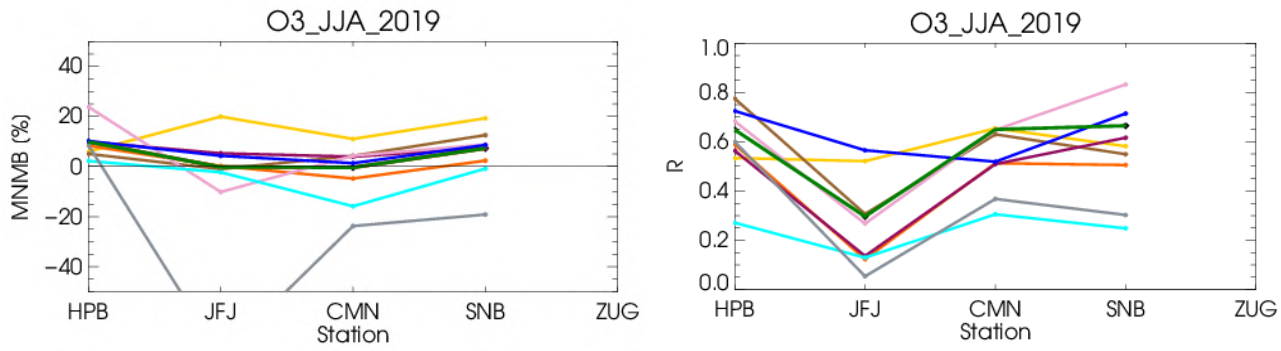

Figure 10.5. MNMBs [%] (left) and correlation coefficients (right) for all models analyses for ozone (red: ensemble, blue: CAMS-global, yellow: CHIMERE, brown: EMEP, orange: SILAM, purple: LOTOS-EUROS, cyan: EURAD-IM, pink: MOCAGE, grey: MATCH). Altitudes are listed in Table 10.1.

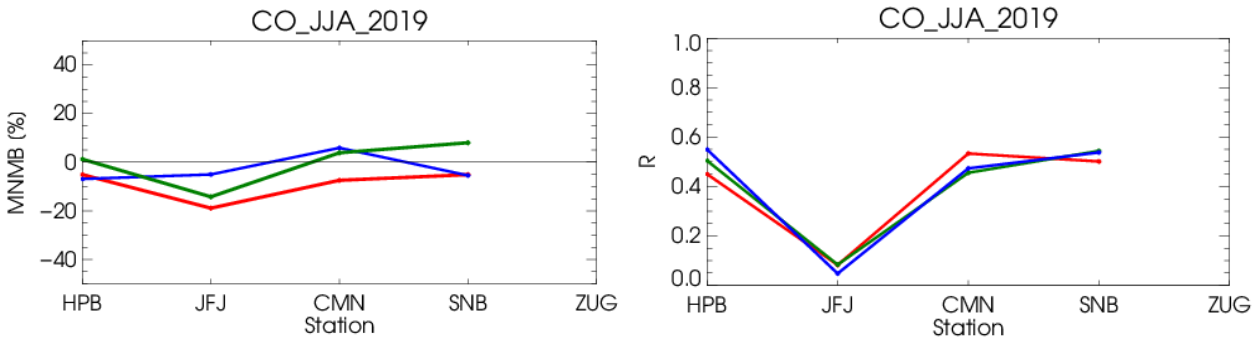

Figure 10.6. MNMBs [%] (left) and correlation coefficients (right) for the ensemble for CO (red: ENSEMBLE forecast, green: ENSEMBLE analysis, blue: CAMS-global).

Results for individual model forecasts:

The models show MNMBs in the range of 27% and -15% for the period June to August 2019 (Fig. 10.4). The CHIMERE model shows larger positive MNMBs than the other models. During JJA, correlation coefficients vary greatly between the individual models and stations (0.3 to 0.64). The EURAD model shows very low correlation coefficients.

Results for the individual model analyses:

For the individual model analyses, MNMBs range between -15% and 23% (without MATCH) and are very similar to the forecast, except for MATCH, which has negative MNMBs up to -75% in the analysis. Same as for the forecast, correlation coefficients vary greatly between the different models and stations. The EURAD and MATCH model show the lowest correlation coefficients.

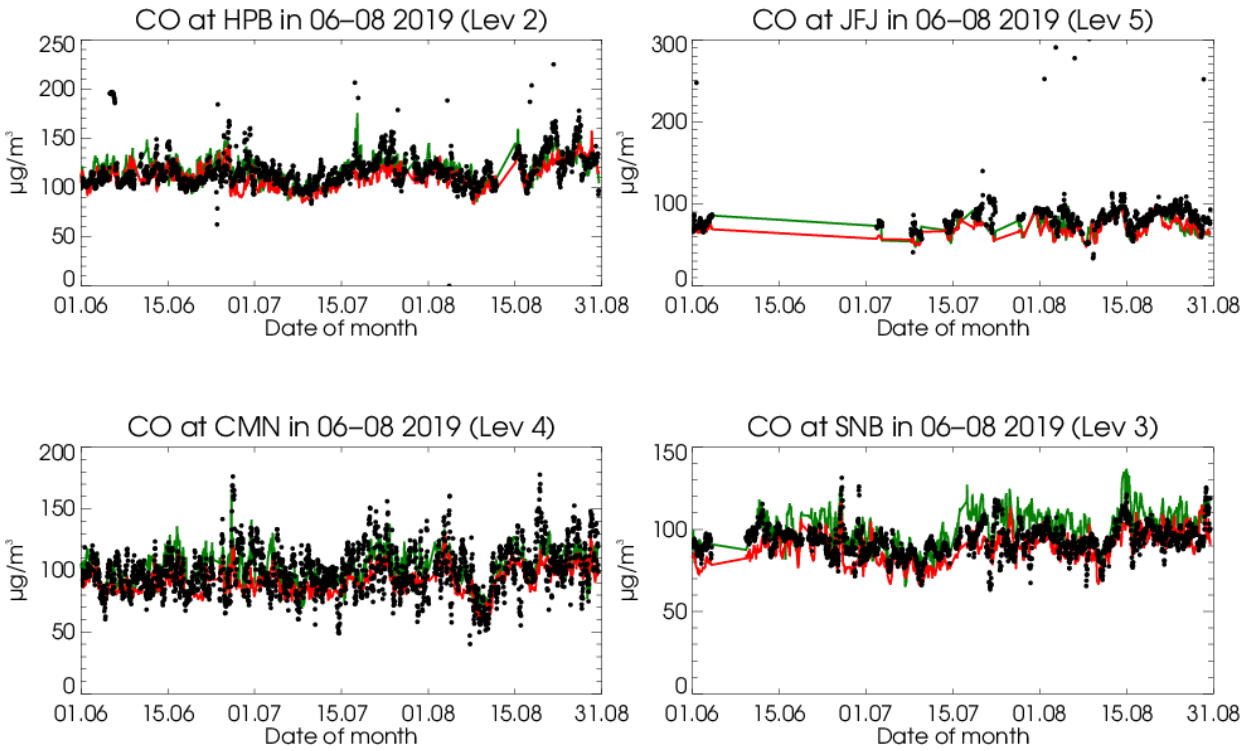

Figure 10.7. Time series plots for the ENSEMBLE forecast (red) and ENSEMBLE analysis (green) for surface CO in comparison with high altitude stations.

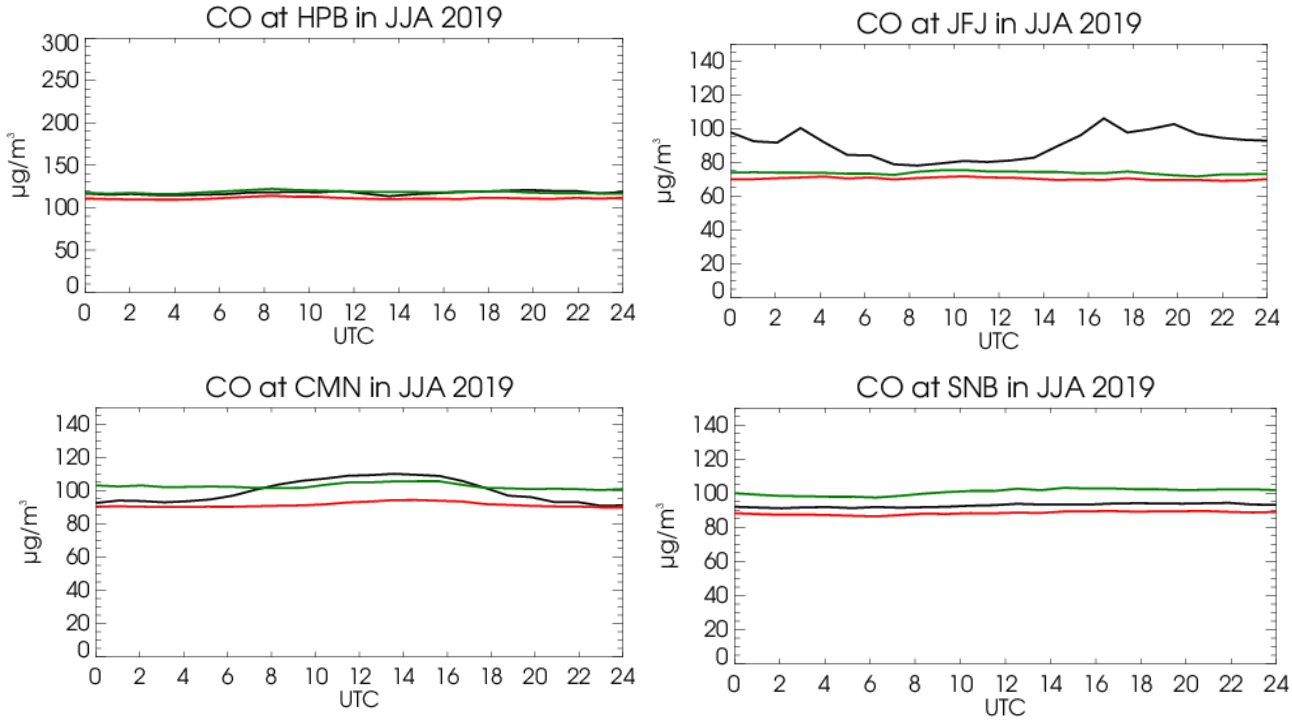

Figure 10.8. Mean diurnal cycle of CO for the ENSEMBLE forecast (red) and ENSEMBLE analysis (green) compared to the observations (black) for the period JJA2019.

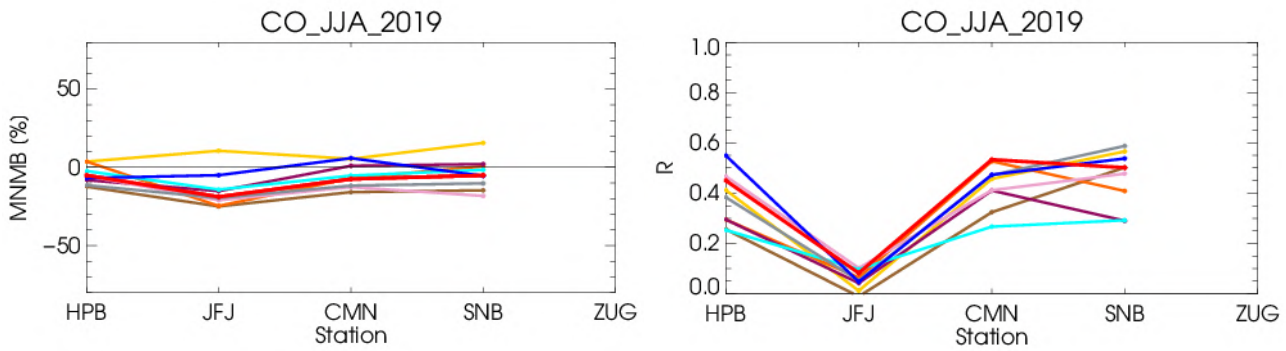

Figure 10.9. CO MNMBs [%] (left) and correlation coefficients (right) for all regional model forecasts, the ensemble and CAMS-global (red: ENSEMBLE forecast, blue: CAMS-global, yellow: CHIMERE, brown: EMEP, orange: SILAM, purple: LOTOS-EUROS, cyan: EURAD-IM, pink: MOCAGE, grey: MATCH). Altitude ranges are listed in Table 10.1.

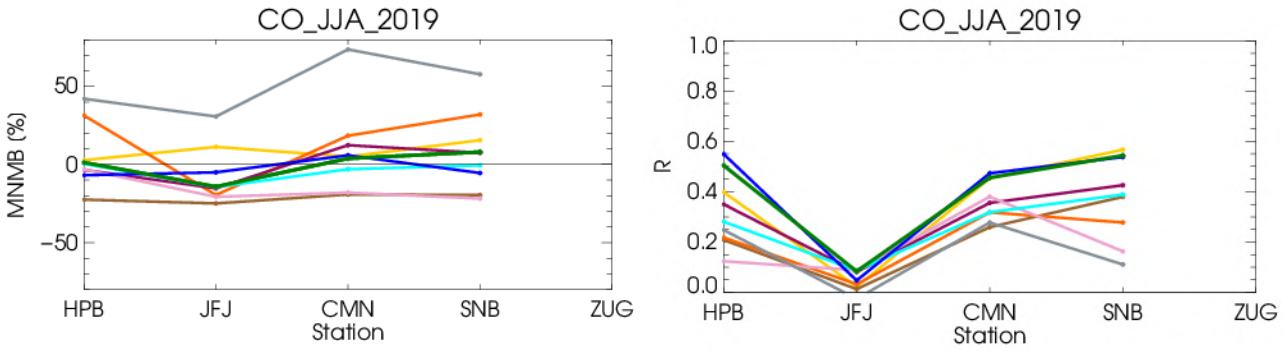

Figure 10.10. CO MNMBs [%] (left) and correlation coefficients (right) for all regional model analyses, the ensemble and CAMS-global (green: ENSEMBLE analysis, blue: CAMS-global, yellow: CHIMERE, brown: EMEP, orange: SILAM, purple: LOTOS-EUROS, cyan: EURAD-IM, pink: MOCAGE, grey: MATCH). Altitude ranges are listed in Table 10.1.

10.4 Carbon monoxide

For CO, the ENSEMBLE forecast and analysis MNMBs range between 8% and -14% for the analysis and between -5% and -18% for the forecast during June to August 2019. Correlation coefficients are between 0.1 and 0.54 for the analysis and forecast (Fig. 10.6). The time series plots (Fig. 10.7) show mostly a very good agreement between model and observations, except for a systematic negative offset for some stations.

The comparison between mean diurnal observations and mean model concentrations show that the forecast mostly has a negative offset for the high-altitude stations. The analysis partly overestimates CO (SNB). For Monte Cimone (CMN) especially the daytime concentrations (between 8 and 18 pm) are slightly underestimated in the forecast. The wave-like structure in the diurnal cycle for JFJ is likely an artefact, see Fig. 10.8.

CO results for individual model forecasts:

CO mixing ratios are underestimated for most stations, with MNMBs between 15% and -20%. The CHIMERE model is the only one that shows positive deviations for most stations, see Fig. 10.9. Correlation coefficients are between 0 and 0.58.

Results for the individual model analyses:

CO mixing ratios are partly underestimated, partly slightly overestimated by all models. CHIMERE and MATCH show only positive MNMBs (up to 73% for the MATCH model). The MATCH model thus behaves differently in the analysis than in the forecast, see Figs. 10.9 and 10.10. Correlation coefficients range between 0 and 0.56.

11 Comparisons with MOPITT CO

11.1 Summary

Due to the data unavailability in the archive system the model results are only evaluated for June 2019. The land part of domain is generally underestimated up to 20% over the eastern part of domain. All the models overestimated areas with very low CO values over the North Atlantic Ocean within 10 % with some regional exceptions. Note, that the data for ENSEMBLE and MOCAGE are only available for the first two weeks on June.

11.2 Method

CO total column forecasts over Europe from seven regional models and the model ensemble are compared with CO total column retrievals from MOPITT Version 8 (thermal infrared radiances) (Emmons et. al., 2009). Modelled CO data were converted from µg/m³ to VMR by using temperature obtained from CAMS-global (o-suite) model. Pressure at the middle of the layers was also interpolated from the global model. Regional model data are available from the surface up to altitude of 5 km. For the comparison with satellite retrievals, the averaging kernels were applied to the modelled data.

Regional model data up to 5 km were merged with CAMS-global data above 5 km in order to minimize uncertainty error. We performed several confidence tests to establish the method. To check the error due to coarse sampling of the profiles up to 5 km as provided by the regional models, CAMS-global data were sampled at the height levels of the regional models up to 5 km and merged with the CAMS-global original levels above 5 km. Comparison of this results with the original CAMS-global data showed that the errors due to coarse sampling of the profiles up to 5 km were very small. Both results showed slight underestimation of the MOPITT data. CAMS-global values up to 5 km sampled at the height levels as the regional models and ENSEMBLE data without merging with the levels above 5km show overestimation of the satellite data over almost entire region. From this we concluded that error due to missing values above 5 km is significant and merging the regional data with CAMS-global values above 5 km is necessary for the proper comparison.

Due to the data unavailability in the archive system the model results are only evaluated for June 2019. The land part of domain is generally underestimated up to 20% over the eastern part of domain. All the models overestimated areas with very low CO values over the North Atlantic Ocean within 10 % with some regional exceptions. Note, that the data for ENSEMBLE and MOCAGE are only available for the first two weeks on June.

MOPITT

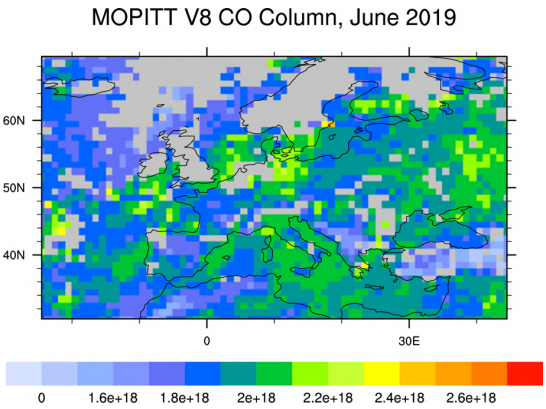

ENS-MOPITT
Forecast (0H24H)

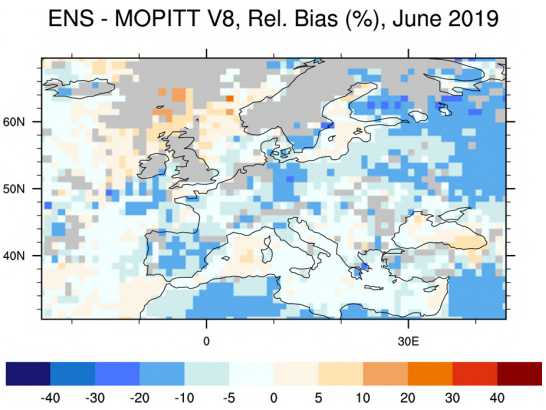

EMEP-MOPITT
Forecast (0H24H)

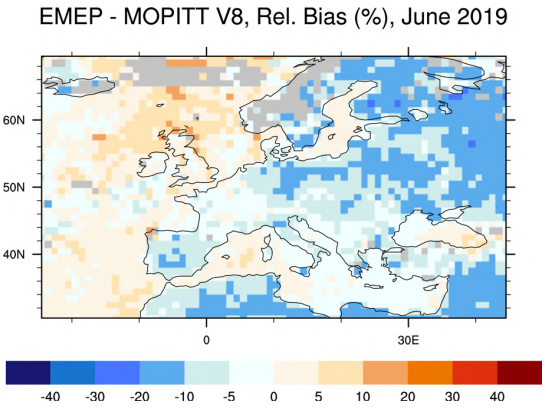

EURAD-MOPITT
Forecast (0H24H)

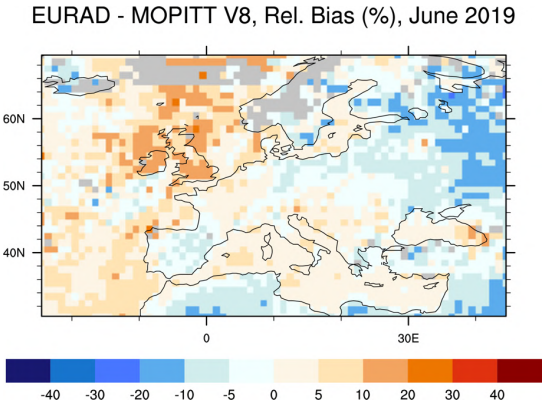

CHIMERE-MOPITT
Forecast (0H24H)

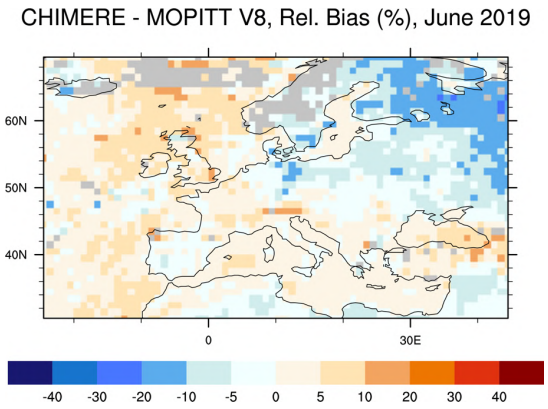

LOTOS-EUROS-MOPITT
Forecast (0H24H)

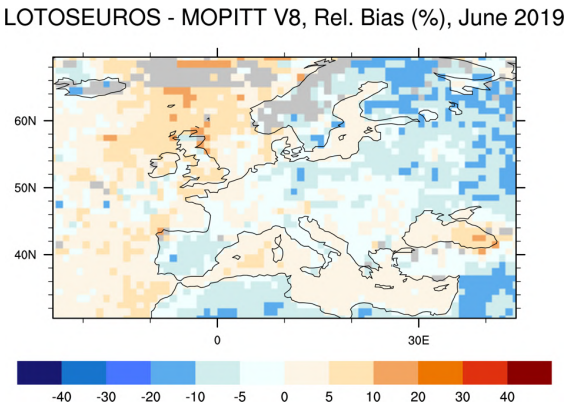

SILAM-MOPITT
Forecast (0H24H)

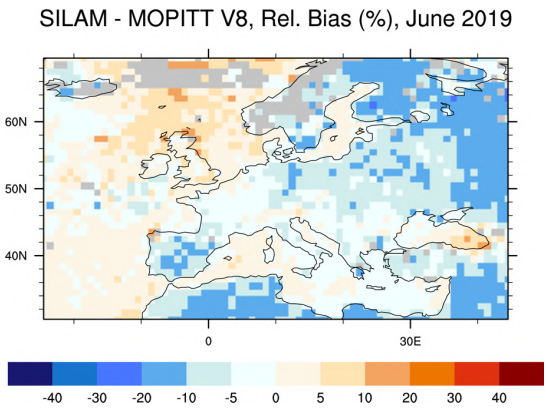

MATCH-MOPITT
Forecast (0H24H)

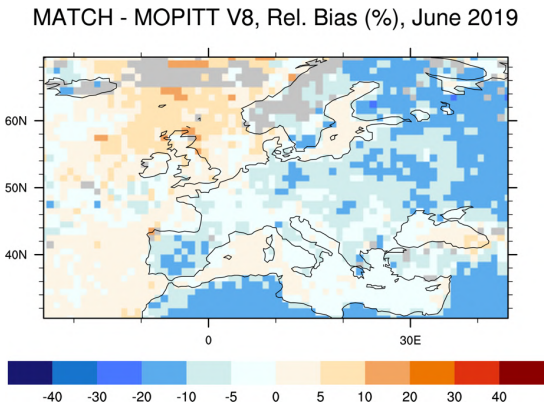

MOCAGE-MOPITT
Forecast (0H24H)

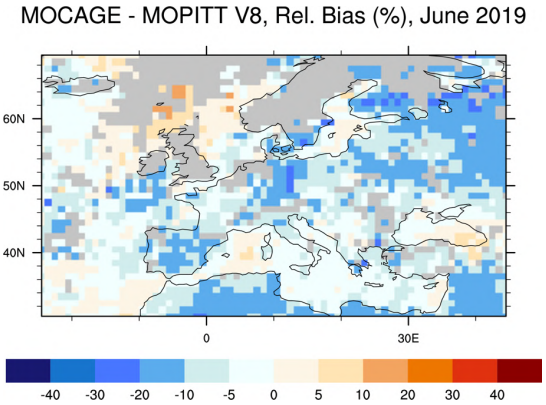

Figure 11.1. CO total column for MOPITT V8 satellite retrievals (top row, in molecules/cm^2), relative difference between the regional forecasts of the seven models and the ENSEMBLE and MOPITT (other rows) for June 2019. Grey colour indicates missing values.

12 Acknowledgements

The authors acknowledge all EARLINET and European ACTRIS/Aeronet data providers for providing aerosol lidar profiles and sun photometer data available from the ACTRIS data portal (http://actris.nilu.no), and the Aeronet NRT data dissemination system respectively (https://aeronet.gsfc.nasa.gov). The ACTRIS 2 project (http://www.actris.eu) has received funding from the European Union's Horizon 2020 research and innovation program under grant agreement No 654109.

We wish to acknowledge the provision of GAW hourly NRT station data by: the National Air Pollution Monitoring Network (NABEL) (Federal Office for the Environment FOEN and Swiss Federal Laboratories for Materials Testing and Research EMPA) for Jungfraujoch station, the Umweltbundesamt (UBA, Germany) for Zugspitze (Schneefernerhaus) station, the Umweltbundesamt (Austria) for Sonnblick station, the Observatory Hohenpeissenberg (Deutscher Wetter Dienst, DWD) for Hohenpeissenberg station, and the Institute of Atmospheric Sciences and Climate (ISAC) of the Italian National Research Council (CNR) for Monte Cimone station.

We wish to acknowledge the provision of ozone sonde data by the World Ozone and Ultraviolet Radiation Data Centre established at EC in Toronto (http://woudc.org), by the Data Host Facility of the Network for the Detection of Atmospheric Composition Change established at NOAA (http://ndacc.org), and by the Norwegian Institute for Air Research (http://nilu.no).

We acknowledge the EEA Air quality e-reporting Network (https://www.eea.europa.eu/data-and-maps/data/aqereporting-8) for the provision of hourly NRT station observations.

We wish to acknowledge the Department of Labour Inspection - Ministry of Labour and Social Insurance, of Cyprus (http://www.airquality.dli.mlsi.gov.cy/) for the provision of hourly NRT ozone data from Mountain Troodos station.

The programmes MOZAIC and CARIBIC, and the current Research Infrastructure IAGOS are operated with support from the European Commission, national agencies in Germany (BMBF), France (MESR), and the UK (NERC), and the IAGOS member institutions (http://www.iagos.org/partners). The participating airlines (Lufthansa, Air France, Austrian, China Airlines, Iberia, Cathay Pacific, Air Namibia, Sabena) supported IAGOS by carrying the measurement equipment free of charge since 1994. The data are available at http://www.iagos.fr thanks to additional support from AERIS (CNRS and CNES).

GOME2 lv1 radiances and irradiances were provided by EUMETSAT.

We acknowledge the NASA Langley Research Center Atmospheric Science Data Center for providing the MOPITT data.

AUTH acknowledges the AUTH Scientific Computing Centre (https://it.auth.gr/en/services) for providing technical and infrastructure support for data analysis performed in this WP.

13 References

*Richter, A., Begoin, M., Hilboll, A., and Burrows, J. P.: An improved NO2 retrieval for the GOME-2 satellite instrument, Atmos. Meas. Tech. , **4**, 1147-1159, doi:10.5194/amt-4-1147-2011, 2011.*

Ackermann, J. (1998). The extinction-to-backscatter ratio of tropospheric aerosol: A numerical study. Journal of atmospheric and oceanic technology, 15(4), 1043-1050.

ACTRIS Deliverable WP6/D6.21,
http://www.actris.net/Portals/97/deliverables/PU/WP6_D6.21_M45v2.pdf

Cattrall, C., Reagan, J., Thome, K., & Dubovik, O. (2005). Variability of aerosol and spectral lidar and backscatter and extinction ratios of key aerosol types derived from selected Aerosol Robotic Network locations. Journal of Geophysical Research: Atmospheres, 110(D10).

Chin, M., Ginoux, P., Kinne, S., Torres, O., Holben, B. N., Duncan, B. N., ... & Nakajima, T. (2002). Tropospheric aerosol optical thickness from the GOCART model and comparisons with satellite and Sun photometer measurements. Journal of the atmospheric sciences, 59(3), 461-483.

Eskes, H.J., S. Basart, A. Benedictow, Y. Bennouna, A.-M. Blechschmidt, S. Chabrillat, Y. Christophe, E. Cuevas, J. Douros, H. Flentje, K. M. Hansen, J. Kapsomenakis, B. Langerock, M. Ramonet, A. Richter, M. Schulz, N. Sudarchikova, A. Wagner, T. Warneke, C. Zerefos, Observations characterisation and validation methods document, Copernicus Atmosphere Monitoring Service (CAMS) report, CAMS84_2015SC3_D.84.8.1.1-2018_observations_v3.pdf, October 2018 (2018). Available from: http://atmosphere.copernicus.eu/user-support/validation/verification-global-services

Eskes, H., Huijnen, V., Arola, A., Benedictow, A., Blechschmidt, A.-M., Botek, E., Boucher, O., Bouarar, I., Chabrillat, S., Cuevas, E., Engelen, R., Flentje, H., Gaudel, A., Griesfeller, J., Jones, L., Kapsomenakis, J., Katragkou, E., Kinne, S., Langerock, B., Razinger, M., Richter, A., Schultz, M., Schulz, M., Sudarchikova, N., Thouret, V., Vrekoussis, M., Wagner, A., and Zerefos, C.: Validation of reactive gases and aerosols in the MACC global analysis and forecast system, Geosci. Model Dev., 8, 3523-3543, doi:10.5194/gmd-8-3523-2015, 2015.

Flemming, J., Huijnen, V., Arteta, J., Bechtold, P., Beljaars, A., Blechschmidt, A.-M., Diamantakis, M., Engelen, R. J., Gaudel, A., Inness, A., Jones, L., Josse, B., Katragkou, E., Marecal, V., Peuch, V.-H., Richter, A., Schultz, M. G., Stein, O., and Tsikerdekis, A.: Tropospheric chemistry in the Integrated Forecasting System of ECMWF, Geosci. Model Dev., 8, 975-1003, doi:10.5194/gmd-8-975-2015, 2015.

Joly, Mathieu, and Vincent-Henri Peuch, Objective classification of air quality monitoring sites over Europe, Atmospheric Environment 47, 111-123, 2012.

Katragkou, E., Zanis, P., Tsikerdekis, A., Kapsomenakis, J., Melas, D., Eskes, H., Flemming, J., Huijnen, V., Inness, A., Schultz, M. G., Stein, O., and Zerefos, C. S.: Evaluation of near-surface ozone over Europe from the MACC reanalysis, Geosci. Model Dev., 8, 2299-2314, doi:10.5194/gmd-8-2299-2015, 2015.

Marécal, V., Peuch, V.-H., Andersson, C., Andersson, S., Arteta, J., Beekmann, M., Benedictow, A., Bergström, R., Bessagnet, B., Cansado, A., Chéroux, F., Colette, A., Coman, A., Curier, R. L., Denier van der Gon, H. A. C., Drouin, A., Elbern, H., Emili, E., Engelen, R. J., Eskes, H. J., Foret, G., Friese, E., Gauss, M., Giannaros, C., Guth, J., Joly, M., Jaumouillé, E., Josse, B., Kadygrov, N., Kaiser, J. W., Krajsek, K., Kuenen, J., Kumar, U., Liora, N., Lopez, E., Malherbe, L., Martinez, I., Melas, D., Meleux, F., Menut, L., Moinat, P., Morales, T., Parmentier, J., Piacentini, A., Plu, M., Poupkou, A., Queguiner, S., Robertson, L., Rouïl, L., Schaap, M., Segers, A., Sofiev, M., Tarasson, L., Thomas, M., Timmermans, R., Valdebenito, Á., van Velthoven, P., van Versendaal, R., Vira, J.,

and Ung, A.: A regional air quality forecasting system over Europe: the MACC-II daily ensemble production, Geosci. Model Dev., 8, 2777-2813, doi:10.5194/gmd-8-2777-2015, 2015.

Morcrette, J.-J., O. Boucher, L. Jones, D. Salmond, P. Bechtold, A. Beljaars, A. Benedetti, A. Bonet, J. W. Kaiser, M. Razinger, M. Schulz, S. Serrar, A. J. Simmons, M. Sofiev, M. Suttie, A. M. Tompkins, and A. Untch: Aerosol analysis and forecast in the ECMWF Integrated Forecast System. Part I: Forward modelling, J. Geophys. Res., 114, D06206, doi:10.1029/2008JD011235, 2009.

Mortier, A., Goloub, P., Derimian, Y., Tanré, D., Podvin, T., Blarel, L., ... & Ndiaye, T. (2016). Climatology of aerosol properties and clear-sky shortwave radiative effects using Lidar and Sun photometer observations in the Dakar site. Journal of Geophysical Research: Atmospheres.

Müller, D., Ansmann, A., Mattis, I., Tesche, M., Wandinger, U., Althausen, D., & Pisani, G. (2007). Aerosol-type-dependent lidar ratios observed with Raman lidar. Journal of Geophysical Research: Atmospheres, 112(D16).

Omar, A. H., Winker, D. M., Vaughan, M. A., Hu, Y., Trepte, C. R., Ferrare, R. A., ... & Kuehn, R. E. (2009). The CALIPSO automated aerosol classification and lidar ratio selection algorithm. Journal of Atmospheric and Oceanic Technology, 26(10), 1994-2014.

Pappalardo, G., A. Amodeo, A. Apituley, A. Comeron, V. Freudenthaler, H. Linne, A. Ansmann, J. Bösenberg, G. D'Amico, I. Mattis, L. Mona, U. Wandinger, V. Amiridis, L. Alados-Arboledas, D. Nicolae, and Wiegner, M.: EARLINET: towards an advanced sustainable European aerosol lidar network, Atmos. Meas. Tech., 7, 2389–2409, www.atmos-meas-tech.net/7/2389/2014/, doi:10.5194/amt-7-2389-2014, 2014.

*Richter, A., Begoin, M., Hilboll, A., and Burrows, J. P.: An improved NO2 retrieval for the GOME-2 satellite instrument, Atmos. Meas. Tech. , **4**, 1147-1159, doi:10.5194/amt-4-1147-2011, 2011.*

Vinken, G. C. M., Boersma, K. F., van Donkelaar, A., and Zhang, L.: Constraints on ship NOx emissions in Europe using GEOS-Chem and OMI satellite NO2 observations, Atmos. Chem. Phys., 14, 1353-1369, doi:10.5194/acp-14-1353-2014, 2014.

Wagner, A., M. Schulz, Y. Christophe, M. Ramonet, H.J. Eskes, S. Basart, A. Benedictow, Y. Bennouna, A.-M. Blechschmidt, S. Chabrillat, H. Clark, E. Cuevas, H. Flentje, K.M. Hansen, U. Im, J. Kapsomenakis, B. Langerock, A. Richter, N. Sudarchikova, V. Thouret, T. Warneke, C. Zerefos, Validation report of the CAMS near-real-time global atmospheric composition service: Period September-November 2018, Copernicus Atmosphere Monitoring Service (CAMS) report, CAMS84_2018SC1_D1.1.1_SON2018_v1.pdf, March 2019.

Copernicus Atmosphere Monitoring Service

ECMWF - Shinfield Park, Reading RG2 9AX, UK

Contact: info@copernicus-atmosphere.eu